UNIVERSITY OF OULU

FACULTY OF INFORMATION TECHNOLOGY AND ELECTRICAL ENGINEERING

Theresa Eleonye

STUDY ON MONITORING BREATHING AND HEART RATES WITH MM-WAVE FREQUENCY RADAR FOR VEHICULAR ENVIRONMENT

Master's Thesis
Degree Programme in Biomedical Engineering
June 2024

ABSTRACT

The physiological parameters of breathing rate and heart rate have been used for vital signs monitoring of the health status of the human subject for the purpose of wellness. As a result, many sensors have been invented and commercialized for the vital signs monitoring. However, the majority of these sensors are contact based or on-body wearable sensors that are best deplored in controlled clinical environments such as hospitals or home care for self-monitoring. These contact based sensors are not suitable for real-life driving situations as they cause distractions to the driver due to discomfort and they encroach on the driver's privacy. These inherent limitations in contact based sensors have led to the surge in alternative non-contact or contact-less based sensors of which the radar-based sensors have achieved some level of success with respect to vital signs monitoring of human subject in a vehicle.

The objective of this work is to compare the breathing rate and heart rate measurements from the millimeter wave radar-based sensor (Texas Instruments 77 GHz AWR1642Boost TI-mm wave sensor) used in vehicular environment to the reference device (Zephyr Technologies BioHarness™ 3.0), investigate the impact of radar's location and azimuthal orientation on the measured vital signs from human subjects situated in an approximating vehicular environment and comparing the results in different gender. The datasets of 5 volunteers (3 males, 2 females) captured from 24 measurement scenarios were pre-processed with bandpass filter of 0.1 to 0.6 Hz and 0.8 to 4.0 Hz respectively. The spectral evaluation of the filtered signal using the peak interval and Fast Fourier Transform (FFT) were used for the vital signs estimation of volunteers. The statistical analysis of the datasets showed weak correlation between the radar-based sensor and the reference device with the $p \leq 0.05$ occurring in the breathing signal only. The Bland Altman plots showed that the radar device overestimated the breathing and heart rates by -5.75 bpm and -7.23 bpm respectively from the reference device due to the presence of outliers. However, the confidence intervals with respect to the zero bias equivalence line validates the interchangeability and good measurement precision of the radar device with the reference device. The vital signs results of all volunteers were comparable within the normal range of 40 to 120 bpm and 5 to 35 bpm for the heart and breathing rates respectively. The range of tilt angles 0° to 45° of the radar-based sensor impacted positively on the accuracy of measured physiological parameters via increase of signal to noise ratio and the highest signal quality is detected at the tilt angle of 30°.

Keywords: millimeter wave, radar-based sensor, vital signs monitoring, performance metrics, non-contact sensor.

TABLE OF CONTENTS

FOREWORD

I give thanks to God Almighty for giving me life, wisdom, courage and sustenance in achieving this laudable feat. It certainly wasn't easy but it is worth it! I will like to express my profound gratitude to my Program coordinator; Professor Tapio Seppänen for his free hand towards the exhaustion of my curiosity in the different spheres of biomedical engineering as well as his Father figure interventions in my academic journey in Oulu, I am indeed very grateful! Special thanks goes to the following supervisors: Dr. Daljeet Singh for his intuitive suggestions, advice, support, and active participation in the experiment. Lukasz Surazynski for his patience, guidance, advice, consent in using his photograph of the experimental setup in this publication, and for reinforcing the can-do spirit in me of conducting the experiment with less supervision even though it is my first time. I will also like to express my deep appreciation to my Principal supervisor; Adjunct Professor Mariella Särestöniemi for accepting my request for thesis supervision on such a short notice while I was still back home in Nigeria. You have indeed being a mentor! I am grateful for your empathy, inspiration, guidance and encouragement throughout the thesis, most especially keeping me on my toes! I will also like to acknowledge Dr. Hany Ferdinando, I can't thank you enough for your accessibility and availability at the critical challenging moments in the thesis. Your impactful insight paved way for the actualization of this thesis. I learnt so much from you in the short period of discussion. I am indebtedly thankful to Associate Professor Teemu Myllylä for accepting to be the second examiner of my thesis and providing the platform to further my thesis in this project. I am indeed honored to have the opportunity and rare privilege to work with great minds in your research unit, the memories will last for a life time. I look forward to leveraging on the information gathered for the benefit of mankind and to the glory of God.

Finally, I am eternally grateful to my parents and siblings for their vigilant prayers, encouragement and moral support in my life's journey. And I will like to say to my late Father who always supported my acquiring a master's degree, "I finally did, Dad!", also to my mother "you are the best Mom!". To all the wonderful people I met in Oulu who helped me through my challenging moments, I say God bless you immensely! I wouldn't have achieved this feat without your support and cooperation both financially and morally. Thanks goes to Frau Judith Lang (elder sister), Nina Onguti, Rashida Abioye, Vijaya, Triana, Iwan, Deepak, Lassi, Martti and Dr. Haque.

Oulu, June.10.2024

Eleonye Theresa Chinyere

LIST OF ABBREVIATIONS AND SYMBOLS

ADAS	Advanced Driver Assistance System
ADC	Analog to Digital Converter
AD	Arctangent Demodulation
BCG	Ballistocardiography
bpm	Beat per minute/Breaths per minute
BR	Breathing rate
BTLE	Bluetooth Low Energy
cECG	Capacitive-coupled Electrocardiogram
CI	Confidence Interval
CSD	Complex Signal Demodulation
CW	Continuous Wave
ECG	Electrocardiogram
EEMD	Ensemble Empirical Mode Decomposition
FCC	Federal Communication Commission
FFT	Fast Fourier Transform
FMCW	Frequency Modulated Continuous Wave
FPGA	Field Programmable Gate Arrays
FSK	Frequency Shift Keying
GHz	Gigahertz
HR	Heart rate
Hz	Hertz
IEEE	Institute of Electrical and Electronics Engineers
IF	Intermediate Frequency
IMF	Intrinsic Mode Function
IR-UWB	Impulse Radio UltraWide Band
ITU	International Telecommunication Union
LLOA	Lower Limit of Agreement
LNA	Low Noise Amplifier
LTE	Long term evolution
MAE/MAD	Mean Absolute Error/Mean Absolute Deviation
MAPE	Mean Absolute Percentage Error
MIMO	Multiple Input Multiple Output
MTI	Moving Target Indicator
MUSIC	Multiple Signal Classification
PA	Power Amplifier
PPG	Photoplethsmography
PPGi	Photoplethsmography Imaging
PRF	Pulse Repetitive Frequency
RADAR	Radio Detection and Ranging
RCS	Radar cross section
RMSE	Root Mean Square Error
R_x	Receiver Antenna
SCG	Seismocardiography
SD	Standard Deviation
S.E	Standard Error
SFCW	Step Frequency Continuous Wave
SNR	Signal to Noise Ratio

STFT	Short Time Fourier Transform
THz	Terahertz
$\mathbf{T_x}$	Transmitter Antenna
ULOA	Upper Limit of Agreement
VCO	Voltage Controlled Oscillator
WHO	World Health Organization

A	Amplitude
B	Bandwidth
c	Speed of light
f_c	Starting frequency
$r(t)$	Receiver chirp signal
$s(t)$	Transmitter chirp signal
t_d	Time delay
T_f	Fast time axis
T_s	Slow time axis

1. INTRODUCTION

In many countries of the world, majority of the population on daily basis spend approximately more than one hour commuting or driving a vehicle on the road [1, 2]. Hence, in recent times it has become imperative to monitor the physiological parameters of the driver to ascertain the health status or well-being in order to reduce injuries or deaths due to the prevalence of road accidents caused by stress, fatigue and drowsiness [3]. The World Health Organization (WHO) in 2020 ranked Finland at number 168 with 215 or 0.44% total deaths recorded from road accidents [4]. Physiological parameters are biosignals produced as a result of bioelectricity, mechanical and heat effects during respiration [5]. These different effects underline the principles of measurement of the different technique approaches. Bioelectricity is observed as surface potentials on the body when the cardiac muscles are excited electrically and this is measured through electrocardiogram (ECG) electrodes or the non-invasive capacitive-coupled ECG (cECG) electrodes. The mechanical effects are observed as the displacement or deformation of body structures or fluids within the thoracic cavity which are measured as surface displacement via radar, ballistocardiography (BCG), seismocardiography (SCG) and camera or video motion, and also as fluid impedance in the thoracic cavity measured as perfusion via photoplethsmography (PPG), photoplethsmography imaging (PPGi), or thoracic impedance through magnetic induction [1, 5]. The heat transfer of conduction or convection between organs and fluids can be measured through thermography [6, 7].

The physiological parameters of a human being provide first-hand information about the health status of an individual and it can be monitored through the breathing rate, heart rate or pulse, blood pressure, temperature of the body and oxygen saturation. The health monitoring is mostly done under controlled environment of clinical setting or home care through contact based methods such as ECG, PPG, BCG, magnetic induction and thermography. These contact based or on-body wearable sensors are not ideal for long term monitoring due to discomfort, as such many research studies have embarked on non-contact or contact-less based monitoring [2, 5]. Non-contact based sensors are apt for long term health monitoring as well as beneficial for patients with sensitive skin (premature babies or burn victims), elderly patients and critically sick ICU patients or COVID patients [8]. The commonly used measurement technique approaches for remote health monitoring of a driver in simulated/controlled laboratory or real vehicular environments are radar, BCG, ECG electrodes, cECG electrodes and thermography via camera or video motion [1]. These contact-less sensors used for driver health monitoring in vehicular environments are either integrated/embedded, attached to car upholstery (seat, steering wheel, seat belt, chassis) or mounted on rear view mirror/side mirrors [1, 2, 5]. However, Leem et al. [9] opined that given the comparative advantage, radar sensors are ideal for non-invasive or contact-less monitoring in vehicular environments since privacy infringements and discomfort of the driver are ameliorated. Furthermore, radar sensors are not susceptible to varying levels of illumination, they can penetrate through non-metal objects (walls or clothing) and they overcome the challenges of dead spots in camera-thermal sensors [2].

Radio waves are electromagnetic waves with very high frequencies which are used for remote radar sensing. The radar was invented by the German inventor named Christian Hülsmeyer in 1904 for collision avoidance between sailing ships detected during a foggy weather [10]. Radar is acronym for Radio Detection and Ranging

made popular by the military in detecting enemy aircraft, ship or armory and used during the second World War (1939 to 1945) [11]. Radar-based sensors used for non-invasive or non-contact vital signs monitoring rely on the radar principles where electromagnetic waves in the microwave or millimeter wave band are emitted from a transmitting antenna directed towards the thoracic cavity of the individual person and the reflected wave from the chest is captured as echo signals at the receiving antenna. The echoes or reflected waves are shifted in phase or frequency from the transmitted frequency due to the periodic mechanical displacement of the organs inside the thoracic cavity such that the extrapolation of the heart rate and breathing rate can be estimated [5].

1.1. Motivation

The earliest applications of radar-based sensors for vital signs monitoring emerged in the 1970s for detection of apnoea on a premature baby with a 10 GHz radar sensor mounted on an infant incubator [12]. Vinci et al. [13] in 2015 used two 24 GHz radar sensors separately for two measurement scenarios in a vehicular environment: the first scenario had the radar sensor positioned on the dashboard at 0.5 m distance in front of the driver and the second radar sensor was embedded or attached to the back of the driver's seat. Over the years to present the applications of radar-based sensor deployed in automotive industry have been geared towards the health monitoring of the driver, driver's safety and comfort which comprises of occupant presence detection, advanced driver assistance system (ADAS), in-cabin child detection, smart vehicle monitoring and recognition of gestures [1, 2].

  In literature, several studies on driver vital signs monitoring either in laboratory setting or real life driving scenarios have focused more on the accuracy of the measured physiological parameters rather than other applications specific to safety or comfort of the driver [2]. The accurate estimation of vital signs parameters potentially can be used for early detection of cardio-pulmonary diseases, cardio-vascular diseases, neurological disorders and their clinical management [1]. The high frequency millimeter wave radars are miniaturized, easily integrated inside the vehicular environment due to small-sized antennas [14] and can reliably to some extent estimate the physiological parameters of a driver [8]. However, the millimeter wave radars also suffer from the challenges of light of sight or other propagation drawbacks [14, 15], artifacts due to body movement [5], signal attenuation and multiple path interference which degrades the measurement accuracy especially the weak heart rate signals [16]. The improvement in vital signs estimation accuracy can be achieved by ameliorating the artifacts from body movements either by hardware or sophisticated signal processing algorithms [5, 16]. The multiple input and multiple output (MIMO) configuration of millimeter wave radar (used in this thesis) with many receiver channels offers high angular resolution that mitigates the multiple path interference [16] and makes possible the simultaneous monitoring of several persons [8]. The line of sight challenge as per placement of the radar-based sensor inside the vehicle for good signal quality (minimal interruption in signal path between radar sensor and human target) was investigated by Yang et al. [17]. Out of the 16 different positions/locations, the rear view mirror was found to have optimal signal quality. The main aim of this thesis which is one of the following research questions asked (second question) is to investigate the impact or effect of angular placement or

positioning of the radar-based sensor on the breathing rate and heart rate accuracy as it is yet to be determined in literature. The research questions are as follows:

1. Are the results from the reference and radar devices comparable?

2. What are the impact or effects of the radar's location and angular orientation with respect to the measured physiological parameters?

3. Are the measured physiological parameters comparable amongst all subjects?

The experiment was conducted in the laboratory with the dimensions and geometry of the vehicular environment factored in the experimental setup. The 77 GHz radar-based sensor AWR1642Boost (Texas Instruments) positioned or mounted on a tripod was placed from the human target at different locations, distances (vertical/horizontal) and corner or angular measurements for optimal performance assessment.

The thesis structure is organised in the following order. Chapter 1 gives an introductory overview of the various measurement techniques used for vital signs monitoring with highlights on the radar sensor and the motivation for the study. Chapter 2 focuses on the literature review in relation to viz-a-viz general theory of radar, fundamental block diagram, types of radar, electromagnetic spectrum with respect to the different frequency bands of radar, commercialized vital signs monitoring using radar sensor, basic principles of high frequency modulated radars, the derivation of the physiological parameters from radar sensing systems, related previous research studies with emphasis on the signal processing algorithms and ground truth or reference devices used in the experiments as well as the challenges of radar sensing systems in driver-centered health monitoring. Chapter 3 discusses the materials and methods in terms of the devices(system model of devices), software and data processing used in this study. Chapter 4 gives the presentation of results obtained from the experimental procedure. Chapter 5 discusses the results with focus on the practical applications, limitations of the results and study. Chapter 6 discusses the conclusion and future directions. Chapter 7 and Chapter 8 contain the references and appendices respectively.

2. LITERATURE REVIEW

Unobtrusive, non-invasive and wireless monitoring of the heart rate and breathing rate of an individual has continued to be a keenly researched topic area because of the huge potential benefits of enhancing healthcare and quality of life. The health monitoring of breathing rate and heart rate can provide early detection or diagnosis of cardio-vascular or cardio-pulmonary disorders, sleep apnoea, stress, fatigue or depression. Recent WHO statistics estimated 1.19 million persons die from road accident injuries [18]. Hence, it is imperative to ascertain the health status of motorists in order to reduce the rates of road accidents, injuries and deaths [2]. The literature review examines the earlier related studies on the vital signs monitoring of a driver using radar-based sensors with broad frequency range of microwave or millimeter wave conducted either in experimental setups (approximated vehicular environments) or in real-life driving scenarios. The review is sectioned into three parts namely: Section 2.1, 2.2 discusses the overview of general theory of radar, radar sensor block diagram, frequency bands of radar in the electromagnetic spectrum and its applications, Section 2.3, 2.4 highlights the different types of radar and their advantages, basic principles of millimeter wave frequency radar and the derivation of vital signs parameters are discussed, Section 2.5, 2.6 focuses on the related works and the challenges of radar sensing systems in vehicular vital signs monitoring.

2.1. General Theory of Radar

The German inventor Christian Hülsmeyer in 1904 received a patent for his sensing device which was based on the principles of radar. The generated radio waves transmitted through one antenna was reflected from ships in close proximity and detected at the receiver antenna. His sensing device called telemobiloscope was mainly used to prevent the collision of ships in foggy weather [10]. The radio waves used for detecting or sensing an object's location was first named "Radar" by the US military (US Navy) in 1940 and used during the second World war to target enemy aircraft or ship [19]. The foremost radar sensor produced through research for the automotive industry dates back to more than four decades ago [20]. In 1998, for the first time the radar was deployed in a commercial vehicle for adaptive cruise control functionality which was later expanded to avoiding collisions on the road [20]. However, for vital signs monitoring, the authors in [12] mounted a radar sensor on an infant incubator for monitoring the physiological parameters of a pre-term baby in 1971.

Radar-based sensors make use of wireless sensing technologies which are largely used to detect the motion and velocity of object(s). Thus, the radar-based sensors can determine the object's position, shape, motion characteristics and trajectory [20]. The general theory of radar is based on the radio detection and ranging principles of which antennas (trans-receiver) emit waves in the microwave or millimeter wave range directed towards the target and receives back echo signals reflected from the target. These echo signals contain information from the target that is being processed to obtain the target's speed, distance, angle and movement directions. This is possible because of the changes in the signal that is reflected from the target as an

echo signal to the sensor, the difference in the signal changes between the transmitted and received is used to identify the target and its position [20, 21, 22].

2.1.1. Radar Sensor Block Diagram

The typical block diagram of an automotive radar sensor in Figure 1 has been extended to medical applications. Some of the research work or related studies have the typical configuration. However, others have integrated different active circuits with the trans-receiver sensor for the purpose of optimization and achieving high signal to noise ratio (SNR) of the output measured signal.
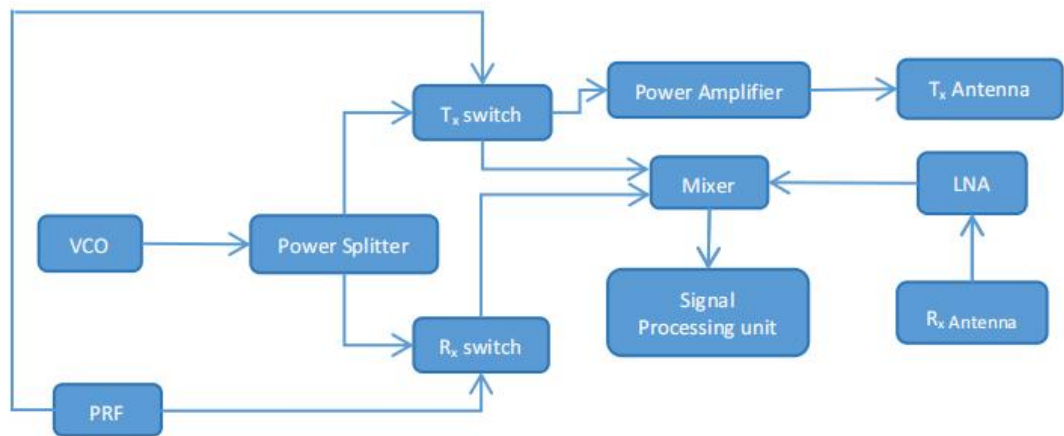

Figure 1. Automotive radar block diagram [21].

The typical automotive radar sensor architecture consists of the following components:

- **Voltage-controlled oscillator (VCO):** The voltage-controlled oscillator is mainly used to generate the output signal whose frequency changes with the amplitude of voltage for an input signal with reasonable frequency range [21].

- **Power Splitter:** The power splitter also known as the power divider is responsible for dividing a single radio frequency (RF) line and splitting the power [21].

- **Power Amplifier (PA):** The power amplifier changes signals from low power to higher power signals [21].

- **Signal Processing:** The signal processing circuit modifies, synthesizes and analyzes signals [21].

- **Mixer:** The mixer converts the feeble RF signals from the low noise amplifier into intermediate frequency (IF). It is used for the generation of frequency's sum and differences which are applied to it [21].

- **Low Noise Amplifier (LNA):** It is an amplifier that amplifies the feeble RF signal received from the antenna. The output from the LNA is fed into the mixer [21].

- **Pulse Repetitive Frequency (PRF):** The pulse repetition frequency is the number of pulses of a repeating signal within a specified time usually measured in seconds [21].

- **Antenna:** The antenna system comprises of the transmit and receive channels. The transmit channels drive and provide beam steering capabilities to different antennas. The multiple receive channels provide angular information about the target which is possible due to the phase difference between signals received by different receive antennas [21].

2.2. Electromagnetic Spectrum

2.2.1. Frequency Bands of Radar

The electromagnetic spectrum consists of electromagnetic waves or radiation in the broad range from two extremes of long radio waves to the short gamma rays which are categorized into different bands either by frequency or wavelength in increasing or decreasing order of magnitude [23, 24]. The electromagnetic radiation contained in the different bands of the electromagnetic spectrum differs from one band to another by virtue of their interaction with matter and their applications [23]. The broad range of electromagnetic spectrum consists of the following:

- Radio waves
- Microwaves
- Infrared light
- Visible light
- Ultraviolet light
- X-rays
- Gamma rays

The millimeter wave electromagnetic radiation falls between the electromagnetic spectrum band of microwaves and infrared having the frequency range of 30 GHz to 300 GHz. It further extends to the lower portion of the frequency range of 0.1 THz to 30 THz in the terahertz domain [27], occupying the extremely high frequency band according to International Telecommunication Union (ITU) [23, 25, 26]. The ITU is an organization that oversees both generation and transmission of different frequency bands in the electromagnetic spectrum in compliance with local regulatory laws of respective countries [30]. Figure 2 shows the frequency bands of radar with emphasis on the portion of millimeter wave band in the electromagnetic spectrum. The frequency bands of the radar especially the millimeter wave differs in penetration capabilities with respect to their frequency range and applications [26, 28, 29]. According to the Institute of Electrical and Electronics Engineers (IEEE), the classified frequency bands of millimeter waves are inclusive of some portions of the

microwaves frequency bands. The IEEE classified frequency bands are important for radar remote sensing, terrestrial mapping and satellite surveillance applications [30]. These frequency bands are highlighted as follows:

(a) Microwaves frequency bands

- L -Band (1 to 2 GHz)
- S -Band (2 to 4 GHz)
- C -Band (4 to 8 GHz)
- X -Band (8 to 12 GHz)
- Ku -Band (12 to 18 GHz)
- K -Band (18 to 27 GHz)
- Ka -Band (27 to 40 GHz)

(b) Millimeter waves frequency bands

- Ka -Band (27 to 40 GHz)
- V -Band (40 to 75 GHz)
- W -Band (75 to 110 GHz)
- Mm or G -Band (110 to 300 GHz)
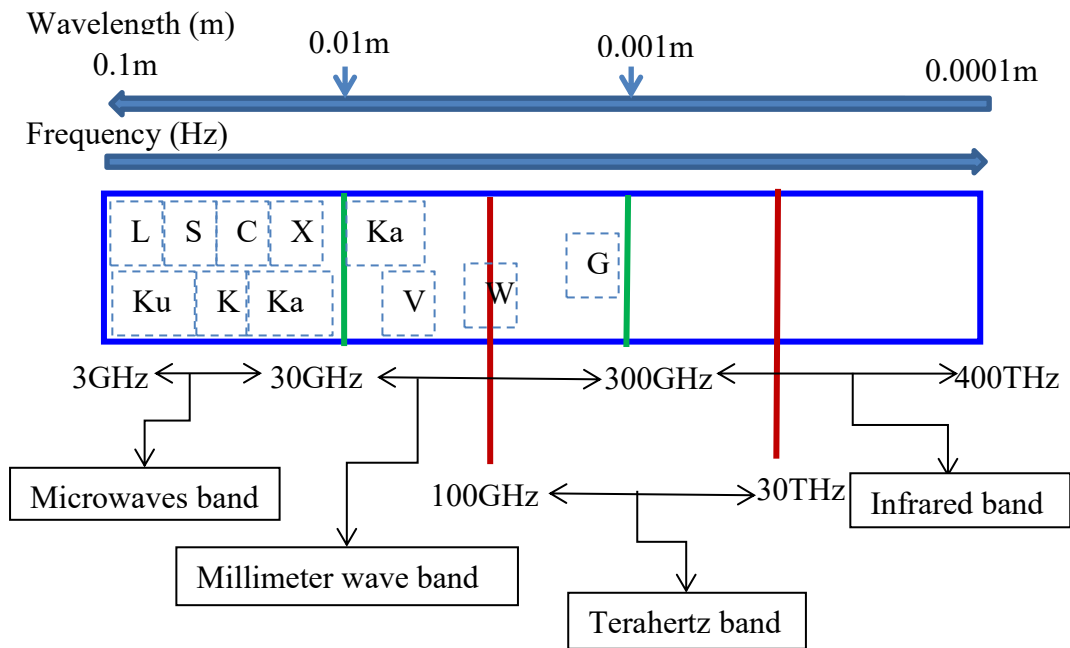
Figure 2. Millimeter wave band portion in electromagnetic spectrum [26].

2.2.2. Applications of Frequency Bands of Radar

The frequency bands of radar differ in frequency range and its applications [14]. However, in the millimeter wave band, the bands dominantly used in the field are the V- band, E - band and W- band which are application specific due to their frequency range [14] and to overcome any interference [2]. In the automotive industry the

microwave band (24 GHz) and millimeter wave band (60 GHz, 77 GHz) categorized in the short-range, mid-range and long-range sensing capabilities are commonly used for (inside and outside) in-cabin monitoring [2]. Currently, there is a growing trend towards the production of portable, miniaturized radar-based sensors (for easy integration) with high sensitivity or detection accuracy of object's location which favours the use of 77 GHz millimeter wave radars in vehicles for applications of vital signs monitoring, ADAS for safety and comfortability of the driver [2, 14]. Although the 24 GHz and 77 GHz radar sensors are used externally for out-cabin monitoring, due to the bulky arrays of the antenna (affected by size of aperture), poor spatial resolution limited by low bandwidth, high consumption of power and noise on microwave 24 GHz radars [14], as earlier mentioned, there is a switch to the 77 GHz millimeter wave radars which is predominantly in use in most vehicles. The V-band frequency range of 60 GHz radars are non-licensed by Federal Communication Commission (FCC) [14]. These radars are used internally for in-cabin monitoring [2], an example is the Infineon Xensiv^{TM} 60 GHz used for in-cabin child detection [40]. The short range of the V-band find application in fast data transfer, high definition (HD) multimedia streaming, wireless communication, object presence detection and vital signs monitoring [14]. The E-band range is used in traffic control around vehicles, ADAS for comfort and safety of drivers. The W-band are used for active imaging in robotic controls, land mapping or surveillance, security scanning and monitoring devices, detecting cancers or malignant cells and physiological parameters monitoring [14]. In general, the frequency bands of radar find application in many fields such as long range tracking or surveillance, terrestrial mapping, satellite surveillance, mining, weather observations, traffic control, quality assurance detectors in manufacturing industries, gesture recognition, ADAS in automobile industry, health monitoring, cancer and tumour detection in healthcare industry, airborne traffic control, security and surveillance at the airports and many more [14, 19, 20, 21, 31]. Table 1 highlights some Texas Instruments radars with their frequency bands and ranges.

Table 1. Frequency bands and ranges of Texas Instruments Radars [31]

Texas Instrument Radar	Frequency Band	Frequency Range
IWR6843AOPEVM	V	60 to 64 GHz
IWR1843	E	76 to 81 GHz
AWRL6432	V	57 to 64 GHz
AWR1843AOPEVM	E	76 to 81 GHz
AWR1642BOOST	E	76 to 81 GHz
IWR1642	E	76 to 77 GHz
IWR1443	E	77 to 79 GHz
AWR1443	E	76 to 81 GHz
IWRL6432	V	57 to 64 GHz
AWR2243BOOST	E	76 to 81 GHz
AWR1243	E	76 to 81 GHz

2.3. Types of Radar

There are different types of radar-based sensors depending on their function, properties, and application [32, 33]. Most health monitoring of driver(s) found in literature depend on the different radar types which is a function of the mode of wave propagation or transmission of the wave to the human target and purpose of investigation [32, 33]. The major radar sensing types shown in Figure 3 used in vital signs monitoring are Impulse radio ultrawide band (IR-UWB) radar, Continuous wave (CW) radar and Frequency Modulated Continuous wave (FMCW) radar. Although, not so popular is the variant of the FMCW radar known as Step Frequency Continuous wave (SFCW) radar [22, 32, 33]. The SFCW radars transmit incremental multiple discrete frequencies in a continuous wave [22, 32]. High frequency range in the microwave (6 to 24 GHz) and millimeter wave (30 to 300 GHz) are preferably used because of their benefits of miniaturization of components and easy integration, high resolution of target detection (at short source-target distance) as the phase modulated echo signals at the receiver antenna are proportional to the micro-motions of the organs in the thoracic cavity [5, 32, 33].

There is a trade-off between lower frequency bands and high frequency bands. Extremely high frequency millimeter waves are susceptible to signal loss or attenuation at long-distances such that the SNR is degraded, range of detection is reduced, and detection accuracy is greatly affected. However, lower frequency has high penetration capabilities for long-distance applications but low resolution with poor detection accuracy due to low bandwidth and spatial resolution [5, 20, 33].
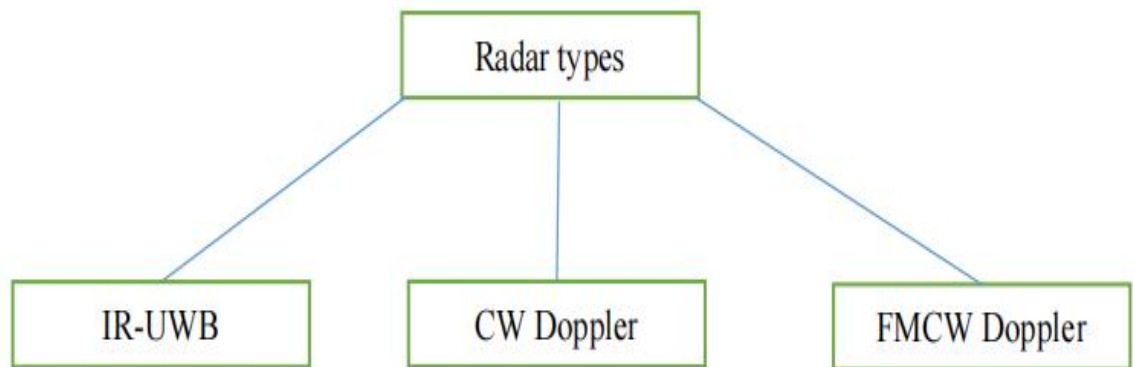

Figure 3. Types of Radar sensor.

IR-UWB radars transmit repeating short radio pulses with wide bandwidth which provides good spatial resolution of objects, high speed and data rates in communication devices. The pulses are transmitted at PRF such that the echo signals reflected from the object are detected between the intervals of transmitted pulses. The ultrawide band operates in the 3.1 to 10.6 GHz range in compliance with the FCC regulations [5, 33, 34].

CW radar-based sensor has the frequency unmodulated but transmit and receive waves simultaneously and continuously such that the shift in frequency is used to compute the speed or distance of the object [20, 33]. However, the FMCW radar-based sensor unlike the CW radar-based sensor has frequency modulation of waves which is time dependent known as chirp. It is based on triangle wave's law where

both the transmit and receive signal have the same triangle wave and same matching frequency but there is time difference between them. The time difference enables the distance calculation of the object [20, 21].

The FMCW radars also use frequency shift keying (FSK) which transmits and receives signals alternately between two frequencies to detect objects [20, 21, 22]. However, there are so many modified/enhanced versions of the sensors that have birthed a lot of variants from the FMCW radars. This modification is possible because they transmit and receive waves based on Doppler effect such that the carrier frequency is selectively modulated for specific applications [5, 21, 22, 32]. For the 1D-CW radar, objects can be detected through their speed. There are different configurations of FMCW radars such as 2D FMCW (FSK) radar which makes use of a transmitter antenna and receiver antenna to detect objects through their speed and distance without the angle or azimuth information [22]. However, the 3D and 4D MIMO FMCW radars have special multiple arrays of transmitters and receivers such that multiple objects with the same speed, distance and angle can be tracked and localized in 2D or 3D space respectively due to enhanced spatial resolution and reduction of interference [22].

2.3.1. Advantages of Radar Sensing Systems

CW radars have simple hardware designs and are cost effective but because of the low detection range, they are mostly used in short distance applications. Unfortunately, they are unable to detect multiple objects and object localization due to their poor range and spatial resolution. CW radars are affected by interference which reduces the SNR of the measured vital signs parameters [32, 33]. Although the IR-UWB radars are excellent for long distance and through the wall applications because of their high penetration capabilities, they are also less prone to interference of which the human target can be located in a buried structure or collapsed building but have limited low frequency range that requires bulky antennas or more complex hardware [5, 32, 33]. However, the FMCW and SFCW radars are widely used as they can track multiple objects and localize objects due to their high velocity and range resolutions [33]. In this thesis, the FMCW radar is used in the experimental procedure.

2.4. Basic Principles of FMCW Radar

In the working principle of the 77 GHz AWR1642Boost shown in Figure 4, the chirp generated is transmitted by the T_x antenna which is reflected from the thoracic cavity of the human target and captured as frequency modulated chirp at the receiver antenna that is a replica of the transmitted chirp but with a delay time t_d. The transmitted T_x chirp and received R_x chirp are both mixed in the mixer to produce a baseband or IF also called the beat frequency. The IF undergoes further signal processing for the vital signs estimation [35].
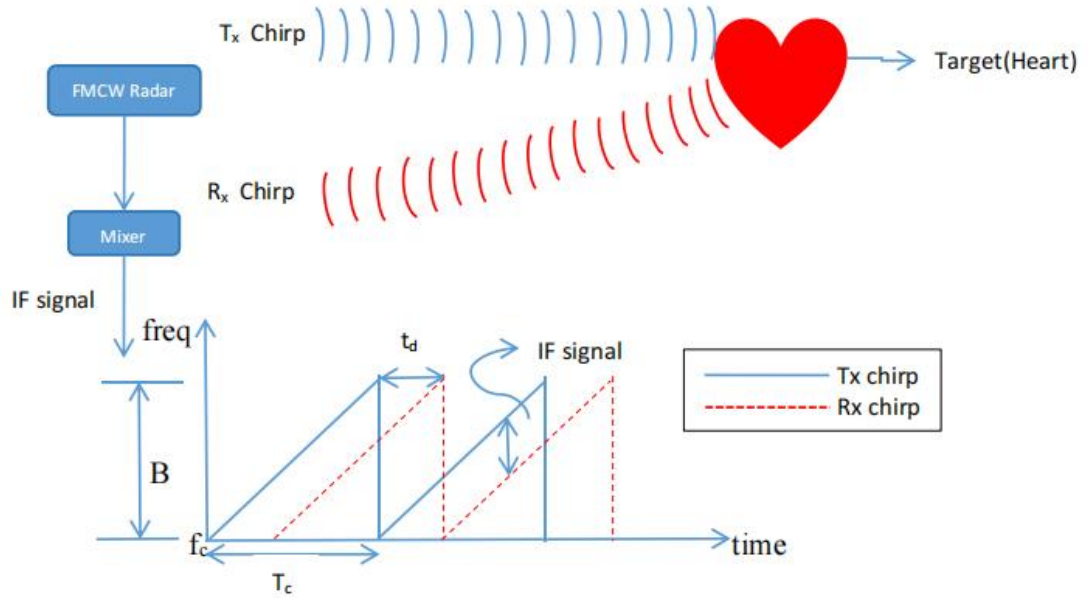
Figure 4. Basic principle of FMCW radar [35].

2.4.1. Derivation of Vital Signs from Radar Sensing System

The time of travel of the transmitted chirp from the T_x antenna to the human target and received at the R_x antenna which is similar to the echo signals can be used to determine the distance or range (R) of the human target from the radar is given by the equation:

$$t_d = 2R/c \tag{1}$$

where R is the distance of the human target to the radar, c is the speed of light and t_d is the time delay.

The time delay is significant in observing the phase shift of the frequency received at the R_x antenna. Because the frequency modulated sinusoid of the T_x chirp given by the expression

$$s(t) = A \cos (2\pi f_c t + (\pi B/T_c) t^2 + \varnothing(t)) \tag{2}$$

where A is the amplitude, f_c is the starting frequency, T_c is the duration and $\varnothing(t)$ is the phase of signal.

On reaching the thoracic cavity of the human target is reflected and the received signal is shifted in phase with a time delay such that the R_x chirp has the form :

$$r(t) = \alpha A\{\cos(2\pi f_c (t-t_d) + (\pi B/T_c) (t-t_d)^2 + \varnothing(t-t_d))\} \tag{3}$$

Both the transmitted T_x chirp and received R_x chirp are mixed and filtered in the mixer component to produce a single IF or baseband or beat signal which is a function of time having the frequency and phase portions given by the expression

$$s(t) * r(t) = A \cos(2\pi f_b t + \varnothing_b(t) + \delta\varnothing(t)) \qquad (4)$$

$$f_b = 2BR/cT_c, \text{ and } \varnothing_b(t) = 2\pi f_c t_d + (\pi B/T_c) t_d^2 \qquad (5)$$

where A is the amplitude of signal received at R_x antenna, f_b is the frequency, and $\varnothing_b(t)$ is the phase.

However, the $\delta\varnothing(t)$ phase component is the residual noise that is negligible for short distance applications. Thus, the periodic micro-motions of the chest or displacement of the thoracic cavity can be estimated from the phase variations of the detected human target range to the radar where the Fast Fourier Transform (FFT) algorithm is applied on the IF to extract the phase measurements for vital signs estimation. The IF sampling rate is obtained from the number of analog-to-digital converter(ADC) samples per chirp such that the ith ADC sample per j^{th} chirp is expressed in the form:

$$s(t) * r(t)[i,j] = A \cos(2\pi f_b i\, T_f + (4\pi/\lambda)R\,(i\,T_f + j\,T_s)) \qquad (6)$$

where T_f is the fast time axis taken after the periodic intervals of ADC samples, T_s is the slow time axis which is used for the estimation of vital signs because the small displacements of the chest which modulates the breathing rate is less than 4 Hz.

Therefore, the breathing rate and heart rate are extrapolated from the slow time axis of the FFT of which the frame consists of two chirps and the first chirp is used for processing of physiological parameters with the sampling frequency related to the repetitive periodic intervals of the frames in FMCW radar systems.

2.4.2. Commercial Vital Signs Monitoring Systems

Contact-less methods of health monitoring of driver's vital signs are still attracting an ongoing surge of high interest. However, some levels of success have been recorded in its application in the automobile industry as some leading brands have proprietary licence of these approaches which comes as ADAS with different brand names such as Driver alert control in Volvo, SmartSenior in BMW and Attention Assist in Mercedes-Benz [5]. Most of the ADAS are mainly integrated into the upholstery of the vehicle and not as stand-alone units [36]. The review work in [1] highlighted that the embedded sensors in current automobiles, apart from the beneficial safety features and comfort they offer, the physiological data acquired can be used for behavioural assessment of the driver which might have some health implications. The commercialized stand-alone vital signs monitoring systems are largely contact based with cables, electrodes, and consumables (gel) used in clinically controlled environments which are of impractical use in vehicular environments. The notable brands of contact based vital signs monitoring systems are General Electric (GE), Philips, Mindray, Schiller, Welch Allyn and many more are used in hospitals [37].

Conversely, the non-invasive or non-contact stand-alone unit built for commercial vital signs monitoring are namely:

> **(i) Vital Signs Radar Aerosense Wavve:** It is a light weight, smart radar sensing device which can detect heart rate, breathing rate, stress levels and sleep disorders operating at 24 GHz FMCW range with the bandwidth of 3 GHz

detection range of 0.3 to 2.5 m, power consumption 5 volts/1 ampere or 110 volts (can use both battery and AC power supply) [38].

(ii) GF Technovation non-invasive vital sensor: The patented technology uses the IR-UWB radar emitting ten million pulses per second within 10 m^2 area. It monitors the heart rate, breathing rate and movement by continuous scanning of the time-of-flight of the signal. It is portable and needs AC power supply, product specifications are available upon request from their website [39].

(iii) Infineon XENSIV^{TM} Radar sensors: The Infineon's XENSIV^{TM} radar sensors range from 24 GHz, 60 GHz and 77/79 GHz millimeter wave, meeting the demand for short, mid and long-range radar sensing capabilities. Infineon XENSIV^{TM} radar sensors are used in the automotive industry for ADAS, autonomous driving functionalities and sensing. However, XENSIV^{TM} 60 GHz radar sensor additionally offers multi-functional novel in-cabin monitoring of child detection, multiple target detection and localization, vital signs monitoring of breathing rate and heart rate which are configurable with excellent security features. XENSIV^{TM} 60 GHz radar sensor operates on 4 GHz bandwidth of FMCW radar with a MIMO array of transceivers. It has low consumption of power, compact design, good thermal stability, free of maintenance, highly accurate measurement and robust to exogenous vehicular factors such as engine vibration or body movement. The long-range XENSIV^{TM} 77/79 GHz radar sensor is located on the front chassis of the vehicle for detecting far distant objects [40].

(iv) Xander Kardian: The Xander Kardian XK300 radar sensor comes in different varieties with different field of view depending on the site location such as beneath the desk or ceiling mounts. The UWB radar sensing system with proprietary signal processing algorithm is commercially available for the vital signs monitoring, presence and motion detection in residential and clinical environments. It can be used with battery, plug in power module or communication module supporting wireless and Long term evolution (LTE) communication platforms [41].

2.5. Related Work

In literature, the CW radar sensor in the microwave frequency range is dominant owing to their low cost and simple hardware design. However, the other radar types like IR-UWB, FMCW and SFCW were also used to ascertain for vital signs estimation in vehicular scenarios [33]. We will discuss the related works in the aspects of the different technologies used with regards to the signal processing methods for vital signs estimation and placement of the radar-based sensor in the vehicle to improve accuracy as well as the verification of results with ground truth or reference devices. The challenges or limitations of radar-based sensors in vital signs monitoring will also be examined.

2.5.1. Signal Processing Methods

In most literature, the research interest of vital signs monitoring in vehicular environments have largely revolved around detection accuracy or the accurate estimation of the breathing and heart rates of the driver which has the potential for clinical applications in terms of early prediction of underlying health disorders/diseases, accurate diagnosis, treatment and management. Hence, researchers have concentrated on solutions geared towards the reduction or possible elimination of noise, interference or signal attenuation which invariably affects the signal quality or accuracy of the measured physiological parameters. Gharamohammadi et al. [2] in their review work recommended for future directions the use of advanced signal processing algorithms that can resolve the phase unwrapping and harmonic non-linearity or discontinuities inherent in radars, placement of the sensor and choice of frequency range can effectively improve the accuracy of the vital signs estimation. The authors in [42] re-echoed the idea of using MIMO millimeter wave radars and machine learning algorithms to ameliorate issues of interference or harmonics which impacts negatively on detection accuracy and accurate estimation of vital signs.

Dai et al. [16] mentioned in their study, that improvement in accuracy of the breathing and heart rates can be achieved through increase in the SNR via hardware in terms of the antenna design or sophisticated signal processing methods. Although, directional antennas such as horn improved the SNR of the vital signs parameters but the radar's field of view is decreased and makes it unsuitable for monitoring several people [16]. Additionally, two antennas on a single radar can be made to mimic the function of a repeater by re-transmitting a transmitted signal [5]. The range resolution is focal to the accurate determination of vital signs parameters which is based on sensor to object distance. Thus, in a recent study in [98], a novel algorithm targeted towards vital signs accuracy in FMCW radars was developed. The authors reiterated two areas in which the accuracy of vital signs estimations can be enhanced: precise range bin selection and advanced signal processing algorithms for eliminating noise for accurate estimation of vital signs.

The placement of radar-based sensors have also been explored in some studies to ascertain positions or locations inside the vehicle with least interference in signal path from radar sensor to human target which can result in improved signal quality devoid of loss or attenuation of signal. In the study [13], Vinci et al. used two 24 GHz CW radar sensor with a 6-port array placed in two different locations inside the vehicle for health monitoring of the driver. The first radar sensor was placed on the dashboard at a distance of 0.5 m with the antenna directed at the driver's chest. The other position has the radar sensing system integrated on the backside of the driver's seat with the antenna directed at the driver's back. Similar work was embarked upon by Lee et al. [43], where a 24 GHz CW radar sensor was integrated at the backside of the driver's seat whereas Izumi et al. [44] integrated the 24 GHz CW radar sensor on the seat belt in front of the driver's chest. Similarly, Schires et al. [45] integrated a commercially patented UWB radar sensor known as Ventricorder impulse radar with operating frequency of 3.9 GHz on the backside of the driver's seat. Different locations or positions for radar-based sensors have been suggested in literature as ideal for good signal quality which are steering wheel, dashboard or control panel or cockpit, seat belt, rear view mirror and backside of the driver's seat [1, 2, 5].

Apart from embedding a 24 GHz CW radar at the backside of the driver's seat, Lee et al. [43] in real-life driving scenario used the multiple signal classification (MUSIC) algorithm to mitigate the artifacts due to body movement and vibration from the vehicle which readily corrupts the weak heart rate signals. A high accuracy of heart rate estimation was achieved with error rate less than 3 beats per minute (bpm) compared with the ground truth devices of ECG and PPG in three different scenarios (stationary vehicle, moving vehicle at 60 km/h and 80 km/h respectively). Park et al. [46], used the Labview controlled data acquisition board DAQ for sampling both outputs of the proposed sensing system or resonators (consisting of two VCOs) and the ground truth sensors which were fed into a digital signal processing unit in the computer. In the raw data captured, the harmonics of the breathing rate interfered with the heart rate such that it was difficult to extract the data separately. Thus, the raw data was fed to a digital bandpass filter with cut-off frequency in the range 0.3 to 2 Hz and 1 to 2 Hz for the extraction of the breathing rate and heart rate respectively. The spectrograms through short-time Fourier transform (STFT) was done for real-time visualization of the results. The results from the resonators were selected after the post processing such that the resonator with expected consistent values was chosen which is dependent on the inverse proportionality of the changes in the derivatives of the reactance of the resonator with distance. The proposed sensing system in [46] was attached to the seat belt and steering wheel and evaluated alongside two reference sensors UFI- Model 1010 (piezoelectric pulse transducer) [47] and UFI- Model 1132 Pneumotrace II^{TM} (piezoelectric respiration transducer) [48] in both static and moving vehicle environment with one male and one female driver respectively. Although, the distance between the driver and the proposed sensing system on the steering wheel was 37 cm, there was similarity and strong correlation in the results of the proposed sensing system and the reference sensors irrespective of the driver's gender.

The study in [17] proposed a novel offline and online signal processing methods where 2-minutes of breathing were acquired from each participant in driver's seat with the radar in 16 different positions alongside the ground truth of a PPG sensor placed on the driver's finger. Each participant mimics the regular driver's motion during the data acquisition for 3 times for the offline signal processing. In the offline signal technique, a customized narrow bandpass filter and peak detection algorithm were used for the extraction of the breathing rate in breaths per minute (bpm). The online signal method was designed for real time vital signs monitoring. The maximum peak value in frequency domain was multiplied with a moving sliding window in 60 seconds time frame. The moving sliding window is same in functionality with the moving target indicator (MTI) for respiratory harmonic cancellation [60]. The sliding windows were constructed for the various respiration situations: stationary normal breathing, normal breathing with driving movement and combination of normal, fast and slow breathing with driving movements. The data analysis on the raw data acquired showed that the online signal processing technique gave a better performance and accuracy than the offline signal processing technique when it involved variations in the breathing rates of the participants with optimal signal performance of the radar situated at the rear view mirror and the backside of the driver's seat. However, in [49], after the linear interpolation was done to eliminate the discontinuities in the signal caused by the RF switching between the echo signals, the Ensemble Empirical Mode Decomposition (EEMD) algorithm was used for the signal processing and extraction of intrinsic mode functions (IMFs) of

the breathing rate and heart rate for multiple subjects simultaneously which improved the SNR as well as the accuracy.

There are some related works with experimental setup in controlled non-vehicular or indoor environment conducted using millimeter-wave range radar sensing system with significant insights [50, 51, 52]. Xiao et al. [50], proposed a Ka-band radar which was positioned at a constant distance of 0.5 m directly opposite the subject that performed normal breathing and reference pulse sensor placed at the index finger of the subject was used as ground truth during the measurement. The IF or baseband output signals from the mixer were filtered and signal processed with the 4th-order butterworth band filter in the 0.1 to 0.7 Hz and 0.9 to 3 Hz range for the recovery of the subject's breathing and heart signals respectively. The butterworth filter is a bandpass filter designed to have a ripple-free, maximal flat frequency response which depends on the additional number of reactive elements (such as resistors, capacitors and inductors) in the filter design circuit and then attenuates to a zero level in the bandstop frequency [53, 54]. There are n-order of butterworth filters determined by the number of reactive elements used in the circuit [54]. The 4th-order butterworth filter frequency range can be varied to detect abnormal heart rate by windowing the filtered baseband signals and autocorrelation. The autocorrelated signals are transformed in the frequency domain through FFT to generate the abnormal breathing rate and heart rate of the subject. The data analysis showed that the vital signs of the subject correlated with the results of the ground truth of which the detected heart rate was in line with the 2 % of reference range as per the heart rate accuracy calculations. However, Chuang et al. [51] had one subject positioned in four different orientations (front side, back side, left side and right side) during the measurement at a distance of 1 m recorded for every 20 seconds interval from the radar sensing system. The subject holds his breath during measurement. The breathing rate and heart rate are captured in both time and frequency domains. The IF output signals from the V-band mixer undergoes further amplification and bandpass filtering for analogue-to-digital conversion into spectral waveforms at the recorder. No specific signal processing algorithms were mentioned in [51]. However, the application of the mathematical formula for receiver sensitivity in communication was adopted for use in data analysis. The breathing rate and heart rate were detected at dominant peaks of 0.3 Hz and 1.4 Hz respectively amongst the smaller observed peaks which are harmonics of these signals. The two scenarios of normal breathing and breath holding were compared and strong breathing rate was detected in the face frontal orientation than from the lateral positions of the subject. Also the amplitude of breathing signal was higher than the heart signal in the same given scenarios. The vital signs of both the human subject and the bullfrog were monitored in [52]. In the study, the vital signs of the human subject were monitored for every 25 secs interval for first normal breathing and holding of breath for 20 secs at a distance of 2 m from the sensing radar while the bullfrog was used because of the effect of the radar cross section (RCS) of a subject which reduces the received power proportionately. The application of the signal processing algorithm, complex signal demodulation (CSD) was used to recover the target's vital signs of the human and bullfrog from the quadrature baseband signals. The results were well correlated with the results from the ground truth of pulse oximeter.

2.6. Challenges in Radar-Based Vehicular Vital Signs Monitoring

The major challenges which affect the SNR and detection accuracy posed in radar-based sensors used for vital signs monitoring of a driver during real life driving situations are as follows:

- Movement artifacts caused by the vibrations from the vehicle engine and body movements of the driver can induce a micro-motion Doppler effect on the operating frequency, which are observed as noise interference masking the physiological parameters [5].

- The extremely high frequency signals suffer significant signal attenuation at far distances as a result there will be increase cost on additional hardware for millimeter wave sensing [59]. The intrinsic null points in the sensor architecture, where signal loss is prominent due to phase cancellation or destructive interference of the transmitted operating frequency and frequency at the receiving antenna. The null points occur repeatedly at every half wavelength of the measured signal such that the signal of the heartbeat is detected at an optimum point and null point interchangeably.

- Interference from clothing material worn by the driver can reduce the SNR of the measured signal as rough surfaces scatter the signal more towards the receiver antenna than smooth reflective surfaces that reflect the signal away from the receiver [56].

- The high frequency millimeter wave radars suffer from line of sight challenges where the signal path from the radar sensor to human target is obstructed by objects which results in signal loss or attenuation which invariably reduces the SNR of the measured signal [14].

- Inability of the radar to discriminate or distinguish the vital signs signals contained in the beat signals or phase data [32] detected at the optimal point. As a result, valid measurement of the physiological parameters are missed or not captured. This issue occurs when the amplitude of movement or vibrations (which do not reflect the vital signs) are equivalent to the wavelength of the operating frequency of the radar [55]. Hence, there is need to control the amplitude or phase waveform of the radar [57] which is analogous to template matching filtering. The proposed algorithm in [55] which is a modified differentiate and cross multiply (DACM) processing algorithm uses an accumulator which replicates the function of an integrator in a digital circuit that takes the input signal and converts to a triangular wave. The triangle waves do no have harmonics except the single fundamental frequency. However, their waveforms show odd harmonics in the series of equal spaced maximum and minimum points, so they find application in control systems that require precision control [61].

- The FMCW radar systems have intrinsic challenge of phase noise generation from the output of the mixer that affects the range resolution as well as the vital signs estimation based largely on the range correlation

principle. The range correlation principle has to do with source (radar sensor) to object (human subject) distance which has direct proportional relation with the phase noise such that increase in the range, results in the increase in phase noise which affects the range resolution due to the alternate generation of null and optimum points as the distance increases [27, 56]. The effects of the intrinsic phase noise of radar sensing systems on vital signs signals are pronounced in long-distance applications [55, 58].

3. MATERIALS AND METHODS

3.1. System Model

3.1.1. Texas Instruments 77GHz AWR1642Boost

Texas Instruments (TI) radar systems for vehicular environment are miniaturized CMOS based chips consisting of small sized patch antennas (virtual arrays for transmitters and receivers), RF front end, electronics and digital control board made possible by the high frequencies in the millimeter wave band at which they operate. The 77 GHz AWR1642Boost in Figure 5 is configured as an FMCW MIMO radar which transmits electromagnetic waves continuously where frequency increases linearly with time called chirp. The chirp parameters are the start frequency f_c, bandwidth B and duration T_c where the slope gives the ramping of the frequency with time. It consists of two transmitter antennas T_x and four receiver antennas R_x thereby increasing the resolution of human target distance or range, velocity and angular measurements [62].
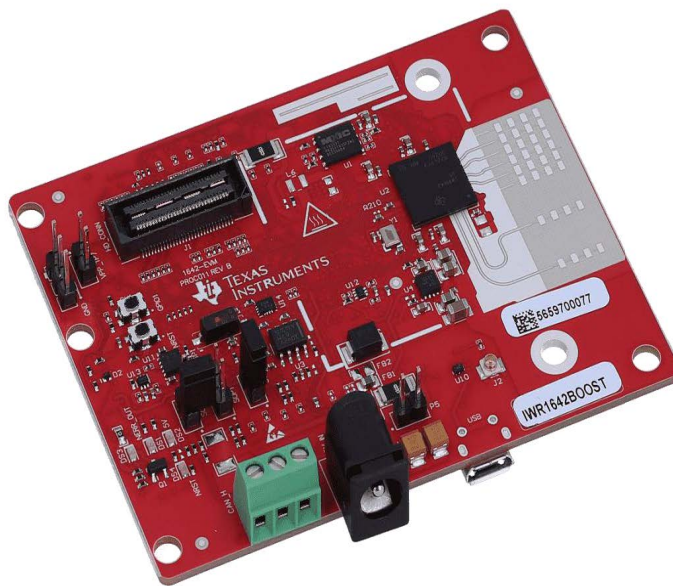

Figure 5. Texas Instruments AWR1642Boost Evaluation Module.

3.1.2. Zephyr Technologies BioHarness 3.0

The Zephyr Technologies BioHarness™ 3.0 is a device using Bluetooth low energy (BTLE) technology for telemetric monitoring of physiological parameters of ECG, heart rate, breathing rate, body postures and physical activity of an adult for purpose of wellness. The device is powered internally by a rechargeable lithium polymer battery and inserted into a receptacle on a chest strap which is worn by the human target. The physiological parameters are wirelessly captured and transmitted via Bluetooth to an external configured device with proprietary software such as a laptop.

The Zephyr technologies BioHarness[TM] 3.0 [63] in Figure 6 is used as a reference device for correlations in measurement performance in the experimental setup of the thesis.

Figure 6. Zephyr Technologies BioHarness[TM] 3.0 Device.

The TI millimeter wave 77 GHz AWR1642Boost ES 2.0 evaluation module (EVM) mounted on a tripod in the experimental setup shown in Figure 7 has two transmit antennas and four receive antennas with a digital signal processing programmable core, low power Arm® R4F controllers, and on-chip memory. The radar sensor has operating frequency of 77 GHz to 81 GHz with a starting frequency of 77 GHz, bandwidth of 4 GHz and duration of 50 μs [62]. The vital signs estimation and waveforms of the heart rate and breathing rate are displayed on the PC-GUI software platform on the configured laptop.
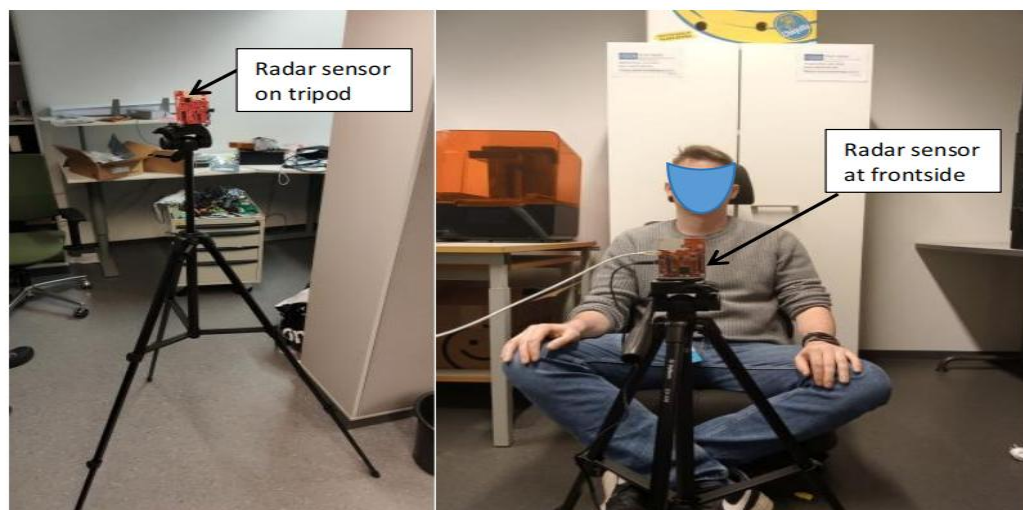

Figure 7. Experimental setup: Human target has to be still for 10 to 15 seconds and at a distance of 0.8 m from the radar at rotation (azimuthal) angle 0° and tilt angle 0° respectively.

3.2. Experimental Setup

The experiment was conducted in the laboratory with estimated dimensions of vehicular environment factored in the experimental setup shown in Figure 7. There were five healthy adult volunteers (3 males and 2 females) used for the study. Before the measurement or collection of data from the human target, the purpose of the experiment and the procedure to be followed were explained to each volunteer. The informed consent form was filled and signed by each volunteer. The height and circumferential diameter measurement of each volunteer was taken. Table 2 shows the information of the participants.

Table 2. Human Subject Information

Subject	Height (cm)	Circumferential diameter (cm)
Subject1 (Male)	173	105
Subject2 (Female)	168	71
Subject3 (Male)	172	85
Subject4 (Male)	178	95
Subject5 (Female)	173	102
Average $\pm$ SD	172 $\pm$ 3.56	91.6 $\pm$ 13.85

The instructions provided for the measurement include the following:

- All items on the clothing of the human target that can cause distraction are removed.

- The human target is trained on how to power on the Zephyr module inserted into a receptacle on the chest strap and properly strapped or fastened on the body of the human target with the correct positioning of the pressure sensor pad on the chest strap moved to the left side of the rib cage just slightly below the sternum for good contact and sensitivity to the variations of the diaphragm displacement.

- The human target with hands folded and relaxed is seated on a car seat positioned on the front side of the radar sensor with its antenna array directed toward the human target.

- For the first measurement, the human target is expected to remain still for 10 to 15 seconds to enable the application to be calibrated and for repeated measurements, the human target will be still for 5 to 10 seconds. However, the Zephyr Technologies BioHarness™ 3.0 device when powered on, starts logging data of biosignals into the internal memory. As a result in order to synchronize or threshold the two sensor signals, the human target was instructed to tap his/her chest 3 times before measurements were taken. The chest tapping was used as an event marker for synchronization.

3.2.1. Parameters of Measurement

There are important measurement parameters required to obtain the precise location of an object or human target in space with the use of the radar sensor. In addition, the transmission of series of set of chirps or frames and the signal processing algorithms applied to the captured phase variations of the transmitter and receiver antennas makes feasible the estimation of vital signs parameters. The measurement parameters used in the measurement setup attached in the appendix are:

- Range: The range is measured on the basis of time as it is the measured horizontal distance of the radar sensor from the human target.

- Elevation/Depression Angle: The upward or downward angle measured from the horizontal to the line of sight from the observer to the human target. In the case of the measurement setup, the depression angle (tilt angle of radar) is considered.

- Azimuth Angle: This is the orientation of the human target's presence in space with respect to clockwise or anticlockwise movement about a certain reference axis based on a convention that the North is taken as the reference axis with 0° and all azimuth angle measurements are done with respect to the North in a clockwise manner such that the East has 90°, South has 180°, West has 270° and back to North with 360° or 0°.

During measurement, there were 24 different measurement scenarios involving the variations of the distance (horizontal and vertical) and angular measurements of the millimeter wave radar sensor AWR1642Boost with respect to the human target. Here, it is assumed that the horizontal distance (range) approximates the front side of a vehicle with the steering wheel, dashboard, cockpit, side view mirrors, side doors, back seats and the perpendicular/vertical height approximates the rear view mirror, car ceiling, and corner points in the car. The millimeter wave radar sensor AWR1642Boost was rotated around the human target in a clockwise manner at some rotation angles of 0°, 45°, 90°, 135°, 180°, 225°, 270°, 315° approximating the perimeter dimensions of the car or vehicular environment as well as the field of view of the radar sensor. In addition, the radar sensor was aligned at different depression/tilt angles of 0°, 30° and 45°. The millimeter wave radar sensor AWR1642Boost can take measurements both at the front and backside which is selected on the PC-GUI software platform.

The unknown quantity of the tilt angles used in the measurements in Figure 8 were derived from simple triangulation [64] and trigonometric calculation such that either the distances between objects or angles between them can be computed. These were applied in the measurement setup in Figure 9. The azimuth is an angular measurement in spherical coordinate system and it is the angle between the perpendicular projection of the object of interest and the known baseline. The principle of triangulation states that if all the three angles and the length of one side of a triangle are known, then by trigonometry the lengths of the remaining sides of the triangle can be calculated [65]. Also, if the coordinates of any vertex of a triangle and azimuth of any side are known, then the coordinates of the remaining vertices can be computed [66]. Already, the horizontal distance, that is, the distance of the

millimeter wave radar sensor AWR1642Boost from the human target either on the front side or backside is predetermined and known as the baseline in the experiment. The baseline ranges from 0 cm to 80 cm. We can determine the perpendicular or vertical height of the radar sensor from the floor which varied from 85 cm to 150 cm (through the extension of the tripod stand) and the tilt angle with the formula:

$$Perpendicular\ distance(h) = base(b) * tan\theta \qquad (7)$$
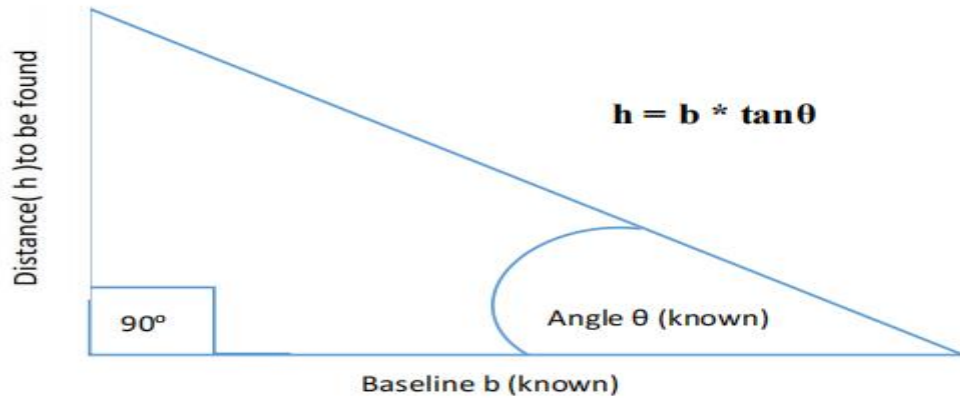
Or

$$\theta = arctan(h/b) \qquad (8)$$
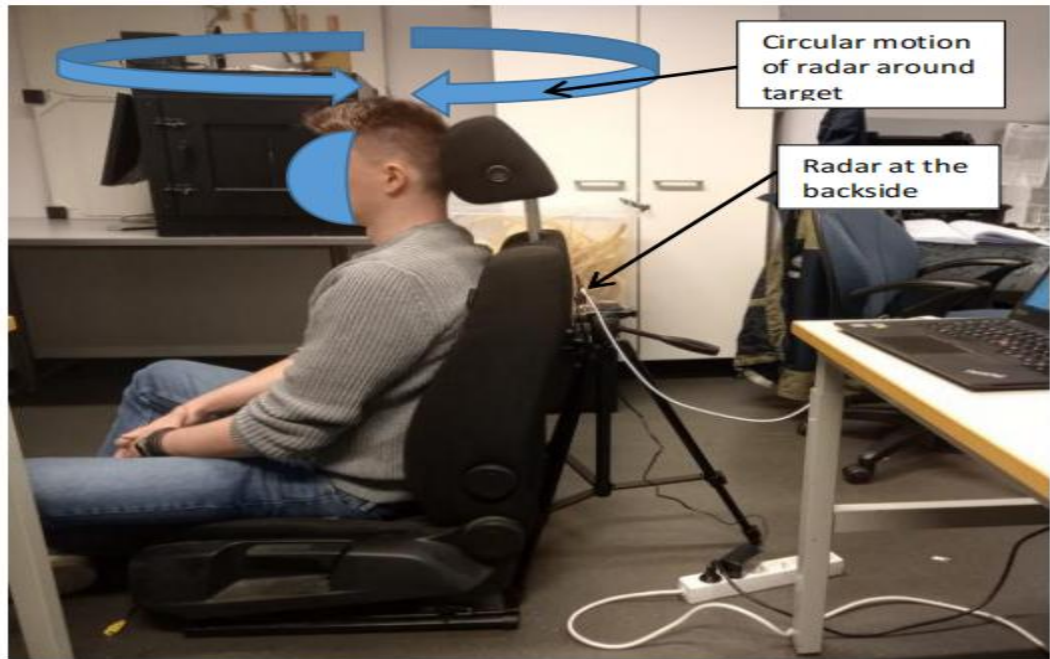

Figure 8. Triangulation Principle.

Figure 9. Experimental setup showing circular path of motion of the radar sensor around the target and at the backside.

3.3. Data Collection

The data collection on 5 volunteers consisting of 3 males and 2 females for purpose of variability in dataset already provided in Table 2 was conducted for the study. The measurement procedure lasted for approximately 2 hours for the total of 24 measurement scenarios per participant. The first 5 measurement scenarios lasted for 3 minutes each while the remaining scenarios lasted for 2 minutes each. For every specific distance, for example, horizontal distance of 80 cm and perpendicular distance of 85 cm for the millimeter wave radar sensor AWR1642Boost from human target is kept constant and the angular measurements of rotation (azimuthal) angles and tilt (depression) angles are varied as data is being captured. A protractor was used to measure the tilt angles from the marked baseline on the tripod where the millimeter wave radar sensor AWR1642Boost was positioned vertically at 0° to the horizontal and tilted forward from the reference point of 0° to align with the different tilt angles of 30° and 45°.

The Zephyr Technologies BioHarness^{TM} 3.0 device can be configured by either wirelessly transmitting data via Bluetooth or logging the data without transmission into an internal memory or both modes are applicable. In the study, the device was configured to internal memory for collection of data of which the proprietary software for Zephyr Technologies BioHarness^{TM} 3.0 produces the raw data as external .csv files of general data, summary and waveforms of all the measurements.

The raw data from the millimeter wave radar sensor AWR1642Boost (EVM) was captured through the USB data port configured on the Texas Instrument proprietary software PC-GUI on a laptop and stored in a database created in \gui_exe folder as a dataOutputFromEVM. bin file. These .csv files and .bin files from the Zephyr module and radar sensor respectively, were imported into the Matlab software for further processing and data analysis.

3.4. Data Processing

In most literature, the signal processing of radar data for vital signs estimation are mainly done in either time or frequency domains or both. However, there are other several algorithms relying on numerical methods, machine learning and mathematical models that have also been used for the estimation of vital signs and improvement on measurement accuracy [16, 32]. The prevalent methods used for analysis in time and frequency domains, are the peak detection and FFT techniques.

The vital signs estimation acquired from the AWR1642Boost radar device through the embedded signal processing algorithm is displayed as heart rate and breathing rate values on the proprietary PC-GUI interface on a configured laptop. The signal processing algorithm of peak detection and FFT are applied on the baseband or IF signal output from the mixer. The IF signal contains both the range and vital signs information that can be extrapolated from the radar system parameters in 2D matrix format of fast time interval axis and slow time interval axis. The fast time interval are obtained from the number of ADC samples per chirp or ADC sampling for the range estimation such that when FFT is applied, the exact distance of the human target from the radar can be estimated. Conversely, the slow time interval are obtained from the periodic repetition of the number of chirps or frames per second. The phase variations between the transmitter and receiver antennas in successive frames can be detected when FFT is applied for the vital signs estimation. However, the Nyquist

sampling theorem greatly influences the resolution of both the range and vital signs estimation since the maximum sampling frequency must be higher than 2 times the rate of sampling or sampling frequency to prevent signal distortion or aliases. Hence, the theorem imposes measurement boundaries on the range estimations through the ramping bandwidth B and the periodic intervals of the frames for the vital signs calculations respectively [36, 58]. The frequency for vital signs estimation range from 0.1 to 4.0 Hz, thus, the sampling frequency for slow time interval is 20 Hz as captured in the radar system parameters in Table 3.

In the data processing steps, after the initial range estimations in frequency domain are determined, they are proceeded by extraction and unwrapping of phase from each corresponding range bins via the arctangent demodulation (AD) algorithm. The differences in the phase undergoes bandpass filtering in the frequency range of 0.1 to 0.6 Hz and 0.8 to 4.0 Hz for the breathing rate and heart rate signals respectively. The spectral evaluation of the vital sign signals in frequency domain are performed with peak detection and FFT. However, due to the susceptibility of the weak heart rate signal to be corrupted by the breathing harmonics or body movement, the embedded signal processing algorithm has threshold mechanism that discards invalid values and places the valid values in a buffer for peak detection, autocorrelation and FFT to estimate the heart rate [67]. The implementation of the signal data processing block diagram in the 77 GHz AWR1642Boost radar sensor is shown in Figure 10.

Table 3. Extrapolation of Vital Signs from Radar system parameters [67]

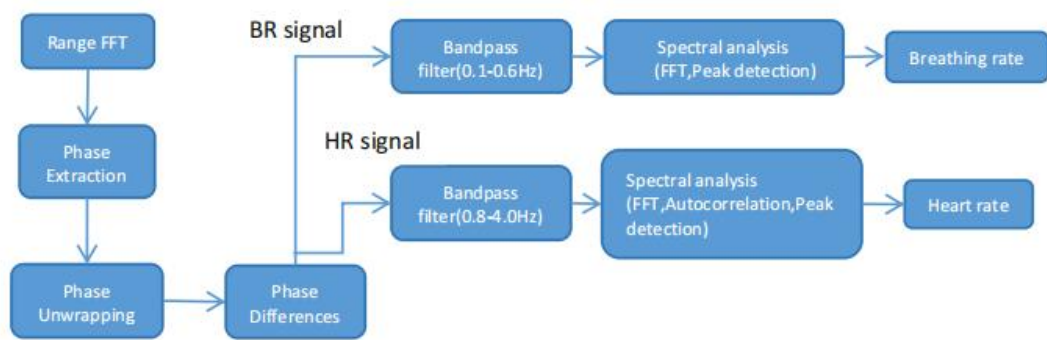| Radar system Parameters	Nominal values
Bandwidth, B	4 GHz
Starting Frequency, F_c	77 GHz
Slow time axis sampling, F_s	20 Hz
Fast time axis sampling, $F_{s\ fast}$	2 MHz
Samples per chirp, N	100
Chirp duration, T_c	50 µs

Figure 10. Block diagram of signal data processing of AWR1642Boost radar sensor [67].

3.4.1. Pre-processing

The data collected from each human target was simultaneously stored in both reference Zephyr and radar devices. The raw ECG data with the sampling frequency of 250 Hz from the Zephyr device was used for the manual alignment or synchronization of the vital signs parameters acquired from both devices because the chest tap event marker can be observed as visible sharp burst or peak for each scenario with respect to the time of occurrence. The raw ECG waveform versus time plot for Subject 1 in Figure 11, showed successive sequence of chest tap event markers for each measurement scenario and their respective time of occurrence. An example of the chest tap event marker zoomed in the raw ECG waveform versus time for the measurement scenario 4 is displayed in Figure 12. The respective time of occurrence of the chest tap event marker on the raw ECG waveform is used for segmenting the physiological parameters of heart rate and breathing rate respectively from the Zephyr device. The pre-processing step of merging the two datasets from reference device and radar sensor required the need to have the same sampling frequency for the purpose of feature extraction or data analysis. The ECG-derived heart rate from the Zephyr device is sampled at 1 Hz, whereas the vital sign signals from the radar device are sampled at 20 Hz respectively. Hence, heart rate and breathing rate from the radar device with the higher sampling frequency of 20 Hz were averaged at 20 values to 1 second to the equivalent sampling frequency of 1 Hz same as the signals from the Zephyr device. The averaged radar data were manually merged or aligned with the Zephyr data with respect to the time of occurrence of the chest tap event for each measurement scenario. Some samples were cut off from the Zephyr data for merging the two dataset signals with the same time vector. Figure 13 shows the two merged datasets with the same time vector. The pre-processing procedure was done on the Matlab 2023 software.
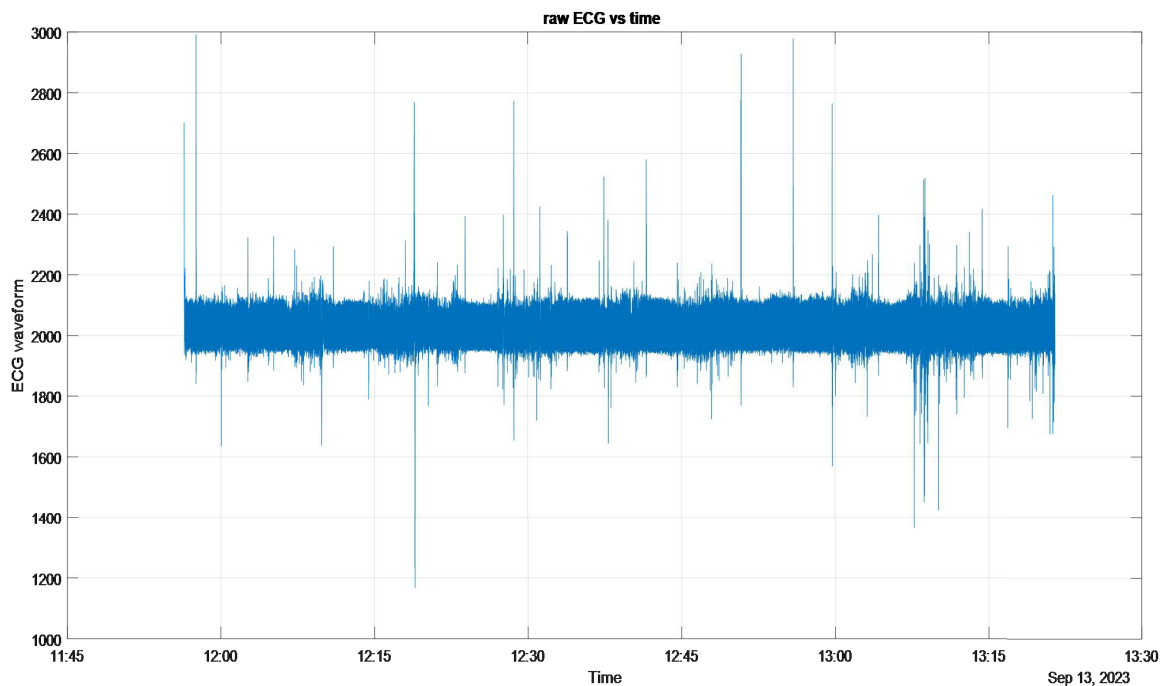

Figure 11. Raw ECG waveform versus Time plot from Zephyr device.
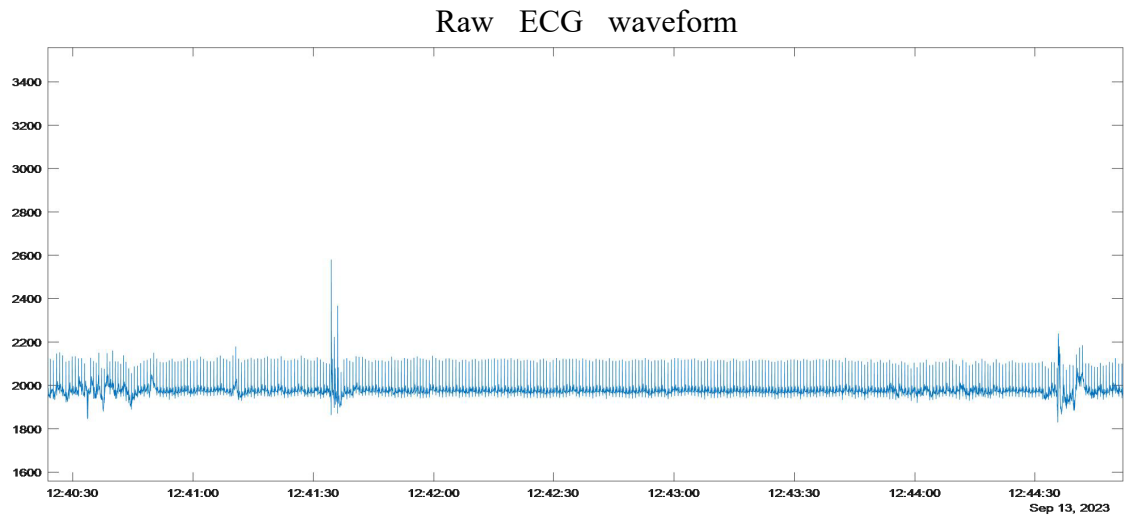
Raw ECG waveform

Figure 12. Zoomed raw ECG waveform versus Time plot showing sharp burst or spike of chest tap event marker for measurement scenario 4 for Subject 1.
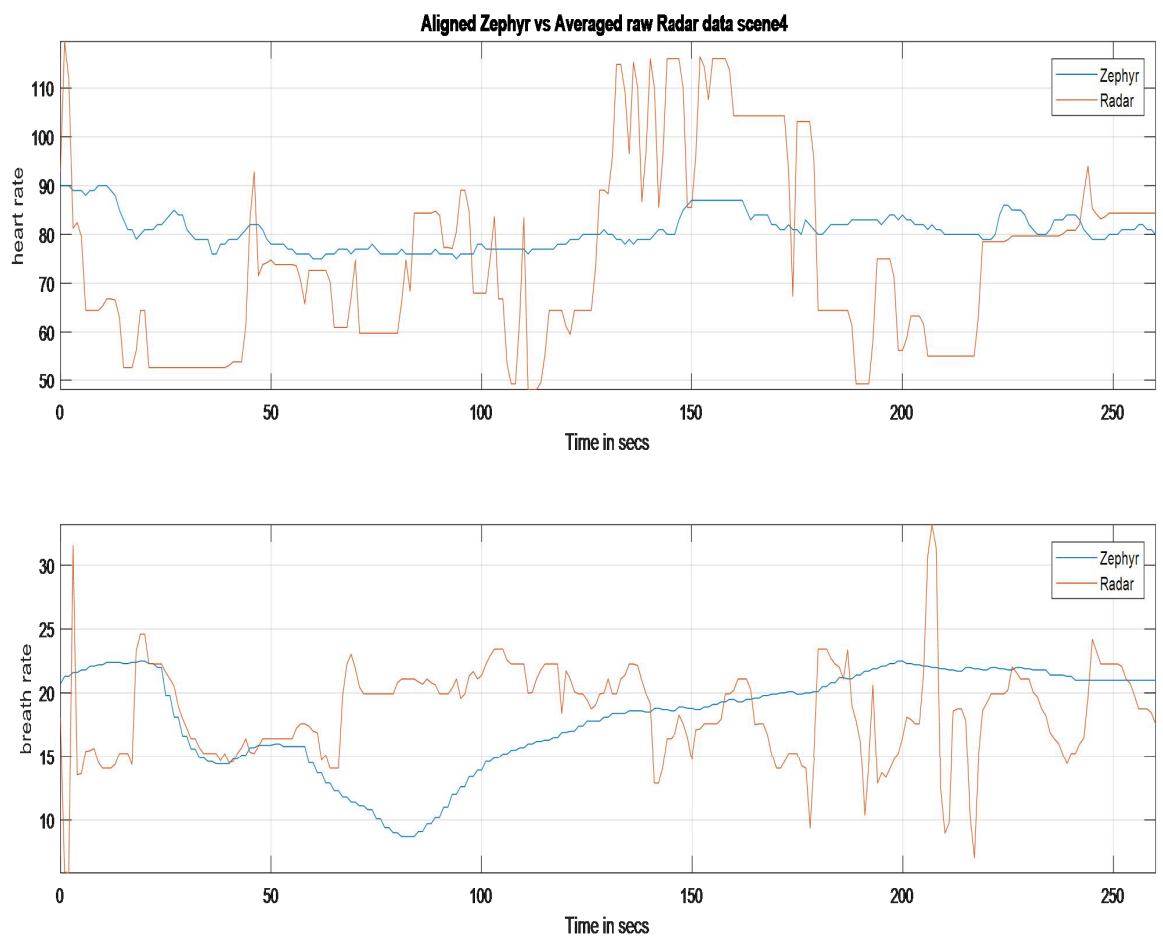

Figure 13. Manually synchronized Zephyr and Radar datasets for measurement scenario 4 in Subject 1. The Breath rate and Heart rate in bpm units.

3.4.2. Statistical Analysis

Different measures of dispersion tools and performance metrics were deployed in the statistical analysis of the datasets which seeks to provide insights to the research questions outlined in the introduction section.

Bland Altman Plot: The Bland Altman's plot is a graphical tool to measure levels of agreement between two devices with different measurement techniques of the same event such as the breathing rate and heart rate. The comparison of two different measurement techniques of same parameter(s) gives room for occurrence of measurement errors or systematic bias. Hence, the plot focuses on the mean differences (bias) and the limits of agreement (Standard Deviation (SD) $\pm$ 1.96). The recommendation is that 95 percent of the sample data points should lie within $\pm$ 1.96 SD of the bias which gives the upper and lower bounds of the limit of agreement. The evaluation of the measure of dispersion from the mean and limits of agreement provides the comparison or agreement level between the two different devices or measurement techniques such that the two devices can be used interchangeably, if there exists extremely low or zero bias and strong levels of agreement. The closer the sample data points are to the mean, the stronger the agreement but the farther the sample data points are from the mean and limits of agreement, the weaker the agreement between the two devices or measurement techniques [68]. However, in [69] the author emphasizes that the interpretation of the Bland Altman's plot should be based on the evaluation of the mean deviations between the two devices rather than agreement levels which might be erroneous. The logic behind the agreement level is based on the assumption that there is equivalence of results of same parameter obtained from two different measurement techniques provided the summation of the mean deviations equals to zero which rarely occurs in reality.

  The sample data points in Bland Altman's plot with the 95 percent confidence interval of the mean deviation is presumed to be Gaussian which is dependent on the large size of the sample data. Hence, the bell-shaped distribution of the sample as a requirement for interpretation must be validated through some statistical test methods [69]. However, in real cases where the requirement is unattainable, the interpretation of the Bland Altman's plot can be evaluated based on the 95 percent confidence intervals of the mean deviations and limits of agreement of which the reliability of the results or measurement precision and statistical inference on population basis can be extrapolated. The width of the confidence intervals of the mean deviations and agreement levels determines the measurement precision which depends on the size of the sample data such that the larger the size of the sample data, the narrower the width with high precision and vice versa. The Bland Altman analysis scatterplots typically assumes the normality of sample distribution such that the larger the sample size, the narrower the widths of the confidence intervals which in most cases are preferred [69]. It is vital to determine a priori the sample size required for comparability studies [96]. Lu et al. [81] developed a template or framework for computation of the sample size determination such that with the minimum sample size calculated, the measurement accuracy obtained will be the exact replica of large pool of sample size. The framework is based on statistical inference theory used for the power analysis calculations of the sample size under varying settings of parameter via a priori known or determined set limits of standard parameters of alpha, beta, mean and standard deviation of the differences between the two measurement

techniques and the clinically acceptable limit or threshold. In [81], the author offered a superior argument to the proposed estimation of sample size by Bland which is drawn from the width of confidence interval and lacking in high level of statistical power [97], whereas in their experimental procedure, Monte-Carlo simulations were performed to validate the proof of concept of the framework with the achievement of high statistical power of 80 percent.

Although, Bland Altman's plot does not infer the acceptance of the mean deviations as standard except a predetermined standardized value prescribed by regulatory body can be used to validate the confidence intervals. According to the American National Standards Institute for cardiac monitoring devices, the measurement accuracy of heart rate must lie within $\pm$ 10 % or $\pm$ 5 bpm deviation based on which one is greater [70].

Pearson Correlation Coefficient: The correlation coefficient is a statistical method used to show similarities or linearity in the relation between two features or parameters which is expressed as a value or coefficient ranging from -1 to +1. It evaluates the strength or magnitude of association and direction between the results obtained from the reference and radar devices via the range of coefficient values to either have a positive or negative correlation or none. The interpretation of the Pearson's correlation coefficient is based on line fitted regression and the decision rule of statistical significance of the p-values with $p \leq 0.05$ satisfying the null hypothesis of significant relationship of the results from both devices [71].

Error Analysis Tools: The assessment of the measurement accuracy will be implemented via the commonly used performance metrics of mean absolute error (MAE) or mean absolute deviation (MAD), root mean square error (RMSE) and mean absolute percentage error (MAPE). The comparison amongst these error analysis tools with provide valuable insights on the validation of the measured results to be used for possible clinical prognosis.

The MAPE is a performance metrics that measures the deviation of a model's prediction from the mean which can be equated to the percentage of MAE/MAD. It is defined as the average absolute percentage difference between predicted outcomes and the actual outcomes/ground truth [72, 73]. The MAE/MAD performance metrics simply measures the mean of the absolute errors without the percentage. Both MAPE and MAE/MAD are robust to outliers and non-differentiable of different errors due to the absolute function that renders opposing signed errors positive. Thus, the errors are equally weighted and these performance metrics linearly increment with rise in errors [74]. Conversely, the RMSE performance metrics is susceptible to outliers, as such blows up the mean errors making them larger since it measures the square root of the mean squared error. Hence, for the RMSE performance metrics larger errors are weighed more and penalized [75]. The variability in errors can be assessed by the simultaneous use of the RMSE and MAE/MAD in error analysis, since usually the RMSE $\geq$ MAE/MAD. If RMSE is higher, the larger the difference between them, the larger the variability of the each error within the observations or measurement data else there is similarity in the magnitude of errors [75].

Coefficient of Variation: The coefficient of variation (CV) is a statistical tool that measures the dispersion of the sample data points from the mean which is given as a ratio of the SD to the average or mean multiplied by 100 percent as it is expressed in

percentage. It measures the variability between two datasets with different scales of measurement or units of different measurement techniques [76, 77]. The higher the CV, the greater the dispersion from the mean resulting in lower measurement precision and vice versa.

Signal to noise ratio: The SNR can be derived from the inverse of CV. It evaluates the quality or strength of signal with respect to the interference levels or noise in the measured signal [77]. The signal quality increases with higher SNR and vice versa and it is measured in decibels (dB). The SNR values calculated from the CV are converted to decibels with the $10\log_{10}(\text{mean/SD})$ [78].

The computation of the SNR will provide insights into the design functionality and performance since the SNR depends on the transmission power, noise figure of the receiver, chirp duration, number of chirps in a frame, the antenna gain pattern of the transceiver and the RCS of the human subject or target which measures the magnitude of energy reflected by the human subject [79].

In addition, the angle at which the radar device makes with the horizontal equivalently relates to the radar's field of view (FOV) such that the radar's tilt angle of 0° equates to 90° FOV which will be viable for the assessment of its impact or effect on the accuracy of the measured physiological parameters. Table 4 shows the tilt angles with their corresponding FOV while Table 5 displays the summary of the measurement scenario with respect to their associated tilt angles.

Table 4. Tilt angles with their corresponding Field of view values

Tilt Angle (degrees)	Field of View (degrees)
0	90
30	60
45	45

Table 5. Summary of Measurement scenarios with respective tilt angles

Measurement Scenarios	Tilt Angle (degrees)
Scenario1	0
Scenario9	45
Scenario17	30
Scenario2	0
Scenario10	45
Scenario18	30
Scenario3	0
Scenario11	45
Scenario19	30
Scenario4	0
Scenario12	45
Scenario20	30

Scenario5	0
Scenario13	45
Scenario21	30
Scenario6	0
Scenario14	45
Scenario22	30
Scenario7	0
Scenario15	45
Scenario23	30
Scenario8	0
Scenario16	45
Scenario24	30

Boxplots: The boxplot statistical tool is used to analyze the variability or spread in a grouped data via the range and interquartile range (IQR). The range reveals the spread of the entire data, and it is the difference between the highest number and lowest number in the dataset whereas the IQR reveals the spread of the middle 50 % of the data, which is the difference between the upper and lower quartiles. The boxplot divides the data into four equal parts of 25 % each or quartiles [80].

The Bland Altman's plot, Pearson's correlation coefficient and error analysis tools (performance metrics) were used to answer the first research question while the coefficient of variation, signal to noise ratio and boxplots were used to answer the second and third research questions respectively. The Microsoft Excel was used for the statistical analysis and data visualization.

4. RESULTS

The total number of 5 human subjects consisting of 3 males and 2 females participated in the study with 24 measurement scenarios observed for approximately 2 hours for each participant. During the course of measurement, there were interventions of adjusting the level of the tripod (mounted with the radar device) for the different stages of measurement involving the varying vertical heights of 85 cm, 130 cm and 150 cm as well as positioning of the human subject and the angular orientation (tilt angle) of the radar device. The expected total of 120 paired measurement data points from 24 measurement scenarios were reduced to 118 paired measurement data points due to missing data for measurement scenarios 23 and 24 for Subject 1 as the rechargeable battery on the reference Zephyr device had gone flat during the period of measurement for those scenarios. Thus, in order to avoid biasing the data, these missing values were excluded from the computation of the statistical analysis.

4.1. Bland Altman Analysis

Heart Rate

The Bland Altman analysis of the physiological parameters from the Zephyr and radar devices were analyzed to assess the agreement and systematic errors between the two devices for the individual human subject. For lack of space in displaying each Bland Altman plot of human subject per scenario, the mean deviations and limits of agreement of the physiological parameters for all human subjects per scenario were averaged to compute the overall mean deviations and limits of agreement used for the Bland Altman's plot in Figures 14 and 18. In Figure 14, the data visualization of the heart rate scatterplot for majority of the subjects per scenario lie within the 95 percent confidence interval alongside some outliers from either or both side of the limits of agreement. It also showed a general trend or proportional bias from high to low values with low systematic errors or bias such that the scatterplots are closer to the mean which means strong agreement between the two devices whereas dispersion of sample data points from the mean are largely observed at extreme low or high values which are outliers generated from the radar device. However, in most of the Bland Altman's plots for each human subject per scenario showed the scatterplots with low and extremely high biases(in some cases) in the physiological parameters which lie within the 95 percent interval for many of the scenarios. There is a remarkable trend in the increase or decline of values in the dataset depicted as proportional bias which impacts on the measurements. An example is the Bland Altman plots of the physiological parameters for Subject 1 in scenario 1 as shown in Figures 15 and 16 in the appendices. The heart rate scatterplots exhibits a trend from high to low values with low bias while the breathing rate with a high bias (in most cases low bias), exhibits random scatterplots reflecting the consistent differences in the measurement between the two devices. Similarly, this general trend is replicated in the remaining human subjects for most scenarios except for the heart rate in scenario 7 for Subjects 3, 4, 5 and scenario 14 for Subjects 2, 3 respectively which showed the trend from the lowest to highest

values. This inverse trend is captured in Figure 17 for Subject 3 in scenario 7. The occurrence of proportional bias can be adduced to the proportional variation between the differences and the mean of the two devices [81]. The proportional bias implies that the radar device either overshoots the high values or undershoots the low values of the physiological parameters. The bias of -7.23 bpm with the 95 percent confidence intervals of 27.24 bpm and -41.22 bpm respectively in Figure 14, showed that the radar device is 7.23 bpm more than the reference device with respect to analyzing the deviations between the two devices [69]. Since the bias obtained from the Bland Altman analysis does not ascertain the acceptability of the limits, the scatterplots of the overall Bland Altman for the heart rate parameter was assessed with respect to the predetermined acceptable limit of ± 5 bpm for physiological parameters [70] shown as red dashed lines in Figures 14 and 18. The deviation of 2 bpm from the acceptable limit of ± 5 bpm by the bias is due to the influence of the observed outliers and proportional bias in the data. However, over 70 % of the heart rate data lies within the acceptable threshold having low biases and narrow agreement levels with few exceptions of high biases and wide agreement levels observed in the scenarios 6, 7, 9, 15, 16, 23 and 24 which are above the threshold limit shown in Table 6 as the summary of the computation of Bland Altman parameters for heart rate (see appendices). The low biases and narrow agreement levels are suggestive of strong agreement between the two devices whereas the high biases and wide agreement levels implies poor agreement levels. Thus, Table 6 showed that more than 70 % of the heart rate data fall within the strong agreement levels.Invariably, there are significant trends in the occurrence of strong agreement levels between the two devices in the measurement scenarios with the human subject. For example, Subjects 1, 2, 4, 5 have low biases in scenario 10 while scenario 11 showed low biases for Subjects 1, 2, 3, 4. The high biases for Subjects 3 and 5 in these respective scenarios could be as a result of the radar sensor overshooting the high values of the individual subject. Similar trends of low bias were also observed for scenarios 1, 2, 3, 4, 5, 8, 12, 13, 14, 17, 18, 19, 20, 21, and 22 which implies that the front side and back displayed good agreement levels at their respective parameters of measurement. The overall average computation of the heart rate for all the participants is estimated at 77.18 bpm.
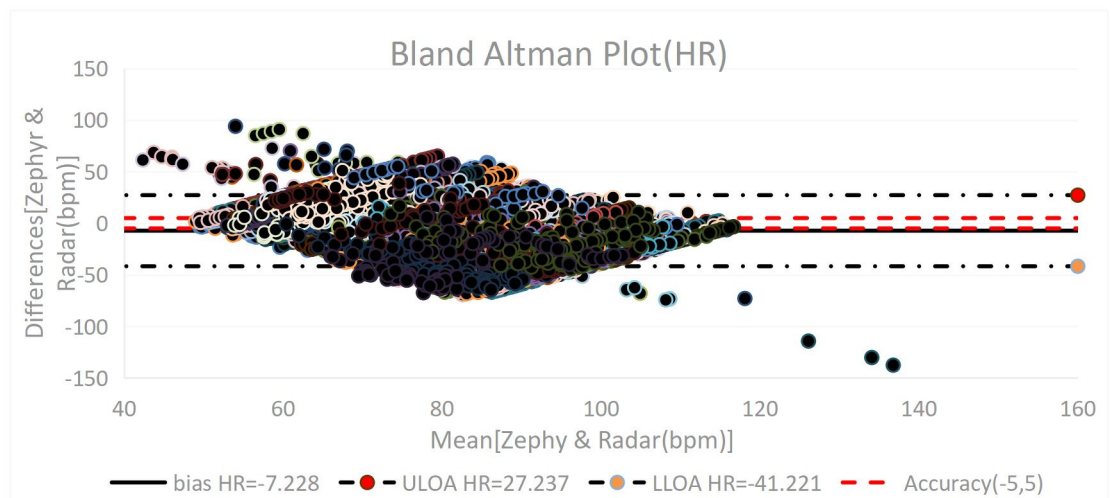

Figure 14. Overall Bland Altman plot for Heart rate(bpm) for all human subject per scenario.

Outliers are common and inevitable occurrences in data measurements which have an overbearing impact on the accuracy of which the statistical mean computation or average is vulnerable. A more robust approach will be the computation of the overall median of the mean deviations and limits of agreement whereby the statistical median computation is not affected by the occurrence of outliers. Table 7 shows the comparison between the overall mean and median computation of the mean deviations and the limits of agreement. The bias of -4.14 bpm, 95 percent confidence intervals of 30.42 bpm and -38.35 bpm obtained from the median computation alludes to the influence of outliers on mean computation as the bias of -4.14 bpm falls within the standard acceptable threshold and the confidence interval with less deviation or width showed strong agreement between the two devices.

Table 7. Comparison between Overall Mean and Median Computation

Bland Altman Parameters	Overall Mean Computation (bpm)		Overall Median Computation (bpm)	
	HR	BR	HR	BR
Bias (mean differences)	-7.228	-5.753	-4.136	-5.036
ULOA*	27.237	5.583	30.418	5.939
LLOA*	-41.221	-17.089	-38.351	-15.952
SD+	17.585	5.784	17.394	5.823

* Upper and Lower limits of agreement, + Standard deviation.

In order to assess the impact of the outliers witnessed in the data on measurement precision, the confidence intervals of the mean deviations and agreement levels were computed in Table 8. The computation of the confidence intervals is based on the assumption of Gaussian distribution of sample data whereby the t-inverse distribution with the corresponding (N-1) degrees of freedom for two-tailed test from Medcalc manual and standard error mathematical formula for mean deviation ($\sqrt{SD^2/N}$) and agreement levels ($\sqrt{3SD^2/N}$) are applied respectively [69, 82].

Table 8. Bland Altman Confidence Intervals for Heart & Breathing rates

Parameters		Test of significance	S. E[a] (bpm)	Confidence Intervals(S.E* t-score) (bpm)	
Mean Deviation	HR	t = 2.78, DF# = 4	8.793	-7.228 ± 24.4	[-31.43, 17.17]
	BR		2.892	-5.753 ± 8.039	[-13.79, 2.29]
ULOA	HR	t = 2.78, DF# = 4	15.229	27.237 ± 42.3	[-15.06, 69.54]
	BR		5.009	5.583 ± 13.925	[-8.34, 19.51]
LLOA	HR	t = 2.78, DF# = 4	15.229	-41.221 ± 42.3	[-83.52, 1.08]
	BR		5.009	-17.089 ± 13.925	[-31.01, -3.16]

[a]standard error, #degrees of freedom.

In [69], the evaluation of measurement precision is validated when the equivalence line of zero bias lies within the confidence intervals of the mean deviation and agreement levels. Conversely, if the zero bias equivalence line lies outside the boundaries of the confidence intervals, then there is an indication of systematic errors such that the results obtained from the radar device overshoots or undershoots in

comparison with the reference device. The visualization of the confidence intervals in Figure 17 clearly showed the overlapping of the zero bias equivalence line falling within the confidence intervals of the mean deviation and limits of agreement indicative of good measurement precision or lack of significant systematic errors. However, the respective width of the confidence intervals for the mean deviation and agreement levels are wide due to the small sample size but a narrower width of confidence intervals with large size of sample would suffice to have a higher level of precision [69].
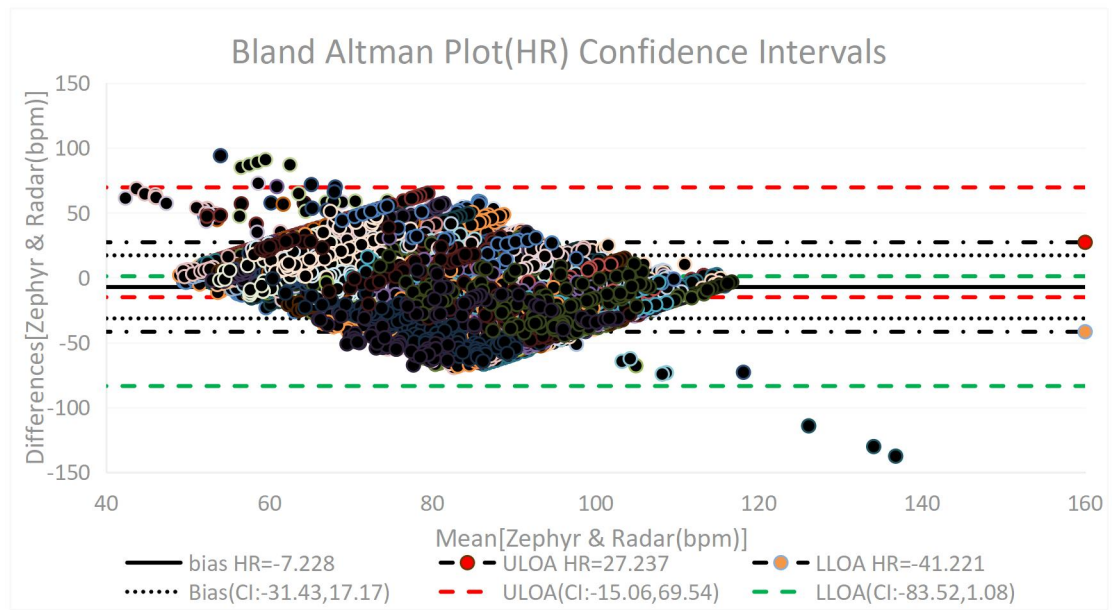

Figure 17. Bland Altman plot of Confidence intervals (Heart rate) for bias and agreement levels.

Breathing rate

The Bland Altman plot in Figure 18 for the breathing rate showed a replica of the general trend or proportional bias from high to low values witnessed in the heart rate with low bias such that the random scatterplots are closer to the mean referencing stronger levels of agreement between the two devices while the scatterplots are divergent or dispersed from the mean from above 10 bpm and at extreme higher values. The divergent trend is observed in the scenarios 1 and 19 for Subjects 3, 4, whereas same is applicable in scenarios 11 and 12 for Subject 5. This trend might be due to the variability of the deviations between the two devices such that there is dispersion in the agreement levels with increasing higher values. Hence, at values close to 10 bpm the values tend towards convergence, less variability, and low bias which implies good agreement between the two devices. An example is the Bland Altman plot for the breathing rate of Subject 3 in scenario 1 in Figure 19 shows the occurrence of the divergence from 8 bpm and it increases with increasing mean values of the two devices with outliers witnessed at lower limit of agreement (see appendices). Thus, we can deduce the influence of proportional bias because as the mean values of the two devices increases the sample data points are closer to the bias line which implies good agreement levels at high values with low bias of -2.913 bpm.

Similarly, in Figure 18 the impact of outliers seen as high values produced from the radar device is reflected in the bias of -5.75 bpm as well as the agreement levels of 5.58 bpm and -17.09 bpm respectively which implies that the radar device estimated beyond the reference device by 5.75 bpm and the wide limits of agreement indicate poor agreement between the two devices. Although with < 1 bpm deviation from the acceptable threshold, more than 80 % of the breathing rate data lies within the acceptable limit with exceptions of high bias occurrence in scenarios 23 and 24 respectively as shown in the summary Table 9 of Bland Altman parameters for breathing rate (see appendices). The significant trend of low biases with narrow limits of agreement and high biases with wide agreement levels witnessed in the heart rate data is replicated in many scenarios for the breathing rate which is captured in Table 9. The calculation of the overall average of the breathing rate for all the participants was estimated at 15.54 bpm.
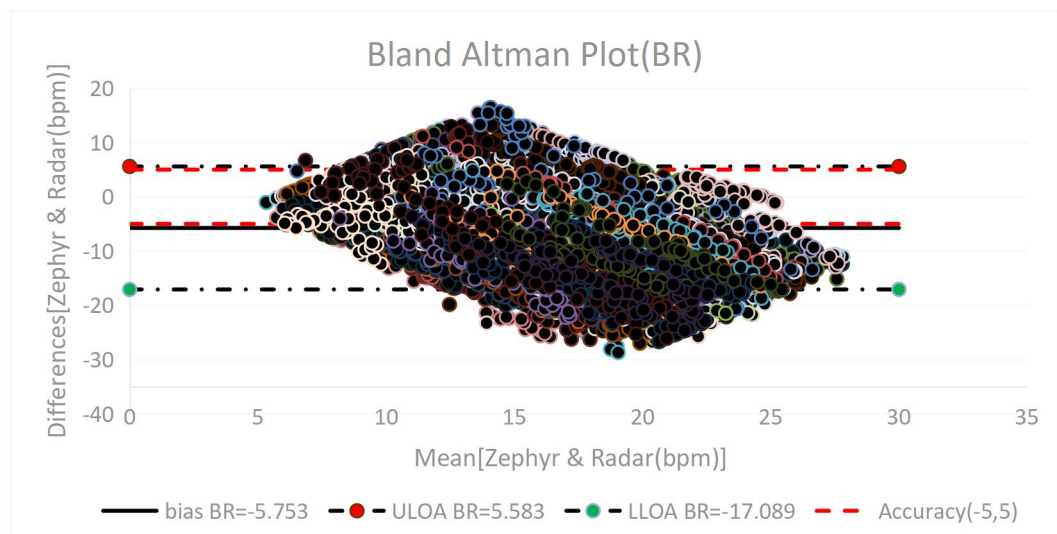

Figure 18. Overall Bland Altman plot for Breathing rate(bpm) for all human subject per scenario.

The overall median computation was performed on the mean deviation and agreement levels for the breathing rate as shown in Table 7. The bias of -5.04 bpm, agreement levels of 5.94 bpm and -15.95 bpm respectively for the median computation compared with the overall mean computation also alludes to the effect of outliers on the data. Although the visualization of the confidence intervals for the Bland Altman plot for breathing rate in Figure 20 mirrors the confidence intervals observed in heart rate but with some exceptions where the equivalence line of zero bias falls only outside the lower bounds of the agreement level signifying errors in the sampling or size of samples (N = 5) [69]. It is noteworthy that for all the 5 human subjects, the scenario 7 (heart rate and breathing rate) with the radar device having the parameters of measurement (azimuth angle:180°, range: 0 cm, height of radar: 85 cm, tilt angle:0°) displayed large bias for the heart rate and low bias for the breathing rate while scenario 11 (heart rate and breathing rate) with the parameters of measurement (azimuth angle:90°, range:40 cm, height of radar:130 cm, tilt angle:45°), displayed low bias for both physiological parameter. However, scenario 12 (heart rate and breathing rate) with parameters of measurement (azimuth angle:270°, range:40 cm, height of radar:130 cm, tilt angle:45°), displayed small bias in both

heart rate and breathing rate for Subjects 1, 4 while the remaining three subjects had high biases for heart rate and breathing rates respectively. The implication for these trends could be as follows: the high bias of the heart rate witnessed at scenario 7 which is at the backside can be related to the influence of proportional bias or systematic errors between the two devices because a low bias of vital signs is expected since the radar is close to the human subject. The scenario 11 which is at the front (right lateral side) witnessed low bias for the physiological parameters is also expected because of its close proximity to the human subject and the same applies to scenario 12 which is on the opposite side of scenario 11. However, the occurrence of low bias of the physiological parameters for only Subjects 1 and 4 on the left as against all participants on the right could be as a result of positioning of the subject with respect to FOV of the radar device. In this case, it can be due to measurement errors as the subject was moved into the different azimuthal angles instead of the radar device (single radar device was used).
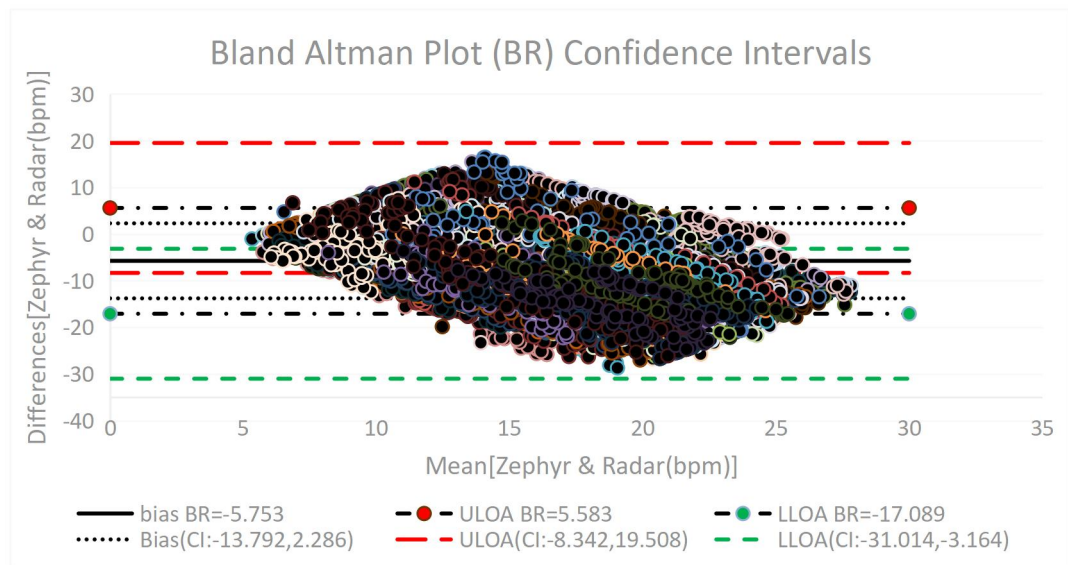

Figure 20. Bland Altman plot of Confidence intervals (Breathing rate) for bias and agreement levels.

4.2. Pearson Correlation Coefficient

The Pearson correlation coefficient was used to assess the strength and direction of the linear relationship between the reference and radar devices for the individual human subject. The correlation plots of each human subject per scenario depicted extremely weak to moderately high correlation coefficient in the range $\pm$ 0.60. The correlation between the two devices in the positive and negative correlation range values were evaluated with p-values for all 5 human subject per scenario. There were some significant relationship for both heart rate and breathing rate especially with respect to the front side and back side scenarios. This implies the similarity in results obtained from the two devices at the front and back respectively. However, there are exceptions to this trend where there were no simultaneous occurrence of statistical significant values obtained on both physiological parameters such as in scenarios 10, 15, 23 and 24 as shown in Table 10 containing the summary of the occurrences of the

p-values with respect to corresponding correlation of each human subject per scenario. This exceptional occurrence is suggestive that either heart rate or breathing rate had statistical significance at any point in time not both at the same time. The positive correlation obtained in the results is indicative that for every 1 bpm increase in the reference device there is a corresponding increase in the radar device and negative correlation depicts inverse relationship. The rejection of the null hypothesis of either the positive or negative correlation validates the similarity between the two devices. An example of positive and negative correlation with p-values set at 0.05 is shown in the correlation plots of the physiological parameters for Subject 1 in scenario 1 in Figures 21 and 22 (see appendices). The disparity witnessed in the Pearson correlation coefficient in Table 10, whereby the positive and negative correlation values occurs alternately between the heart rate and breathing rate can be adduced to the differences in height and body type of each subject which can be linked to the RCS. Other possible factors can be the differences in physical anatomical structure of each human subject with respect to the heart's location within the thoracic cavity and in the distribution of adipose tissue in the body [83]. Additionally, the FOV of the radar sensor is affected by the vertical height which determines the angular tilt orientation of the radar. Hence, as the vertical height is increased, the radar sensor with the antenna patch should be tilted to an angle that can accommodate the FOV for good signal quality.

The overall averaged correlation were computed and plotted in Figures 23 and 24 for all the human subject per scenario for the heart rate and breathing rate showed a weak positive correlation of 0.08[CI: -0.863, 0.899], and 0.24[CI: -0.815, 0.926] with p-values of 0.388 and 0.008 respectively [84]. The Pearson correlation coefficient is not robust against outliers as such the overall averaged correlation coefficient for the heart rate though observed a weak positive correlation but has no statistical significance which implies lack of similarity between the reference Zephyr device and radar device. However, the impact of the outliers on the breathing rate data was not so pronounced as there is statistical significance between the two devices. This result is expected given the obvious factors of the location of the lungs within the thoracic cavity (lungs are sandwiched between the heart and the back), the displacement of the chest during respiration and the strong amplitude of the breathing signal makes it possible for both devices with different measurement techniques (contact based pressure pads and non-contact based radar) to detect the breathing signal. However, the breathing signal can be weakened by the presence of outliers. Additionally, the heart signals are weak and easily corrupted by influential interference of the breathing harmonics as well as body movement can affect the accurate estimation of the heart rate by the radar device. Therefore, it suffices that correlation coefficient with statistical significance is being observed in the breathing rate only.

Table 10. Summary of occurrences of Correlation coefficient with p ≤ 0.05

Measurement Scenarios	Participant	Correlation [HR & BR, p ≤ 0.05]
Scenario1	Subject 4	Both negative
Scenario2	Subject 3	Both positive
Scenario3	Subject 4	Positive and negative
Scenario4	Subject 1	Positive and negative

| Scenario5	Subject 1	Both positive
	Subject 4	Both negative
	Subject 5	Both positive
Scenario6	Subject 4	Both negative
	Subject 5	Both negative
Scenario7	Subject 2	Both positive
Scenario8	Subject 4	Both negative
Scenario9	Subject 5	Positive and negative
Scenario10	none	none
Scenario11	Subject 4	Both negative
Scenario12	Subject 5	Both positive
Scenario13	Subject 1	Positive and negative
Scenario14	Subject 4	Positive and negative
Scenario15	none	none
Scenario16	Subject 1	Both negative
Scenario17	Subject 1	Both positive
Scenario18	Subject 3	Positive and negative
Scenario19	Subject 5	Negative and positive
Scenario20	Subject 5	Negative and positive
Scenario21	Subject 1	Negative and positive
	Subject 3	Negative and positive
Scenario22	Subject 1	Both positive
	Subject 2	Both negative
	Subject 3	Negative and positive
Scenario23	none	none
Scenario24	none	none
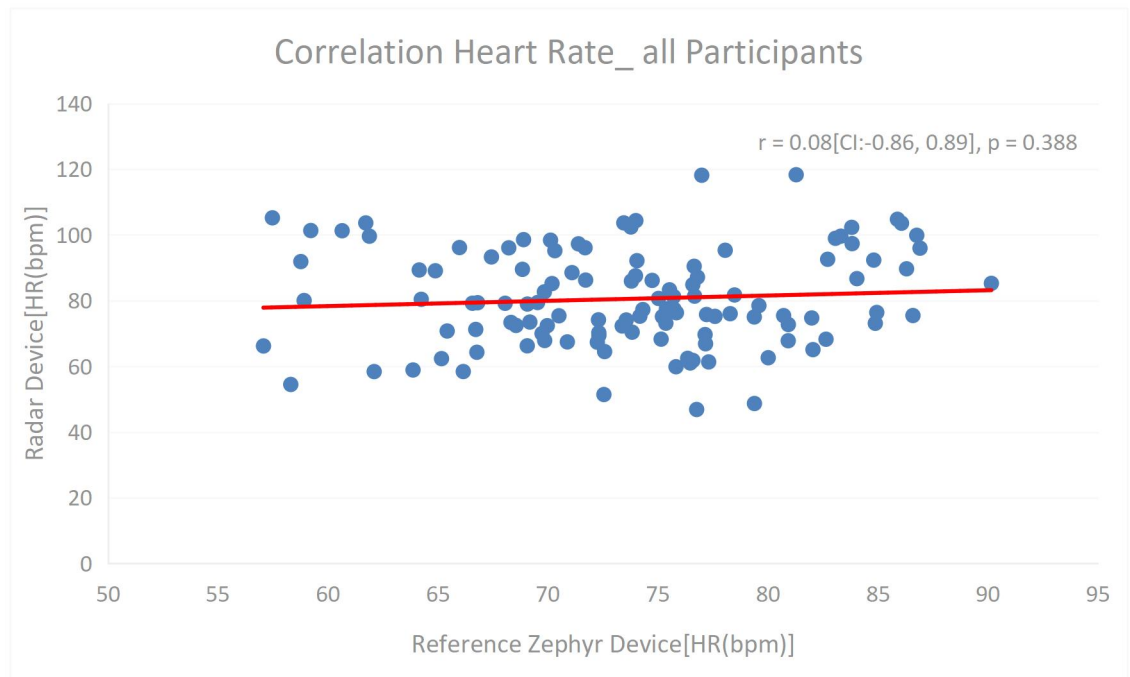
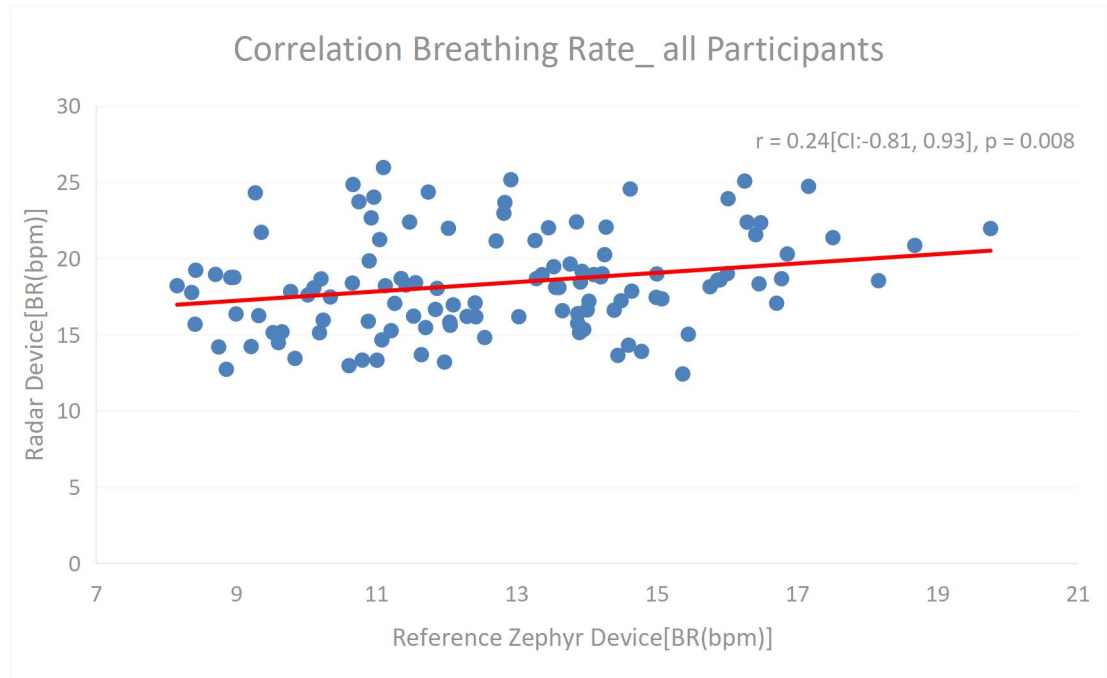Figure 23. Overall Pearson correlation coefficient of heart rate for all participants.

Figure 24. Overall Pearson correlation coefficient of breathing rate for all participants.

4.3. Error Analysis

The performance metrics of mean absolute error or mean absolute deviation (MAE/MAD), root mean square error (RMSE) and mean absolute percentage error (MAPE) were applied or computed to assess the measurement accuracy. Table 11 shows the comparison among the performance metrics tools.

Table 11. Performance metrics for measurement accuracy of Radar device

Performance metrics	HR	BR
MAE/MAD	13.14 bpm	5.75 bpm
RMSE	17.21 bpm	6.70 bpm
MAPE	18.48 %	50.05 %

The measurement accuracy of the Zephyr Technologies BioHarness[TM] 3.0 used with ECG and breathing emulators were estimated at ± 1 bpm and ± 2 bpm for the heart rate and breathing rate respectively as specified by the manufacturer [63]. On the contrary, the measurement accuracy of the vital signs parameters for the radar sensor obtained in this study using the performance metrics of MAE/MAD, RMSE and MAPE were estimated at 13.14 bpm, 17.21 bpm, 18.48 % for the heart rate and 5.75 bpm, 6.70 bpm, 50.05 % for the breathing rate respectively. The breathing rate has better performance metrics of MAE/MAD and RMSE compared with the heart rate which can be alluded to the feeble heart rate signal and its susceptibility of being corrupted by breathing harmonics or movement of the body as a result the heart rate

measurements have poor accuracy. This implies that the breathing rate can be accurately determined even with minimal signal processing due to their strong amplitude than the heart rate. However, in terms of measurement accuracy the radar device had a poor accuracy with error rates of 13.14 bpm and 5.75 bpm for the heart and breathing rates compared to the reference device. A critical look at the values of the MAE and RMSE for the physiological parameters shows small margin of errors between them of 4 bpm and 0.95 bpm for the heart rate and breathing rate respectively. This implies that there is less variability of each error within the observations of the measurement data which can be alluded to the FOV of the radar device which increases the SNR. Thus, the tilt angles related to the FOV of the radar device indeed has positive impact on the accuracy. The MAPE values of the radar device was poor at 18.48 % and 50.05 % for heart rate and breathing rate respectively. This implies that both heart and breathing rates deviated from the mean by 18.48 % and 50.05 % each which can be due to the influence of outliers observed in the measurement data. These MAPE values conflict with the MAE and RMSE metrics as it shows that the heart rate has a higher accuracy than the breathing rate. This exceptional case of the MAPE value of 50.05 % for the breathing rate showed that the accuracy in measurement decreases with time and will require calibration. Furthermore, the measurement accuracy of the breathing rate declines at higher frequencies [85] due to the phase ambiguity of null point occurring at the displacement of the human subject greater than half of the wavelength of the carrier frequency as well as the increase in the breathing harmonics as the frequency becomes higher [86] and in [32] suggests deploying in the signal processing, harmonic cancellation algorithm for the vital signs estimation.

   Therefore, as the frequency increases with time since it is an FMCW radar sensor, the accuracy of measurement for the breathing rate will reduce which will require calibration to be performed similar to the time dependent calibration for blood pressure in [87]. Alternatively, the chirp system parameters can be configured or adjusted to operate at the optimal frequency where the distance of human subject is less than half of the wavelength of the carrier's frequency in order to reduce the degradation in the breathing rate and heart rate detection accuracy [88].

4.4. Coefficient of Variation

The CV is used to assess the dispersion of the sample data points from the mean and infer the accuracy in measurement. The results of the CV for the measurement data revealed a general trend of low CV values in heart rate and breathing rate in the reference Zephyr device with less dispersion from the mean which is suggestive of high estimates of precision compared to the observed high CV values of physiological parameters from the radar device. This trend is clearly evident in the CV plots of the physiological parameters and scenarios for each human subject. The data visualization of the CV of the heart rate and breathing rate for each human subject per measurement scenario for the reference Zephyr device and radar device are shown in Figures 25A-D (see the appendix). For example, Subject 1 showed a remarkable low CV values of the reference device for all the scenarios in heart rate data compared to other human subject, whereas Subject 5 showed the inverse in Figure 25A. The contrasting trend in Subjects 1 and 5 needs to be investigated because they have similar human parameters except for differences in sex. A device

can not be accurate for one person and inaccurate for another except there is a factory defect. However, there are exceptions which conversely varies against this general trend in the different measurement scenarios for each human subject captured in the remaining Figures 25B-D. Hence, there are cases where the reference device has high CV values while the radar device has low CV values. This implies that the radar device outperformed the reference device in some scenarios per human subject. Table 12 provides the summary of the occurrences of low CV of the heart rate and breathing rate for each human subject at different measurement scenarios from the radar device. The averaged CV of the physiological parameters for all participants at each measurement scenario in Figures 26 and 27 showed a remarkably low and high CV for the heart rate at scenarios 7 and 15 respectively in comparison with the other measurement scenarios. Similarly, the occurrence of significantly low and high CV compared to other measurement scenarios for the breathing rate is replicated in the measurement scenarios 23 and 15 respectively. The trend of the low CV values for the physiological parameters observed in the averaged CV versus scenarios plots for all participants suggest that the heart rate and the breathing rate can be accurately determined at scenarios 7 and 23 respectively for all participants. Although, the physiological parameters can be measured at scenario 15 with less accuracy due to the high CV values obtained, it can be resolved by widening the FOV to 60° or by increasing the vertical height of the radar device with a reduced tilt angle accommodating a wide FOV. In addition, the overall occurrence of the low CV in measurement scenarios 7 and 23 as well as high CV at measurement scenario 15 for the physiological parameters converges at the back side for all participants with the common parameters of measurement of azimuthal angle of 180° and range of 0 cm but with different corresponding vertical height of 85 cm, 130 cm, 150 cm and tilt angles of 0°, 30° and 45°. This implies that the proximal location of the radar device at the backside with respect to the human subject, the vertical height of the radar device and tilt angle can accurately estimate the physiological parameters. Thus, the varying vertical height and tilt angle have impact on the measurement accuracy with respect to the low or high CV because the measurement scenarios 7 and 23 have the vertical height and tilt angle at 85 cm, 150 cm and 0°, 30° respectively, we have low CV whereas the measurement scenario 15 has the vertical height and tilt angle at 130 cm and 45°, we have high CV. The differences in the CV at the backside can be adduced to the FOV which is affected by the vertical height that determines the angular tilt orientation of the radar through an inverse relationship.

The low CV values of the physiological parameters from the radar device shown in Table 12 reflects the predominance of the breathing rate over the heart rate which differs for each human subject per scenario. This implies that the breathing rate can be accurately measured than the heart rate which alludes to the strong amplitude or harmonics of the breathing signal. As per the scenarios, it is evident that the low CV values of the physiological parameters were observed in the front side of each human subject for the respective parameters of measurement with the azimuthal angles ranging from 0°, 45°, 90° and 270° with the isolated case of the angle 315° having low CV occurring in participants Subject 2 and Subject 3 only. Similarly, the back side of each human subject witnessed low CV for the corresponding parameters of measurement with the azimuthal angles ranging from 135° to 225°. This implies that the breathing rate and heart rate can be measured reliably at the front side with the azimuthal angles of 0°, 45°, 90°, 270° and back side with azimuthal angles of 135°, 180°, 225° alongside the respective corresponding parameters of measurement for all

participants. However, the exceptional case of low CV at the frontal side of the azimuthal angle of 315° and range of 80 cm for only Subjects 2 and 3 alludes to the characteristics of the subject in the form of RCS of which the Subjects 2 and 3 have the lowest height of 168 cm and 172 cm with the circumferential diameter of 71 cm and 85 cm respectively. Apart from the RCS, the other factors that can be linked to the inter-person variations in occurrence of the low CV values in different scenarios are the proximity of the radar device to the human subject, vertical height of the radar device which affect the FOV, and tilt angle.

Table 12. Low Coefficient of Variation & High Signal to Noise ratio of Radar device for each participant

| Participant	HR (Low CV/High SNR)	BR (Low CV/High SNR)
Subject 1		Scenario1
		Scenario2
		Scenario4
		Scenario6
		Scenario12
Subject 2	Scenario14	Scenario3
		Scenario4
		Scenario17
		Scenario21
		Scenario23
		Scenario24
Subject 3	Scenario2	Scenario1
	Scenario7	Scenario5
	Scenario11	Scenario7
	Scenario16	Scenario8
	Scenario17	Scenario11
	Scenario18	Scenario20
	Scenario20	
Subject 4	Scenario7	Scenario3
	Scenario15	Scenario8
	Scenario16	Scenario9
	Scenario24	Scenario10
		Scenario18
Subject 5	Scenario3	Scenario2
	Scenario6	Scenario10
	Scenario7	Scenario12
	Scenario11	Scenario17
	Scenario12	Scenario23
	Scenario16	
	Scenario18	
	Scenario19	
	Scenario23	
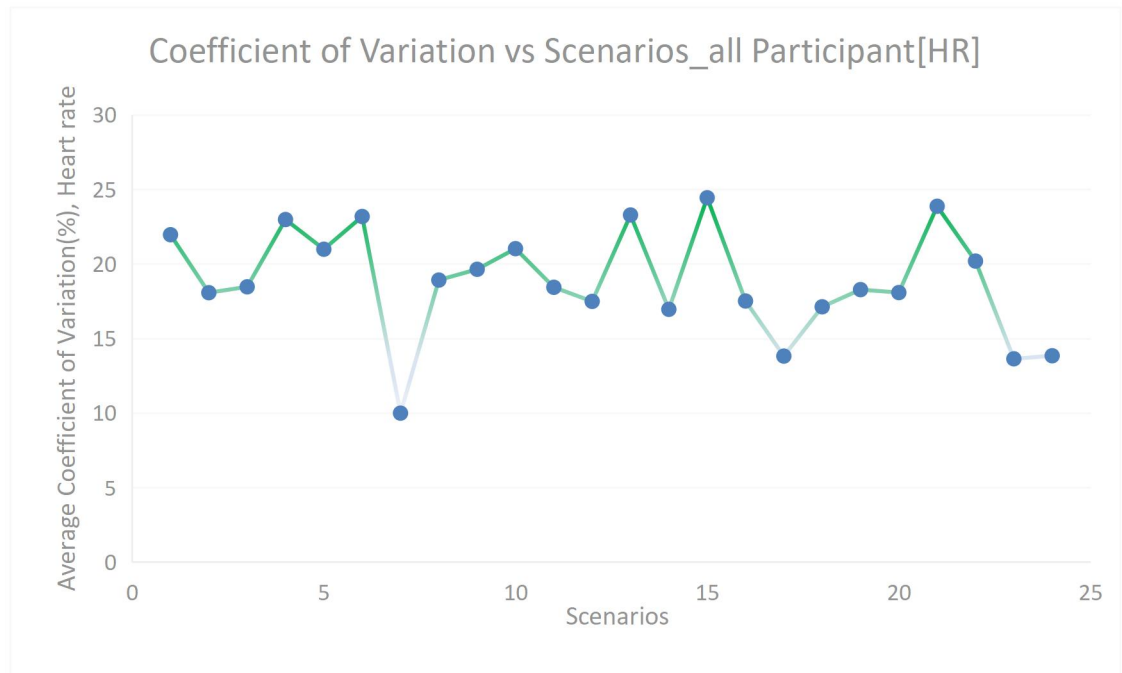
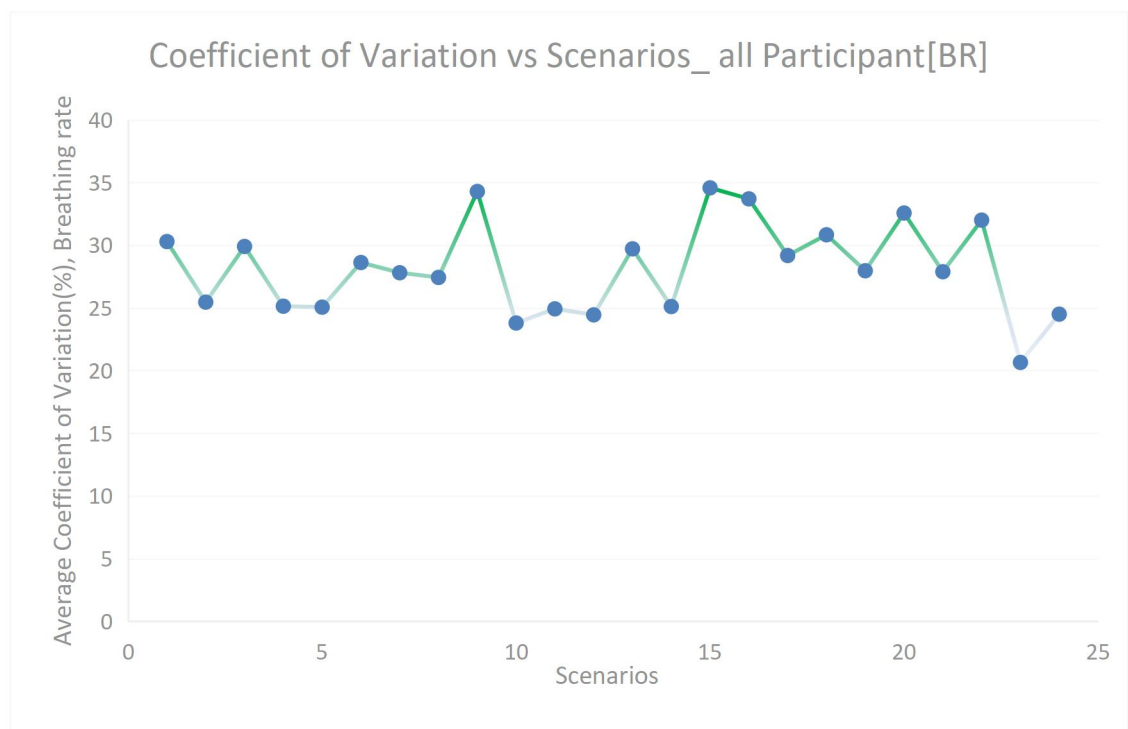Figure 26. Averaged Coefficient of Variation per scenario of heart rate for all participant.

Figure 27. Averaged Coefficient of Variation per scenario of breathing rate for all participant.

4.5. Signal to Noise Ratio

The analysis of the CV is replicated in the SNR of which high SNR is correlated to low CV values observed in Table 12. Low CV values indicate accuracy or precision of measurement. The SNR is the inverse of CV as such reflects the inverse trend of the CV, so high SNR indicates accuracy. Similarly, the general trend of high SNR is witnessed in the reference device compared to the radar device. The radar device outperformed the reference device in some measurement scenarios which were captured in Table 12. The data visualization of the SNR ratio of the heart rate and breathing rate for each human subject per measurement scenario for the reference Zephyr device and radar device are shown in Figures 28A-D reflects the SNR trends between the two devices (see the appendix). In Figure 28A, Subjects 1 and 5 showed contrasting trends in the SNR for the heart rate among all the participants where Subject 1 had the highest SNR for all the scenarios while Subject 5 had the least SNR for majority of the scenarios compared to others for the reference device. Again, it is unclear the causal factors of this significant trend and further investigations need to be done because both of them have the same height and circumferential diameter. In the same vein, high SNR values were dominant for all participants in the breathing signal than the heart rate in the different measurement scenarios indicative of high accurate measurement of the breathing signal by the radar device. In Figure 28B, a significant trend of high SNR for the heart rate observed on measurement scenario 7 for participants Subjects 3, 4, 5 implies that the backside with the range of 0 cm, azimuth angle of 180°, tilt angle of 0° and vertical height of 85 cm has good detectability. Furthermore, high SNR for the heart rate were recorded at the backside of the human subject having the azimuth angles of 135°, 180° and 225° at vertical heights of 85 cm, 130 cm, 150 cm with their respective tilt angles. The front side notable for good signal quality have the azimuth angle ranging from 0°, 45°, 90° and 270° with their corresponding parameters of measurement. These similar trends are observed in the remaining Figures 28C-D. However, the front side azimuth angle range of 315° with high SNR for measurement scenarios 5 and 21 only occurred for Subjects 2 and 3 with average heights of 168 cm and 172 cm respectively which implies that persons of average height will have good signal quality of the vital signs parameter detected within this angle. Figures 29 and 30 showed the averaged SNR of the vital signs parameter for all participants per measurement scenario with the notable peaks and valleys of occurrences of the signal quality replicating the inverse of CV of heart rate observed at measurement scenarios 7 and 15 as well as measurement scenarios 23 and 15 respectively for the breathing rate.
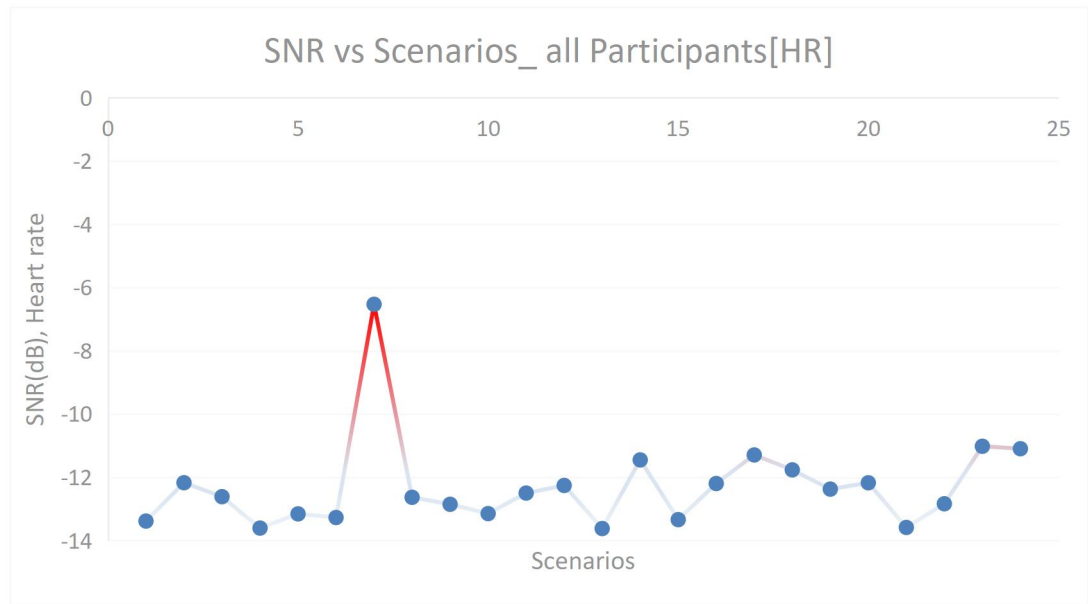
Figure 29. Averaged Signal to noise ratio per scenario of heart rate for all participants.
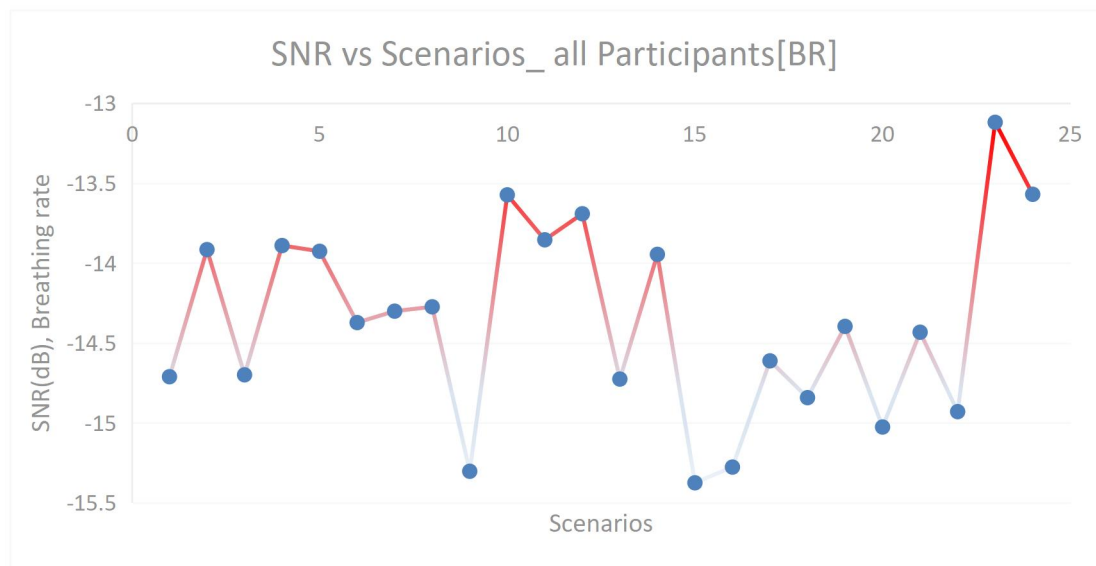

Figure 30. Averaged Signal to noise ratio per scenario of breathing rate for all participants.

In the data visualization of the SNR (dB) versus the angular orientation of the radar's different tilt angles, the measurement scenarios were grouped with respect to the corresponding parameters of measurement of azimuth angles and range which were constant while the vertical height of the radar device and the tilt angles varied. The plots of SNR (dB) versus tilt angle was performed in order to assess its impact on the measured physiological parameters from individual human subject. The measurement scenarios at the front side (1, 2, 3, 4, 5, 9, 10, 11, 12, 13, 17, 18, 19, 20, 21) and the back scenarios (6, 7, 8, 14, 15, 16, 22, 23, 24) witnessed an increasing trend in SNR in all the plots culminating at 30° tilt angle for Subjects 2, 3, 4, 5 with either Subject 2 or 3 having the highest SNR. However, Subject 1 mostly achieved a

high SNR at 45° tilt angle in majority of the plots. For example, in scenario 18 Subject 3 has the highest SNR at 30° tilt angle shown in Figure 31B (see appendices) with the parameters of measurement (azimuth: 45°, range: 80 cm, height of radar: 150 cm) whereas Subject 2 has the highest SNR at 30° tilt angle in scenario 11 with parameters of measurement (azimuth: 90°, range: 40 cm, height of radar: 130 cm), not shown here for concise presentation as similar trend was witnessed/replicated in all front scenarios. This implies that persons within the height range of 168 cm to 172 cm will have good signal quality at the front side compared to others. For the back scenarios, Subjects 2, 4 and 5 had the highest SNR at different tilt angles of 45°, 0° and 30°. Subject 2 had the highest SNR at 45° (scenario 22), Subject 4 at 0° (scenario 7) with a positive SNR, and Subject 5 at 30° (scenario 24). Exceptional cases were observed in the back scenarios. Again, for the sake of brevity, all figures could not be displayed here. However, a notable case is the occurrence of high positive SNR by Subject 4 in scenario 7 shown in Figure 31G (see appendices). This could be due to the characteristics of the subject as per RCS, anatomy and distribution of adipose tissue in the body. Hence, it can be inferred that tall persons will have better signal quality at the back compared to others since Subject 4 is the tallest in the group with the height of 178 cm. The SNR (dB) versus tilt angle plots for all participants reveal that the tilt angles ranging from 0° to 45° positively impacts with different magnitude in good signal quality on the captured vital signs parameter from each human subject irrespective of the other corresponding parameters of measurement. The SNR ranges from -15 dB to +5 dB. However, the general trend of highest signal quality is noticeable at tilt angle 30° for majority of the measurement scenarios for each participant with some few exceptions observed at tilt angles 0° or 45° respectively. This implies that the performance of the radar is largely hinged on the FOV captured by the radar device which is dependent on several factors such as the layout of the antenna patch on the printed circuit board, the position or location of the radar within the domiciled environment, the angular orientation of the radar and the system or chirp parameters that are tuned in the configuration files [89]. Another factor is the bore-sight of the radar which is the angular orientation of the radar at which the power received at the antenna is at its peak or highest magnitude which ideally occurs at 0° for azimuth and elevation angles respectively. The typical angles of the radar's bore-sight range from 20° to 30°. The FOV of the radar sensor array of antennas can be derived from the antenna spacing d which is equal to half of the carrier's wavelength. Thus, the FOV is highest at the range of $\pm\ 90^\circ$ [79]. The work in [36] asserts that angular resolution of the array of antennas of the radar device's bore-sight can be estimated as 29°. Apart from the antenna spacing, the antenna gain pattern also influences the detectability of an object (range resolution) from the radar at different angles such that ideally antennas would have a maximum gain at one angle, usually at 0° which is directly facing the front of the antenna and then the antenna gain will reduce as the angle increases. Therefore, alluding to the fact of good measurability at the frontal side of the human subject. The tilt angle which is related to the FOV such that 0° tilt angle which relates to 90° FOV has the highest SNR and as the tilt angle increases, the FOV of the radar decreases thereby affecting the SNR which in turn reduces the detection accuracy. Hence, the curved lines in the plots of SNR (dB) versus tilt angle such that at 30° (bore-sight angle) the highest power is received at the antenna.

4.6. Analysis of Boxplots

The boxplots for the 5 human subjects for all 24 measurement scenarios of the breathing rate and heart rate showed some consistency in lower values while high variability in higher values were observed with outliers in most measurement scenarios for the heart rate. However, the general range of the heart and breathing rates in all measurement scenarios for all participants lie within 40 to 120 bpm and 5 to 35 bpm respectively. Thus, these observed spread of the data correlates with resting heart and breathing rates in adults [67]. The measurement data is riddled with outliers that affected the measure of spread of the range and mean since the range relies on the minimum and maximum values in the dataset. In addition, there are similarities in the shape of the boxes and whiskers, the median and IQR for most of the scenarios show less to moderate overlapping of the median or boxes. An example is the boxplot of the physiological parameters for measurement scenario 20 for all participants shown in Figure 32 (see the appendix). The boxplot of the heart rate versus the individual human subject showed that the Subjects 1, 2 and 3 dataset are riddled with outliers which can be due to body movement but the Subjects 4 and 5 are without outliers. These outliers impacted on the measure of spread as the minimum or maximum values are taken as outliers since outliers are 1.5 times IQR either below/above the lower and upper quartiles respectively. The outliers in this case do not affect the median or the IQR which are robust because they depend on the upper and lower quartiles. The shape of the box and whisker are similar for Subjects 4 and 5 with same range and median but there is more variability in Subject 5. This implies that there is comparability or association between Subjects 4 and 5 in the heart rate values but the middle 50 % of Subject 5's data has more spread than Subject 4 which is consistent or precise. Similarly, Subjects 1 and 2 have the same median but different ranges of which Subject 1 has more spread and variability than Subjects 2 and 3. The Subjects 1, 2 and 3 have outliers which affected their ranges. Thus, the middle 50 % data of Subject 1 is more spread out than Subjects 2, 3 and their true accurate value is impacted by outliers. The median of Subjects 4 and 5 are 5 bpm more than Subject 2 which has the least spread of data and is 2 bpm more than Subject 3. Less overlapping of the median of two boxes means association and vice versa, so Subjects 1, 2, 3, 4 and 5 with less overlapping in the median or centers are associated which is indicative of similarity in the spread of the heart rate data.

 In like manner, the boxplot of the breathing rate showed outliers in Subjects 1 and 5 except for Subjects 2, 3, and 4. There is similarity in the IQR range for Subjects 1 and 4 as well as Subjects 1 and 3 with the exception of Subject 5 which has less variability. The shape of the box and whiskers are shorter at the lower values compared to the longer upper values so there is clustering or consistency in lower values. Subjects 4 and 5 have the same median while the median of Subject 2 is 5 bpm more than all the subjects having the highest median. Thus, there is comparability among the gender as there is less overlap of their median.

 There are few isolated cases in the boxplot for heart rate where the IQR is zero. An example is the measurement scenario 7 shown in Figure 33 (see the appendix). Subjects 1, 3, 4, 5 all have outliers with the exception of Subject 2. However, Subjects 3, 4 and 5 all have their IQR equal to zero, meaning that there is no variability or spread in the middle 50 % data. Therefore, the values of the middle 50 % data for the three subjects are identical. The interesting thing here is their position in the boxplot. Both Subjects 3 and 4 have heart rate values close to 120

bpm while Subject 5 has heart rate greater than 80 bpm. The heart rate of 120 bpm is indicative of heart problem or tachycardia but the participants are healthy adults, so it only showed that the radar device overestimated the high values of heart rate in Subjects 3, 4 and probably 5 which is greater than 80 bpm. However, Subjects 1 and 2 had variability in the middle 50 % with the median of Subject 1 higher than the median of Subject 2.

5. DISCUSSION

This research study seeks to provide insights and contribution towards driver vital signs monitoring in vehicular environments which would reduce injuries and deaths caused by road accidents with the possibility of harnessing smart vehicle monitoring of motorists. The vital signs monitoring of breathing rate and heart rate of a human being provides insights into the well-being and quality of life of an individual. Furthermore, the information is valuable to physicians as it holds the potential of providing adequate healthcare and increasing life expectancy as per early diagnosis of underlying medical conditions and clinical evaluation of diseases leading to timely interventions or treatment. The advantages of the millimeter wave radars in terms of contact-less sensing, convenience, privacy infringement mitigation, portability and high detection accuracy due to the high bandwidth makes them ideal for continuous monitoring of vital signs in vehicular environments. In recent times till present, there is still an on-going research focused on accurate estimation of vital signs in literature [5] to ameliorate the inherent challenges posed by radar sensing systems through the implementation of sophisticated signal processing algorithms, machine learning, hardware or sensor fusion [5, 31, 59] geared towards increasing the SNR and accuracy improvement. The discussion highlights the significance of the results alongside the limitations of results/study and future direction.

This study investigated the impact or effect of placement of radar sensor in angular orientation (tilt angles) on the accuracy of vital signs estimation from human subjects, validated the measured results by comparing the radar sensor with a reference device as well as comparing the results amongst the different gender. The main aim of the study has been achieved as per the findings, since it is yet to be documented in literature the positive impact of tilting the radar sensor to 30° can optimally increase the SNR which invariably improves measurement accuracy. As recommended in [69], the assessment of agreement between the two devices were performed in this study using the Bland Altman analysis alongside with the Pearson correlation coefficient for strength of association of the results obtained from both devices. The Bland Altman results presented showed good agreement levels between the FMCW radar sensor and reference device. Although proportional bias and outliers were observed in the scatterplots, the presence of outliers did not affect the measurement precision but it affected the accuracy as confirmed by the computation of the robust approach of overall median of mean deviations and limits of agreement of which results obtained fell within acceptable threshold of $\pm$ 5 bpm. The interchangeability or comparability of the radar device with the reference device and good measurement precision was validated by the computation of the confidence intervals of the mean deviation and limits of agreement with respect to the location of zero bias equivalence line falling within its region of breathing and heart rates. Thus, confirming the reliability of results obtained from the radar device and that it can be used in practice for continuous vital signs monitoring. The results of overall average for the heart rate and breathing rate for all participants used in the study were estimated at 77.18 bpm and 15.54 bpm respectively which falls within the adult range for heart rate and breathing rate [32, 67], correlating the results of 20 volunteers (10 females and 10 males) in an earlier study [90] which reported heart rate (77.827 bpm, 78.587 bpm) and breathing rate (19.23 bpm,19.959 bpm) respectively. Quality time is expended in commuting which can be harnessed for health checkups of the driver such that the extraction of the vital signs can be used

for the continuous monitoring of blood pressure since the resting heart rate has a positive correlation with peripheral or systolic blood pressure and a negative correlation with central blood pressure clinically used to evaluate heart/kidney related disorders [91]. This will go a long way in bridging the gap of intermittent measurement of blood pressure, whereby some salient events are missed. It will enhance effective blood pressure management and interventions. The vital signs parameters can be used for driver detection and identification which can be infused into Internet of Things devices for ubiquitous sensing or ADAS for health status monitoring. Machine learning algorithms can be used on the large pool of human target generated radar data to develop a model to accurately classify and detect health abnormalities as the dataset covers different nationalities as such the model will be generalisable. The model can be trained to classify changes in cardiac output in the different gender and developed as a wearable cardiac output sensor using the Google Soli miniaturized radar sensor [92] together with an algorithm to implement the mathematical estimation (stroke volume multiplied by heart rate) [93]. The results of the Pearson's correlation coefficient presented showed positive and negative linear relationship between the radar device and reference device for the vital signs in different measurement scenarios which can be factored to RCS, location of the heart differs from each subject and distribution of adipose tissue [83]. The differences in body type and height linked to RCS can be used for a classification system for group-related maladies. For example, apnoea is prevalent among elderly persons and children below five years [59], the negative correlation of height and cardio-vascular disorders poses height as a risk factor [94]. The negative heart-height association can be used to monitor heart rhythmic dysfunctionalities [95]. The computation of overall averaged correlation coefficient revealed weak positive correlation in both vital signs parameters with statistical significance in the breathing signal only. This trend is possibly due to the presence of outliers and correlation coefficient is highly sensitive to them. However, the correlation coefficient range from - 0.60 to + 0.60 was achieved for all of the participants which is by standard a moderately high correlation, although it would have been higher in the absence of outliers. Thus, correlating with higher accuracy rate reported by earlier studies [16, 17, 46, 49, 50, 51, 52, 58].

The low values of CV indicate high accuracy and vice versa. Thus, the results of the overall averaged CV presented showed low values of CV for all tilt angles (0°, 30°, 45°) in measurement scenarios 7 and 23 while scenario 15 has high value. These measurement scenarios are all referenced to the backside of the human subject (180° azimuth angle, 0 cm range) with the radar device at various vertical heights of 85 cm, 150 cm and 130 cm respectively. Since the backside is closest to the human target, then lower CV is expected. Raheel et al. [59], suggested that the SNR can be enhanced via mitigating the effects of signal-attenuation factors and optimizing the radar's location with reference to the backside. Apart from 180° azimuth angle, the radar sensor can be positioned at angles 135° or 225° at the back which showed low CV. Both the CV and SNR values presented showed the predominance of the breathing rate at the front side than the heart rate while the heart rate could reliably be measured from the front lateral sides and the back which resonates with the conclusion in [51]. Similarly, Berenschot [99] in his work, achieved better heart rate results from the lateral sides and higher breathing rate results from the front side of the human subject. Similar factors that affected the correlation coefficient are replicated here resulting in high CV. However, low CV were recorded in the front

side and in practice, the radar device can be positioned both at the front and back of the human target in a vehicle. The scenario 15 can have low CV at tilt angle 30º with a wider field of view than at the current tilt angle of 45º.

The results of the SNR presented, inversely replicated the trends in CV. However, the visual plots of the SNR versus tilt angle presented showed the curved or parabolic line with a peak at 30º tilt angle in majority of the measurement scenarios with some exceptions at 0º and 45º respectively. Thus, optimal SNR is achieved when the radar device is tilted to 30º (radar's bore-sight). The range of the SNR for all the tilt angles and all the participants is estimated at -15 dB to + 5 dB. The placement or positioning of the radar sensor at the 30º tilt angle irrespective of the range and vertical height increases the SNR which affects the range resolution/detection accuracy and ultimately improves the accuracy of the vital signs estimation. Although, it is widely assumed that the directionality of the radar affects accuracy but in [46, 83], this assumption is disproved since the radar's FOV accommodates a wide area of the body surface as such the directionality or specific aligning of the antenna is inconsequential. Thus, the tilt angles which relates to the FOV of radar device has affirmed this assertion. The radar sensor can be integrated in a smart/biometric seat positioned at a tilt of 0º/30º at the back/headrest respectively. In future work, the radar device positioned at rear view mirror and tilted to 30º will be used in real-life driving scenario as line of sight issues are reduced and accuracy is improved. An audacious thinking might be to have an AI robotic arm fitted with the radar device inside the vehicle to detect, identify and map the human parameters of the driver to optimal tilt angle for vital signs monitoring.

The results of the error analysis presented showed that the breathing rate had better performance metrics compared to the heart rate with error rate of 5.75 bpm and 13.14 bpm respectively. Heart rate signals are weak and easily affected by breathing harmonics or body movements which impacts on their accuracy. Interestingly, the MAPE metrics gave a conflicting result that needs to be investigated. The small margin of error between the MAE/MAD and RMSE showed less variability in the observations between the two devices. Comparatively, the accuracy measures obtained in this study were poor with reference to some related work that reported lower error rates of under 3 bpm [43].

The results of the boxplot analysis showed association or comparability among the different gender using the key indices of range and IQR for the analysis. Thus, the analysis showed that the normal adult range for vital signs were obtained in majority of the scenarios with very few exceptions of very high pulse rate close to 120 bpm in some subjects which can be due to stress or systematic errors of overestimation of the high values from the radar device.

The limitation of the results are largely observed as outliers which can be due to several factors such as movement of the body during measurement as it is not convenient to maintain a static position for sometime period which is being required in the experiment. Thus, the presence of outliers were prevalent in the dataset, thereby negatively impacting on the accuracy, Bland Altman analysis, correlation results and so on. It has been proven in literature that the FFT algorithm is inadequate for the accurate estimation of heart rate in real-life driving scenarios [43], as it achieved less accuracy than the MUSIC algorithm used by the authors. Currently, the arctangent demodulation and FFT algorithms are implemented in the signal processing chain of the TI FMCW radar, so for future work, the chirp system parameters will be optimized and MUSIC algorithm implemented at the receiver side

to extract the vital sign parameters or the robust modified DACM algorithm (which is non-dependent on distance and amplitude) will be implemented in real-life driving scenario. Also, the radar sensor with the modified DACM algorithm will be used for home sleep monitoring at far distance of 5 m [59] alongside with communication gadget in the same frequency range to validate its compatibility. Furthermore, giving one of the setbacks of the MAPE performance metric of imploding on low or small datasets, it will be interesting to use this accuracy metric in future work on larger datasets to test the veracity of the assertion of inaccurate breathing rate at higher frequencies.

   The limitation of the study are numerous which include small sample size, reference device used, a single radar sensor, a chair, protractor, 3 m measuring tape, measurement setup and procedure. The sample size of 5 persons were used in the study but there is variability in the dataset comprising of diverse backgrounds of 2 Europeans (male & female), 2 Africans (male & female) and 1 Asian (male). However, a larger sample size will be sufficient for either artificial intelligence or machine learning algorithms to be used to train a model. So going forward, there will be proper planning and advertisement on the study in order to recruit more volunteers. Another important aspect is the sample analysis that must be computed to ascertain the sample size required for the Bland Altman plot analysis before embarking on the experiment which is relevant for determination of accurate measurement. The relative average height used in the study can not be for wide population conclusions as the height bracket did not include the two extremes of short or tall persons. Also, the participants were without any medical condition so dataset cannot be used to train a model for pattern recognition of some medical disorders.

   The reference Zephyr module is a wellness device used by professional athletes. Thus, it is not a medical grade device which would have improved the validation of the outcomes of this study. The charging time of the battery is 3 hours for longer use, so i had to charge the battery overnight after the experience of flat battery with the first human subject. A medical grade device(s) or clinically validated commercial off the shelf Hexoskin will be used in aforementioned future directions.

   The measurement setup and procedure required the human subject to be stationary during measurement of 2 to 3 minutes each which is quite a difficult task to achieve. A close eye was kept on the volunteers to monitor compliance to the instruction. Unfortunately, some measurements had to be repeated twice because of large body movement from the human subject which made the measurement duration to go a little over the stipulated 2 hours period. A single radar device connected to a laptop was used for the 24 measurement scenarios which involved intermittent adjustment of the radar device mounted on a tripod to the different parameters of measurement (range, vertical height and azimuthal angle). A protractor was used to estimate the tilt angles to which the mounted radar device was to be tilted. However, a measuring tape with laser light will be used in future to conveniently aid accurate centering and measurement. Since the mounted radar device connected to the laptop cannot conveniently be moved around the human subject mimicking the azimuthal angles in clockwise direction of 0º, 45º, 90º, 135º, 180º, 225º, 270º, 315º, 360º/0º, the human subject was adjusted into those angular positions. In order to accommodate all these movements, some markings had to be made to account for the azimuthal angles. Hence, a chair (differs in dimension to car seat) was used for the experiment because it would have been very inconvenient using a car seat as the volunteer must stand up for the car seat to be adjusted for each measurement scenario. These setbacks can

introduce errors in measurement due to the approximations of the parameters. A man-machine interface in form of virtual reality or simulator can be developed using computer graphics and machine vision to overcome the challenges of the intermittent adjustment of human subject and a single radar device in the laboratory. Alternatively, for future work as mentioned in [40] four radar devices can be used to capture four body postures (front, back, left side and right side) and superimposing the FFTs in a laptop.

6. CONCLUSION

This research highlights the study of driver's vital signs monitoring using millimeter wave radar device for vehicular environment. The results obtained from the radar sensor and reference device were compared, the impact or effect of the radar's location and azimuthal or angular orientation on the physiological parameters were assessed as well as the comparison of the results of the breathing rate and heart rate among the different gender. The 24 measurement scenarios captured during measurement of the human subjects were pre-processed with the bandpass filter of 0.1 to 0.6 Hz and 0.8 to 4.0 Hz respectively. The peak interval and FFT algorithms were applied for the extraction of the vital signs estimation.

The SNR is affected by the chirp duration, bandwidth, transmitted power, FOV of radar device and the RCS which reduces the received power. This study has demonstrated that the depression/tilt angles of 0º, 30º and 45º of the angular orientation of the radar device which is related to the FOV also influences the SNR which is evident in the range of -15 dB to +5 dB obtained. The slim marginal error between the MAE/MAD and RMSE metrics further validates the positive impact of the tilt angles in the measurement accuracy of the vital signs estimation. However, majority of the measurement scenarios irrespective of the parameters of measurement showed high signal quality of the vital signs parameters at 30º tilt angle which is related to the bore-sight of the radar device. The line of sight common challenge of the radar system can be resolved by the radar's tilt angle resolution of 30º. In addition, it has disproved the norm of directionality of the radar device to the chest as a pivotal factor for achieving accuracy because the tilt angle is related to the FOV which affects the SNR and the SNR influences the range resolution for detection accuracy.

The strength of this study is that it is yet to be documented in literature the impact or effect of the angular orientation of the radar device with respect to the depression or tilt angles on the measured physiological parameters from human subjects. Furthermore, the new finding observed with respect to the decline of the breathing rate accuracy with higher frequencies as time progresses needs to be investigated if the radar device is to be used for continuous monitoring and premium is placed on accuracy. Limitation of the study is visible in the sample size and outliers which affected the measurement accuracy, as well as the reference Zephyr device which is a wellness device yet to be clinically evaluated and validated. In addition, the system parameters has to be adjusted with optimal settings in order to achieve higher performance of accuracy.

In future work, the Hexoskin wearable device can be used for comparability studies with the radar device to validate the feasibility of the radar sensor to be used in clinical setting or environment. The power analysis for the sample size estimation for Bland Altman analysis will be performed to have good measurement accuracy.

The modified optical-based (DACM) signal processing algorithm is quite robust against disparities in various range of RFs which impacts positively on high measurement detection accuracy and the optimum SNR attained at tilt angle of 30º related to the radar's bore-sight irrespective of the corresponding parameters of measurement resolves the line of sight challenges suffices as potential solution to the deployment of the millimeter wave frequency radar device in vehicular environment for proactive and preventative healthcare.

7. REFERENCES

[1] Wang J., Warnecke J. M., Haghi M., & Deserno T. M.(2020) Unobstrusive health monitoring in private spaces: The Smart Vehicle. Sensors, 20(9), 2442. URL: https://doi.org/10.3390/s20092442

[2] Gharamohammadi A., Khajepour A., & Shaker G.(2023) In-vehicle monitoring by Radar: A Review. IEEE Sensors Journal. URL: https://doi.org/10.1109/JSEN.2023.3316449

[3] Taylor A. H., & Dorn L.(2006) Stress, fatigue, health and risk of road traffic accidents among professional drivers: the contribution of physical inactivity. Annual review of public health, 27, 371-391. URL: https://doi.org/10.1146/annurev.publhealth.27.021405.102117

[4] World Life Expectancy. URL: https://www.worldlifeexpectancy.com Accessed on 28th May 2024.

[5] Leonhardt S., Leicht L., & Teichmann D.(2018) Unobstrusive Vital Sign monitoring in Automotive Environments- A Review. Sensors, 18(9), 3080. URL: https://doi.org/10.3390/s18093080

[6] Fei J., & Pavlidis I.(2007) Visual thermistor. Annual International Conference of the IEEE Engineering in Medicine and Biology Society. IEEE Engineering in Medicine and Biology Society. Annual International Conference, 2007, 250-253. URL: https://doi.org/10.1109/IEMBS.2007.4352271

[7] Fei J., & Pavlidis I.(2010) Thermistor at a distance: unobtrusive measurement of breathing. IEEE Transactions on Bio-medical Engineering, 57(4), 988-998. URL: https://doi.org/10.1109/TBME.2009.2032415

[8] Adiprabowo T., Wang T. H., & Lin D. B.(2019) 77GHz FMCW Radar based Simultaneous Vital Signs Measurements. In 2019 IEEE Conference on Antenna Measurements & Applications(CAMA), 1-3. IEEE.

[9] Leem S. K., Khan F., & Cho S. H.(2017) Vital Sign Monitoring and Mobile Phone Usage Detection Using IR-UWB Radar for intended use in car crash prevention. Sensors. (Basel, Switzerland), 17(6), 1240. URL: https://doi.org/10.3390/s17061240

[10] History of Radar. URL: https://en.wikipedia.org/wiki/History_of_radar Accessed on 28th May 2024.

[11] Radar and Sonar. URL: https://www.history.navy.mil/browse-by-topic/exploration-and-innovation/radar-sonar.html Accessed on 28th May 2024.

[12] Caro C. G., & Bloice J. A.(1971) Contactless apnoea detector based radar. Lancet(London, England), 2(7731), 959-961. URL: https://doi.org/10.1016/s0140-6736(71)90274-1

[13] Vinci G., Lenhard T., Will C., & Koelpin A.(2015) Microwave Interferometer radar-based vital sign detection for driver monitoring systems. In Proceedings of the IEEE MTT-S International Conference on Microwaves for Intelligent Mobility(ICMIM), Heidelberg, Germany 2015. pp. 1-4. URL: https://doi.org/10.1109/ICMIM.2015.7117940

[14] Mallat N. K., Ishtiaq M., Ur Rehman A., & Iqbal A.(2020) Millimeter-Wave in the Face of 5G Communication Potential Applications. IETE Journal of Research, 68(4), 2522-2530. URL: https://doi.org/10.1080/03772063.2020.1714489

[15] Kotecha H., & Mundarath J. C.(2019) Method and Apparatus for Fast Wireless Communication Systems. CA, USA: Google Patents, 2019.

[16] Dai T. K. V., Oleksak K., Kvelashvili T., Foroughian F., Bauder C., Theilmann P., Fathy A. E., & Kilic O.(2021) Enhancement of Remote Vital Sign Monitoring Detection Accuracy Using Multiple-Input Multiple-Output 77GHz FMCW Radar. IEEE Journal of Electromagnetics, RF and Microwaves in Medicine and Biology, 6(1), 111-122.

[17] Yang Z., Bocca M., Jain V., & Mohapatra P.(2018) Contactless Breathing Rate Monitoring in Vehicle Using UWB Radar, in Proceedings of the 7th International Workshop on Real-World Embedded Wireless Systems and Networks, in RealWSN'18. New York, NY, USA: Association for Computing Machinery, 13-18. URL: https://doi.org/10.1145/3277883.3277884

[18] Road Traffic Injuries. URL: https://www.who.int/news-room/facts-sheets/detail/road-traffic-injuries Accessed on 28th May 2024.

[19] Bhatta N. P., & GeethaPriya M.(2017) Radar and its Applications. IJCTA, 10(03), pp. 1-9. International Science Press. URL: https://www.researchgate.net/publication/316696944_RADAR_and_its_applications Accessed on 28th May 2024.

[20] The Ultimate Guide to Radar Sensor. URL: https://hardwarebee.com/the-ultimate-guide-to-radar-sensor Accessed on 25th March 2024.

[21] What is a Radar Sensor: Working & Its Applications. URL: https://www.elprocus.com/radar-sensor Accessed on 25th March 2024.

[22] Innovative Radar Technology. URL: https://www.innosent.de/en/radar Accessed on 25th March 2024.

[23] Electromagnetic spectrum- Wikipedia, the free encyclopedia. URL: https://en.wikipedia.org/wiki/Electromagnetic_spectrum Accessed on 28th May 2024.

[24] Introduction to the Electromagnetic Spectrum. URL: https://science.nasa.gov/ems/01_intro/ Accessed on 28th May 2024.

[25] What is millimeter wave(mmWave)? URL: https://www.techtarget.com/searchnetworking/definition/millimeter-wave-MM-wave Accessed on 28th May 2024.

[26] What are mmWaves or millimeter waves? URL: https://www.everythingrf.com/community/what-are-millimeter-waves Accessed on 28th May 2024.

[27] Lawrence N., Ng B., Hansen H., & Abbott D.(2017) 5G Terrestrial Networks: Mobility and Coverage-Solution in Three Dimensions. IEEE Access. 5. 8064-8093. URL: https://doi.org/10.1109/ACCESS.2017.2693375

[28] Radar Frequency bands. URL: https://www.pepperl-fuchs.com/global/en/51480.htm Accessed on 28th May 2024.

[29] Chen P. -Y., Lin H. -Y., Zhong Z. -H., Pai N. -S., Li C. -M., Lin C. -H.(2024) Contactless and Short-range Vital Signs Detection with Doppler Radar Millimeter-wave(76 to 81 GHz) sensing firmware. Healthcare Technology Letters. 1-10(2024). URL: https://doi.org/10.1049/htl2.12075

[30] An Overview of Frequency Bands and Their Applications. URL: https://resources.pcb.cadence.com/blog/2022-an-overview-of-frequency-bands-and-their-applications Accessed on 28th May 2024.

[31] Soumya A., Krishna Mohan C., & Cenkeramaddi L. R.(2023) Advances in mmWave-Radar-Based Sensing, Its Applications and Machine Learning Techniques: A Review. Sensors(Basel, Switzerland), 23(21), 8901. URL: https://doi.org/10.3390/s23218901

[32] Kebe M., Gadhafi R., Mohammad B., Sanduleanu M., Saleh H., & Al-Qutayri M.(2020) Human Vital Signs Detection Methods and Potential Using Radars: A Review. Sensors, 20(5), 1454. URL: https://doi.org/10.3390/s20051454

[33] Bin Obadi A., Soh P. J., Aldayel O., Al-Doori M. H., Mercuri M., & Schreurs D.(2021) A Survey on Vital Signs Detection Using Radar Techniques and Processing With FPGA Implementation, in IEEE Circuits and Systems Magazine, vol. 21, no. 1, 41-74, First quarter 2021. URL: https://doi.org/10.1109/MCAS.2020.3027445

[34] ISM radio band- Wikipedia, the free encyclopedia. URL: https://en.wikipedia.org/wiki/ISM_radio_band (Accessed on 10 February 2024)

[35] Iovescu C., & Rao S.(2017) The Fundamentals of millimeter wave sensors. Texas Instruments, May 2017.

[36] Li X., Wang X., Yang Q., & Fu S.(2021) Signal Processing for TDM MIMO FMCW millimeter-wave radar sensors. IEEE Access, 9, 167959-167971. URL: https://doi.org/10.1109/ACCESS.2021.3137387

[37] Medical Device Depot- Vital Signs Monitors. URL: https://www.medicaldevicedepot.com/Vital-Signs-Monitors-s/259.htm Accessed on 28th May 2024.

[38] Aerosense Wavve Elderly Care System. URL: https://www.ax-end.com/product/hub Accessed on 28th May 2024.

[39] Vital Signs Monitoring. URL: https://www.gftechnovation.com.hk/en/smart-care/vital-sensor Accessed on 28th May 2024.

[40] Radar Sensors. URL: https://www.infineon.com/cms/en/product/sensor/radar-sensors Accessed on 28th May 2024.

[41] Precise Vital Signs Monitoring Powered by Radar Technology. URL: https://xkcorp.com/products/health-care/xk-300 Accessed on 28th May 2024.

[42] Vorobyov A., Daskalaki E., Roux E. L., Farserotu J., & Dallemagne P.(2020) Contactless Vital Signs Sensing: A survey, preliminary results and challenges, 2020 XXXIIIrd General Assembly and Scientific Symposium of the International Union of Radio Science, Rome, Italy, 2020. IEEE, pp. 1-4. URL: https://doi.org/10.23919/URSIGASS49373.2020.9232160

[43] Lee K. J., Park C., & Lee B.(2016) Tracking driver's heart rate by continuous-wave Doppler radar. Annual International Conference of the IEEE Engineering in Medicine and Biology Society. IEEE Engineering in Medicine and Biology Society. Annual International Conference, 2016, 5417-5420. URL: https://doi.org/10.1109/EMBC.2016.7591952

[44] Izumi S.(2017) A contactless heart rate sensor system for driver health monitoring.Available[Online]:https://pdfs.semanticscholar.org/9059/6a41f8642c5854f88e02a3e121a151747434.pdf

[45] Fathy A. E., Ren L., Nahar S., & Kilic O.(2017) Overview of Human Vital Signs Detection Using Radar Techniques, in 2017 IEEE International Symposium on Antennas and Propagation & USNC/URSI National Radio Science Meeting, 1229-1230. IEEE. URL: https://doi.org/10.1109/APUSNCURSINRSM.2017.8072657

[46] Park J. K., Hong Y., Lee H., Jang C., Yun G. H., Lee H. J., & Yook J. G.(2019) Noncontact RF Vital Sign Sensor for Continuous Monitoring of Driver Status. IEEE Transactions on Biomedical Circuits and Systems, 13(3), 493-502. URL: https://doi.org/10.1109/TBCAS.2019.2908198

[47] Model 1010 Piezoelectric Pulse Transducer. URL: https://www.ufiservingscience.com/model_1010.html Accessed on 28th May 2024.

[48] UFI Model 1132 Pneumotrace II™. URL: https://www.ufiservingscience.com/model_1132.html Accessed on 28th May 2024.

[49] Fang G. W., Huang C. Y., & Yang C. L.(2020) Switch-based Low Intermediate Frequency System of a Vital Sign Radar for Simultaneous Multitarget and Multidirectional Detection. IEEE Journal of Electromagnetics, RF and Microwaves in Medicine and Biology, 4(4), 265-272. URL: https://doi.org/10.1109/JERM.2020.2969100

[50] Xiao Y., Lin J., Boric-Lubecke O., & Lubecke M.(2006) Frequency-tuning Technique for Remote Detection of Heartbeat and Respiration using Low-power Double-SideBand Transmission in the Ka-band. IEEE Transactions on Microwave Theory and Techniques, 54(5), 2023-2032. URL: https://doi.org/10.1109/TMTT.2006.873625

[51] Chuang H. R., Kuo H. C., Lin F. L., Huang T. H., Kuo C. S., & Ou Y. W.(2011) 60-GHz Millimeter-wave Life Detection System(MLDS) for Noncontact Human Vital-Signal Monitoring. IEEE Sensors Journal, 12(3), 602-609. URL: https://doi.org/10.1109/JSEN.2011.2118198

[52] Ma X., Wang Y., Lu L., Zhang X., Chen Q., You X., Lin J., & Li L.(2020) Design of a 100-GHz Double-SideBand Low-IF CW Doppler Radar Transceiver for Micrometer Mechanical Vibration and Vital Sign Detection. IEEE Transactions on Microwave Theory and Techniques, 68(7), 2876-2890. URL: https://doi.org/10.1109/TMTT.2020.2981613

[53] Butterworth Filters. Wikipedia, the free encyclopedia. URL: https://en.wikipedia.org/wiki/Butterworth_filter Accessed on 28th May 2024.

[54] Butterworth Filter: What is it?(Design and Applications). URL: https://www.electrical4u.com/butterworth-filter/ Accessed on 28th May 2024.

[55] Wang J., Wang X., Chen L., Huangfu J., Li C., & Ran L.(2013) Noncontact Distant and Amplitude-Independent Vibration Measurement Based on an Extended DACM Algorithm, in IEEE Transactions on Instrumentation and Measurement, vol. 63, no. 1, pp. 145-153. URL: https://doi.org/10.1109/TIM.2013.2277530

[56] van Berlo B., Elkelany A., Ozcelebi T., & Meratnia N.(2021) Millimeter Wave Sensing: A Review of Application Pipelines and Building Blocks, in IEEE Sensors Journal, vol. 21, no. 9, pp. 10332-10368. URL: https://doi.org/10.1109/JSEN.2021.3057450

[57] Wang G., Munoz-Ferreras J. M., Gu C., Li C., & Gomez-Garcia R.(2014) Application of Linear-Frequency-Modulated Continuous-Wave(LFMCW) Radars for Tracking of Vital Signs, in IEEE Transactions on Microwave Theory and Techniques, vol. 62, no. 6, pp. 1387-1399. URL: https://doi.org/10.1109/TMTT.2014.2320464

[58] Alizadeh M., Shaker G., De Almeida J. C. M., Morita P. P., & Safavi-Naeini S.(2019) Remote Monitoring of Human Vital Signs Using mm-Wave FMCW

Radar. IEEE Access, 7, 54958-54968. URL: https://doi.org/10.1109/ACCESS.2019.2912956

[59] Raheel M. S., Tubbal F., Raad R., Ogunbona P., Coyte J., Patterson C., Perlman D., Iranmanesh S., Odeh N., & Foroughi J.(2024) Contactless Vital Sign Monitoring Systems: A Comprehensive Survey of Remote Health Sensing for Heart rate and Respiration in Internet of Things and Sleep Applications. Available[Online]: http://dx.doi.org/10.1039/D4SD00073K

[60] Lazaro A., Girbau D., & Villarino R.(2010) Analysis of Vital Sign Monitoring Using an IR-UWB Radar. Available[Online]: https://www.researchgate.net/publication/270083592 Accessed on 4th June 2024.

[61] Analyzing The Mathematical Properties of Triangular Waves. URL: https://fastercapital.com/topics/analyzing-the-mathematical-properties-of-triangular-waves.html Accessed on 6th June 2024.

[62] TI mmWave Device Documentation, Texas Instruments, 2024. URL: https://dev.ti.com/tirex/explore/node Accessed on 6th June 2024.

[63] Zephyr BioHarness User Manual. URL: https://www.manualslib.com/products/Zephyr-Bioharness-13364461.html Accessed on 6th June 2024.

[64] Triangulation. Wikipedia, the free encyclopedia. URL: https://en.wikipedia.org/wiki/Triangulation Accessed on 28th May 2024.

[65] Triangulation trigonometry. URL: https://www.britannica.com/science/triangulation-trigonometry Accessed on 28th May 2024.

[66] Triangulation Calculation. URL: https://homework.study.com/explanation/complete-a-triangulation-calculation-to-measure-the-distance-between-actual-objects-in-or-near-your-home-include-a-well-labeled-diagram.html Accessed on 6th June 2024.

[67] TI mmWave Labs-Driver Vital Signs- Developer's Guide, Texas Instruments, 2024. URL: https://dev.ti.com/tirex/explore/node?node=A__ADZIzSoqYpsJx3iqoalh2A__com.ti.mmwave_automotive_toolbox__AocYeEd__LATEST Accessed on 6th June 2024.

[68] Bland J. M., & Altman D. G.(1999) Measuring Agreement in Method Comparison studies. Statistical methods in medical research, 8(2), 135-160. URL: https://doi.org/10.1177/096228029900800204

[69] Giavarina D.(2015) Understanding Bland Altman Analysis. Biochemia medica, 25(2), 141-151. URL: https://doi.org/10.11613/BM.2015.015

[70] ANSI/AAMI. Cardiac monitors, Heart rate meters and Alarms. Arlington: American National Standards Institute, Incorporated 2002.

[71] Pearson Product-Moment Correlation. URL: https://statistics.laerd.com/statistical-guides/pearson-correlation-coefficient-statistical-guide-2.php Accessed on 15th March 2024.

[72] Mean Absolute Percentage Error. Wikipedia, the free encyclopedia. URL: https://en.wikipedia.org/wiki/Mean_absolute_percentage_error Accessed on 6th June 2024.

[73] Mean Absolute Percentage Error(MAPE): What you need to know. URL: https://arize.com/blog-course/mean-absolute-percentage-error-mape-what-you-need-to-know/ Accessed on 6th June 2024.

[74] Mean Absolute Error. Wikipedia, the free encyclopedia. URL: https://en.wikipedia.org/wiki/Mean_absolute_error Accessed on 6th June 2024.

[75] Mean Absolute Error(MAE) and Root Mean Square Error(RMSE). URL: https://resources.eumetrain.org/data/4/451/english/msg/ver_cont_var/uos3/uos3_ko1.htm Accessed 6th June 2024.

[76] Coefficient of Variation- Wikipedia, the free encyclopedia. URL: https://en.wikipedia.org/wiki/Coefficient_of_variation Accessed on 15th March 2024.

[77] Thangjai W., & Niwitpong S. A.(2020) Confidence Intervals for Common Signal-to-noise-ratio of Several Log-Normal Distributions. Iranian Journal of Science and Technology, Transactions A: Science, 44(1), 99-107. URL: https://doi.org/10.1007/s40995-019-00793-3 Accessed on 15th March 2024.

[78] Signal-to-noise-ratio. URL: https://www.techtarget.com/searchnetworking/definition/signal-to-noise-ratio Accessed on 15th March 2024.

[79] Dham V.(2020) Programming Chirp Parameters in TI Radar Devices, Texas Instruments, Dallas Texas USA. Application Report SWRA553A, February 2020. URL: https://www.ti.com/lit/an/swra553a/swra553a.pdf? Accessed on 15th March 2024.

[80] Boxplot. Wikipedia, the free encyclopedia. URL: https://en.wikipedia.org/wiki/Box_plot Accessed on 15th March 2024.

[81] Lu M. J., Zhong W. H., Liu Y. X., Miao H. Z., Li Y. C., & Ji M. H.(2016) Sample size for Accessing Agreement between Two methods of Measurement by Bland-Altman Method. The International Journal of Biostatistics, 12(2). URL: https://doi.org/10.1515/ijb-2015-0039

[82] MedCalc Manual: t-distribution table(two tailed test). URL: https://www.medcalc.org/manual/t-distribution-table.php Accessed on 15th March 2024.

[83] Shi K., Schellenberger S., Will C., Steigleder T., Michler F., Fuchs J., Weigel R., Ostgathe C., & Koelpin A.(2020) A dataset of Radar-Recorded Heart sounds

and Vital Signs Including Synchronised Reference Sensor Signals. Scientific Data, 7(1), 50. URL: https://doi.org/10.1038/s41597-020-0390-1

[84] Confidence Interval for a Correlation Coefficient. URL: https://www.statology.org/confidence-interval-correlation-coefficient/ Accessed on 15th March 2024.

[85] Bakhtiari S., Elmer T. W., Cox N. M., Gopalsami N., Raptis A. C., Liao S., Mikhelson I., & Sahakian A. V.(2011) Compact Millimeter-wave sensor for Remote Monitoring of Vital Signs. IEEE Transactions on Instrumentation and Measurement, 61(3), 830-841. URL: https://doi.org/10.1109/TIM.2011.2171589

[86] Tariq A.(2012) Vital Signs Monitoring Using Doppler Radar and on-Body Antennas. Ph.D Thesis. URL: https://etheses.bham.ac.uk/id/eprint/4332/1/Tariq13Ph.D.pdf Accessed on 20th March 2024.

[87] Hahnen C., Freeman C. G., Haldar N., Hamati J. N., Bard D. M., Murali V., Merli G. J., Joseph J. I., & van Helmond N.(2020) Accuracy of Vital Signs Measurements by a Smartwatch and a portable Health Device: Validation Study. JMIR mHealth and uHealth, 8(2), e16811.

[88] Liu K., Ding C., & Zhang Y.(2020) A Coarse-to-Fine Robust Estimation of FMCW Radar Signal for Vital Sign Detection. In 2020 IEEE Radar Conference(RadarConf20), 1-6. IEEE.

[89] Best Practices for Placement and Angle of mmWave Radar Devices, Texas Instruments, Dallas Texas USA. Application Brief SWRA758, January 2023. URL: https://www.ti.com/lit/ab/swra758/swra758.pdf? Accessed on 28th May 2024.

[90] Srihari P., s Vandana G., & s Raghavendra B.(2021) Measurement and Evaluation of Human Vital Sign Using 77GHz AWR1642 FMCW Radar Sensor. In 2021 IEEE 18th India Council International Conference(INDICON), 1-5. IEEE.

[91] Reule S., & Drawz P. E.(2012) Heart rate and Blood pressure: Any possible implications for management of Hypertension?. Current Hypertension reports, 14(6), 478-484. URL: https://doi.org/10.1007/s11906-012-0306-3

[92] J. Zhang et al.,(2023) A Survey of mmWave-Based Human Sensing: Technology, Platforms and Applications, in IEEE Communications Survey & Tutorials, vol.25, no. 4, pp. 2052-2087, Fourthquarter 2023.

[93] Koenig J., Hill L. K., Williams D. P., & Thayer J. F.(2015) Estimating cardiac output from blood pressure and heart rate:The liljestrand & zander formula. Biomedical sciences instrumentation, 51, 85-90.

[94] Smulyan H., Marchais S. J., Pannier B., Guerin A. P., Safar M. E., & London G. M.(1998) Influence of body height on pulsatile arterial hemodynamic data.

Journal of the American College of Cardiology, 31(5), 1103-1109. URL: https://doi.org/10.1016/s0735-1097(98)00056-4

[95] Infeld M., Avram R., Wahlberg K., & Silverman D.(2020) An Approach towards Individualized Lower Rate Settings for Pacemakers. Available[Online]: https://www.researchgate.net/publication/344588799_An_Approach_towards_Individualized_Lower_Rate_Settings_for_Pacemakers Accessed on 8th June 2024.

[96] Bell M. L., Teixeira-Pinto A., McKenzie J. E., & Olivier J.(2014) A myriad of methods: Calculated Sample size for Two proportions was dependent on the choice of sample size formula and software. Journal of Clinical Epidemiology, 67(5), 601-605. URL: https://doi.org/10.1016/j.jclinepi.2013.10.008

[97] Bland J. M.(2004) How can I decide the sample size for a study of agreement between two methods of measurement? URL: https://www-users.york.ac.uk/~mb55/meas/sizemeth.htm Accessed 5th March 2024.

[98] Zhang X., Yang C., Xiao Z., Lu B., Zhang J., Li J., & Liu C.(2023) A novel target state detection method for accurate cardiopulmonary signal extraction based on FMCW radar signals. Frontiers in Physiology, 14, 1206471. URL: https://doi.org/10.3389/fphys.2023.1206471

[99] Berenschot L.(2022) Vital signs monitoring with an FMCW MMwave radar sensor. Available[Online]: http://essay.utwente.nl/91720/1/Berenschot_BA_EEMCS.pdf Accessed on 7th June 2024.

8. APPENDICES

Appendix 1.

Table 6. Computation of the overall mean deviations and limits of agreement (HR)

Scenarios	Bland Altman Parameters	Subject1	Subject2	Subject3	Subject4	Subject5	Average
Scenario1	Bias HR	-2.149	-5.049	8.541	4.894	-12.834	-1.3194
	ULOA HR	31.063	25.306	46.43	39.462	31.566	34.7654
	LLOA HR	-35.361	-35.404	-29.348	-29.674	-57.235	-37.4044
Scenario2	Bias HR	-5.535	-0.25	2.078	-17.276	-1.871	-4.5708
	ULOA HR	28.009	23.799	17.623	18.703	33.169	24.2606
	LLOA HR	-39.079	-24.3	-13.466	-53.256	-36.911	-33.4024
Scenario3	Bias HR	-1.668	2.882	2.364	-7.532	-14.548	-3.7004
	ULOA HR	30.934	21.413	43.976	30.562	34.671	32.3112
	LLOA HR	-34.27	-15.648	-39.247	-45.628	-63.769	-39.7124
Scenario4	Bias HR	5.265	-3.908	-5.643	13.114	-1.095	1.5466
	ULOA HR	40.806	29.946	28.878	41.192	30.378	34.24
	LLOA HR	-30.275	-37.763	-40.164	-14.964	-32.568	-31.1468
Scenario5	Bias HR	7.254	-11.144	4.335	-15.906	-13.583	-5.8088
	ULOA HR	42.735	30.078	32.349	28.736	15.135	29.8066
	LLOA HR	-28.226	-52.368	-23.679	-60.55	-42.301	-41.4248
Scenario6	Bias HR	15.951	-5.344	30.684	-10.034	-18.879	2.4756
	ULOA HR	55.788	39.738	54.677	45.543	25.496	44.2484
	LLOA HR	-23.884	-50.428	6.691	-65.612	-63.256	-39.2978
Scenario7	Bias HR	-18.117	-12.567	-41.174	-37.038	-10.366	-23.8524
	ULOA HR	16.901	24.021	-16.738	-20.205	15.737	3.9432
	LLOA HR	-53.136	-49.157	-65.61	-53.871	-36.47	-51.6488
Scenario8	Bias HR	-30.217	-4.524	15.93	-13.533	-9.058	-8.2804
	ULOA HR	-6.449	21.613	51.131	32.431	30.052	25.7556
	LLOA HR	-53.985	-30.662	-19.27	-59.498	-48.168	-42.3166
Scenario9	Bias HR	-24.414	-25.183	10.288	-11.428	-12.172	-12.5818
	ULOA HR	6.278	17.722	35.646	32.208	23.332	23.0372
	LLOA HR	-55.106	-68.089	-15.069	-55.065	-47.677	-48.2012
Scenario10	Bias HR	3.434	4.968	11.764	1.085	2.215	4.6932
	ULOA HR	28.695	26.838	45.496	47.863	45.311	38.8406
	LLOA HR	-21.826	-16.901	-21.967	-45.693	-40.881	-29.4536
Scenario11	Bias HR	1.979	3.684	-0.488	-3.251	7.721	1.929
	ULOA HR	31.276	21.988	23.819	49.605	50.072	35.352
	LLOA HR	-27.317	-14.618	-24.797	-56.107	-34.629	-31.4936
Scenario12	Bias HR	-4.896	-33.121	11.113	0.053	16.95	-1.9802
	ULOA HR	18.818	-0.603	35.619	47.336	53.981	31.0302
	LLOA HR	-28.611	-65.638	-13.393	-47.229	-20.079	-34.99
Scenario13	Bias HR	-17.438	-21.116	1.423	-9.898	1.075	-9.1908
	ULOA HR	21.268	8.403	48.734	21.982	48.242	29.7258
	LLOA HR	-56.144	-50.635	-45.887	-41.78	-46.091	-48.1074
Scenario14	Bias HR	-24.896	3.818	17.38	15.43	-13.131	-0.2798
	ULOA HR	14.303	17.983	41.918	67.509	20.937	32.53
	LLOA HR	-64.095	-10.346	-7.158	-36.648	-47.199	-33.0892
Scenario15	Bias HR	21.11	-9.138	13.902	29.882	-25.574	6.0364
	ULOA HR	57.332	33.682	52.227	56.126	22.567	44.3868
	LLOA HR	-15.11	-51.959	-24.422	3.638	-73.716	-32.3138
Scenario16	Bias HR	-25.906	-47.73	14.788	-30.361	-30.178	-23.8774
	ULOA HR	21.341	-8.083	41.166	11.515	22.215	17.6308
	LLOA HR	-73.154	-87.377	-11.589	-72.239	-82.572	-65.3862
Scenario17	Bias HR	-29.677	2.476	3.42	2.25	-9.897	-6.2856
	ULOA HR	1.577	20.372	28.462	20.641	22.906	18.7916
	LLOA HR	-60.932	-15.418	-21.62	-16.141	-42.701	-31.3624
Scenario18	Bias HR	-4.311	8.072	-0.556	8.187	-15.015	-0.7246
	ULOA HR	29.822	32.32	14.436	46.329	23.186	29.2186
	LLOA HR	-38.445	-16.175	-15.55	-29.953	-53.217	-30.668
Scenario19	Bias HR	-20.688	4.888	-2.962	14.375	-7.77	-2.4314
	ULOA HR	17.322	14.632	25.525	60.625	39.852	31.5912
	LLOA HR	-58.709	-4.854	-31.45	-31.875	-55.393	-36.4562
Scenario20	Bias HR	2.807	2.808	7.467	-4.711	-12.643	-0.8544
	ULOA HR	28.871	15.889	29.782	38.155	54.519	33.4432
	LLOA HR	-23.255	-10.272	-14.846	-47.577	-79.806	-35.1512
Scenario21	Bias HR	-2.415	-27.856	-13.813	-2.66	-16.162	-12.5812
	ULOA HR	47.062	7.166	24.454	40.975	40.778	32.087
	LLOA HR	-51.893	-62.879	-52.082	-46.297	-73.102	-57.2506
Scenario22	Bias HR	-28.281	-24.212	6.855	-3.392	-17.496	-13.3052
	ULOA HR	3.813	13.447	54.932	46.265	14.142	26.5198
	LLOA HR	-60.376	-61.872	-41.222	-53.049	-49.135	-53.1308
Scenario23	Bias HR	0.0000	-41.931	-28.646	-16.315	-37.73	-31.1555
	ULOA HR	0.0000	-24.571	3.43	4.088	-5.077	-5.5325
	LLOA HR	0.0000	-59.291	-60.724	-36.719	-70.383	-45.4234
Scenario24	Bias HR	0.0000	-42.114	-8.289	-18.5	-40.631	-27.3835
	ULOA HR	0.0000	-16.962	37.36	10.442	-8.043	5.69925
	LLOA HR	0.0000	-67.267	-53.939	-47.443	-73.22	-60.46725
Overall Average	Bias HR						-7.22845
	ULOA HR						27.23677291
	LLOA HR						-41.2207854

Appendix 2.   Second appendix

Table 9. Computation of the overall mean deviations and limits of agreement (BR)

Scenarios	Bland Altman Parameters	Subject1	Subject2	Subject3	Subject4	Subject5	Average
Scenario1	Bias BR	-5.864	-2.261	-2.913	-2.722	-10.045	-4.761
	ULOA BR	3.622	7.759	11.892	6.753	3.679	6.741
	LLOA BR	-15.352	-12.281	-17.719	-12.199	-23.77	-16.2642
Scenario2	Bias BR	-5.563	-3.556	-4.677	-10.83	-3.894	-5.704
	ULOA BR	3.216	7.581	6.948	0.329	3.843	4.3834
	LLOA BR	-14.342	-14.695	-16.303	-21.99	-11.633	-15.7926
Scenario3	Bias BR	-2.196	-3.572	-2.039	-8.44	-2.498	-3.749
	ULOA BR	7.65	7.231	8.597	6.977	10.771	8.2452
	LLOA BR	-12.043	-14.375	-12.676	-23.857	-15.768	-15.7438
Scenario4	Bias BR	-0.374	-4.932	-2.35	-3.749	-8.048	-3.8906
	ULOA BR	10.964	3.3	4.522	3.108	5.253	5.4294
	LLOA BR	-11.713	-13.165	-9.222	-10.607	-21.351	-13.2116
Scenario5	Bias BR	-2.171	-7.32	-2.529	-8.548	-2.996	-4.7128
	ULOA BR	9.296	2.609	5.273	4.227	8.749	6.0308
	LLOA BR	-13.638	-17.251	-10.331	-21.325	-14.741	-15.4572
Scenario6	Bias BR	-3.848	-4.868	-4.999	-8.015	-15.021	-7.3502
	ULOA BR	6.437	7.394	5.187	10.532	-3.715	5.167
	LLOA BR	-14.133	-17.131	-15.186	-26.564	-26.327	-19.8682
Scenario7	Bias BR	-2.689	-7.957	-3.597	-2.271	-7.121	-4.727
	ULOA BR	11.454	4.395	5.673	5.142	-0.715	5.1898
	LLOA BR	-16.833	-20.31	-12.869	-9.685	-13.527	-14.6448
Scenario8	Bias BR	-5.853	-4.045	2.949	-12.238	-12.344	-6.3062
	ULOA BR	5.099	7.954	13.179	1.289	1.948	5.8938
	LLOA BR	-16.806	-16.045	-7.279	-25.766	-26.638	-18.5068
Scenario9	Bias BR	-1.869	-10.182	-1.225	-9.823	-1.38	-4.8958
	ULOA BR	10.645	3.984	6.063	4.732	13.683	7.8214
	LLOA BR	-14.384	-24.349	-8.514	-24.379	-16.444	-17.614
Scenario10	Bias BR	-3.979	-7.571	-3.861	-1.236	-4.664	-4.2622
	ULOA BR	4.66	6.51	2.31	7.671	3.376	4.9054
	LLOA BR	-12.619	-21.654	-10.034	-10.144	-12.706	-13.4314
Scenario11	Bias BR	-2.453	-7.264	0.291	-4.538	-5.382	-3.8692
	ULOA BR	4.061	4.427	10.022	8.24	7.235	6.797
	LLOA BR	-8.967	-18.956	-9.439	-17.318	-18.001	-14.5362
Scenario12	Bias BR	-6.84	-9.78	-3.768	0.427	-5.919	-5.176
	ULOA BR	1.865	5.31	5.324	6.359	3.746	4.5208
	LLOA BR	-15.546	-24.87	-12.862	-5.503	-15.585	-14.8732
Scenario13	Bias BR	-3.423	-5.784	-4.536	-8.533	-5.986	-5.6524
	ULOA BR	9.638	4.444	8.418	4.99	8.138	7.1256
	LLOA BR	-16.485	-16.013	-17.49	-22.057	-20.112	-18.4314
Scenario14	Bias BR	-8.433	0.886	-5.435	-4.807	-5.143	-4.5864
	ULOA BR	5.057	7.288	2.613	1.647	7.023	4.7256
	LLOA BR	-21.923	-5.515	-13.483	-11.261	-17.311	-13.8986
Scenario15	Bias BR	0.807	-1.867	-5.598	-3.204	-2.237	-2.4198
	ULOA BR	13.412	8.921	5.369	9.578	12.028	9.8616
	LLOA BR	-11.797	-12.656	-16.566	-15.988	-16.502	-14.7018
Scenario16	Bias BR	-7.77	-3.758	-10.238	-9.943	-6.087	-7.5592
	ULOA BR	10.532	7.831	1.555	5.813	7.138	6.5738
	LLOA BR	-26.073	-15.347	-22.033	-25.701	-19.312	-21.6932
Scenario17	Bias BR	-2.38	-2.608	-2.31	-4.579	-4.984	-3.3722
	ULOA BR	9.05	12.05	5.189	8.552	4.906	7.9494
	LLOA BR	-13.81	-17.266	-9.809	-17.711	-14.875	-14.6942
Scenario18	Bias BR	-2.701	-6.829	-4.851	-5.704	-0.348	-4.0866
	ULOA BR	8.895	3.171	7.724	7.55	11.015	7.671
	LLOA BR	-14.299	-16.831	-17.427	-18.958	-11.711	-15.8452
Scenario19	Bias BR	-4.483	-9.392	-7.719	-3.137	-3.157	-5.5776
	ULOA BR	5.533	2.48	5.236	7.368	3.897	4.9028
	LLOA BR	-14.5	-21.264	-20.675	-13.643	-10.213	-16.059
Scenario20	Bias BR	-5.524	-10.795	-6.163	-5.215	-4.835	-6.5064
	ULOA BR	5.274	3.142	11.527	7.577	2.405	5.985
	LLOA BR	-16.322	-24.732	-23.853	-18.008	-12.076	-18.9982
Scenario21	Bias BR	-4.763	-11.727	-10.906	-7.074	-7.35	-8.364
	ULOA BR	4.333	3.136	1.006	3.522	2.539	2.9072
	LLOA BR	-13.86	-26.59	-22.819	-17.671	-17.24	-19.636
Scenario22	Bias BR	-8.814	-12.607	-6.92	-1.885	-7.556	-7.5564
	ULOA BR	2.14	4.049	6.374	14.76	5.707	6.606
	LLOA BR	-19.77	-29.263	-20.215	-18.53	-20.82	-21.7196
Scenario23	Bias BR	0.0000	-13.049	-12.961	-7.895	-10.138	-11.01075
	ULOA BR	0.0000	-4.088	-2.483	1.112	1.303	-1.039
	LLOA BR	0.0000	-22.009	-23.44	-16.903	-21.58	-20.983
Scenario24	Bias BR	0.0000	-14.173	-8.935	-9.926	-14.855	-11.97225
	ULOA BR	0.0000	-3.83	9.525	-1.292	-6.012	-0.40225
	LLOA BR	0.0000	-24.517	-27.397	-18.56	-23.698	-23.543
Overall Average	Bias BR						-5.75283333
	ULOA BR						5.582989583
	LLOA BR						-17.0894666

Appendix 3.

Bland Altman Plots of vital signs parameters for Subjects 1 & 3 in Scenario 1
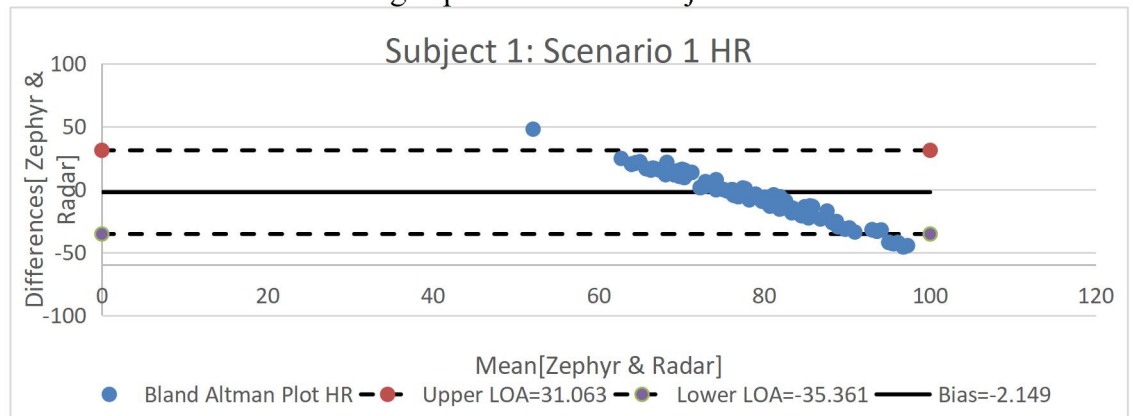

Figure 15. Bland Altman plot for Heart rate (bpm) for Subject 1 in scenario 1.
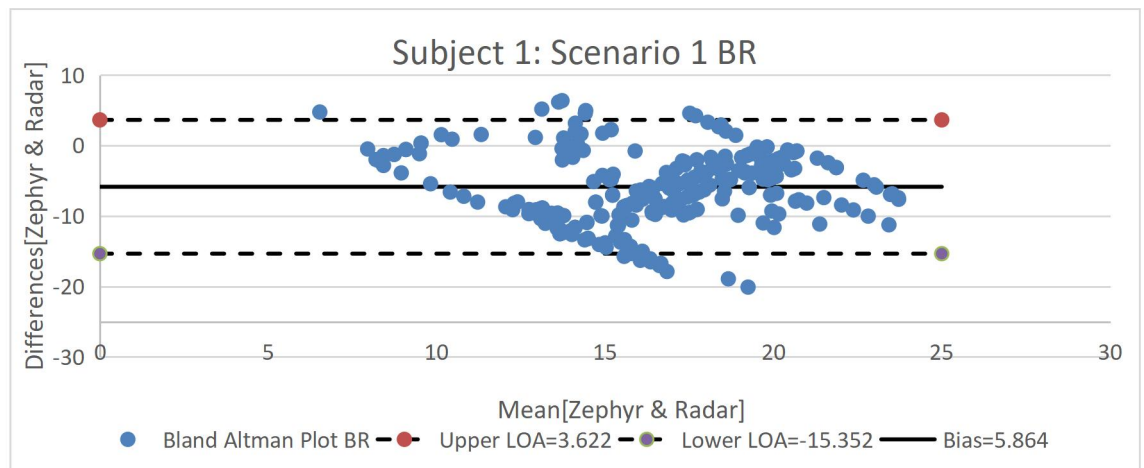

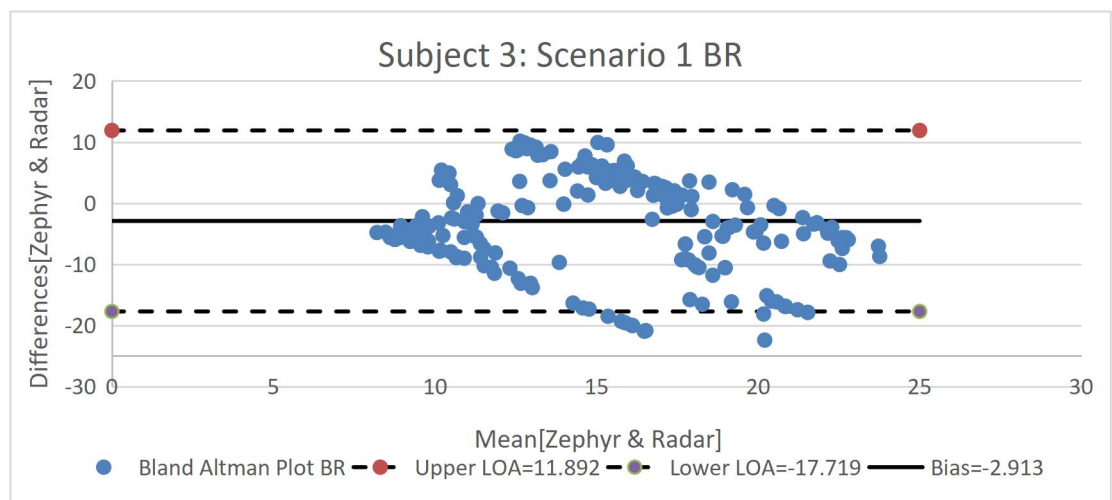Figure 16. Bland Altman plot for Breathing rate (bpm) for Subject 1 in scenario 1.

Figure 19. Bland Altman plot for Breathing rate (bpm) for Subject 3 in scenario 1.

Appendix 4.

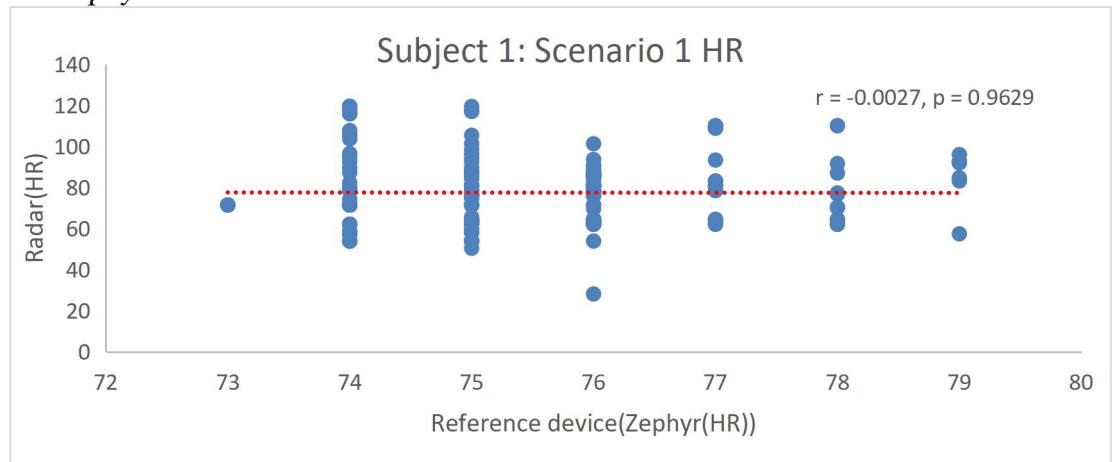Correlation Plots of Heart and Breathing rates for Subject 1 & CV Plot of Heart rate for Zephyr

Figure 21. Correlation plot of Heart rate for Subject 1 in scenario 1.
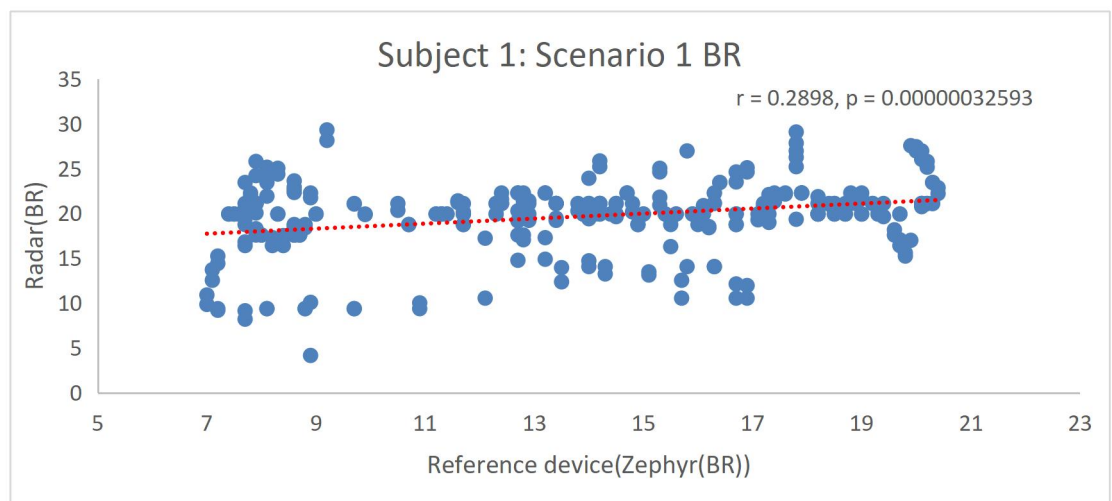
Figure 22. Correlation plot of Breathing rate for Subject 1 in scenario 1.
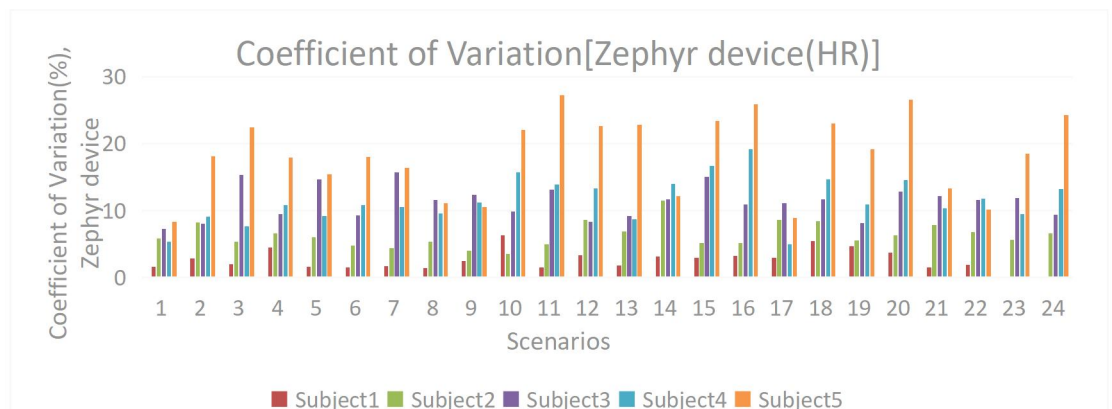
Figure 25A. Coefficient of variation per scenario of heart rate for reference device.

Appendix 5.

CV Plots of Heart and Breathing rates for Zephyr and Radar
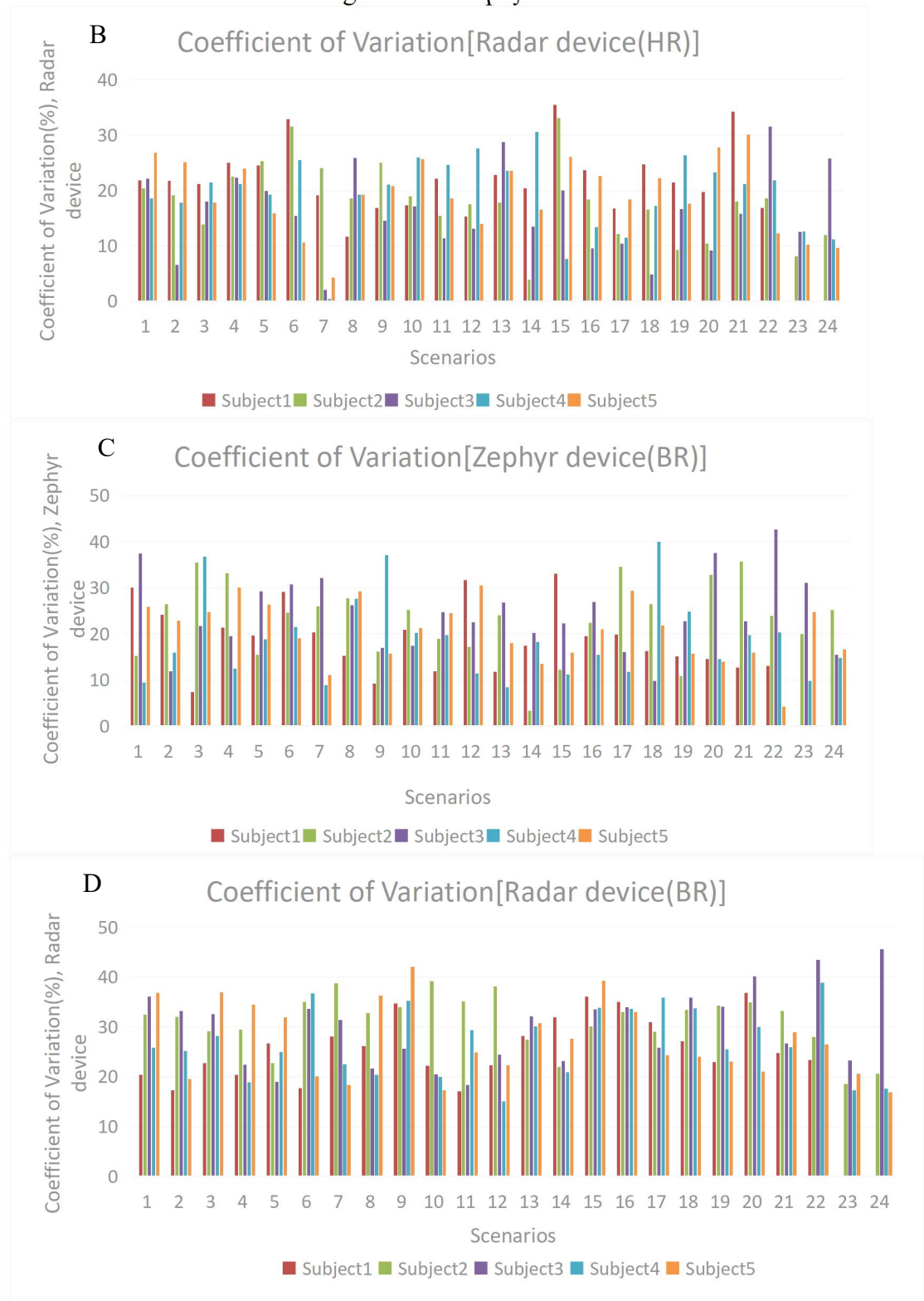
Figure 25. Coefficient of Variation per scenario of B) Heart rate for Radar device C) Breathing rate for reference device D) Breathing rate for Radar device.

Appendix 6.

SNR Plots of Heart and Breathing rates for Zephyr and Radar
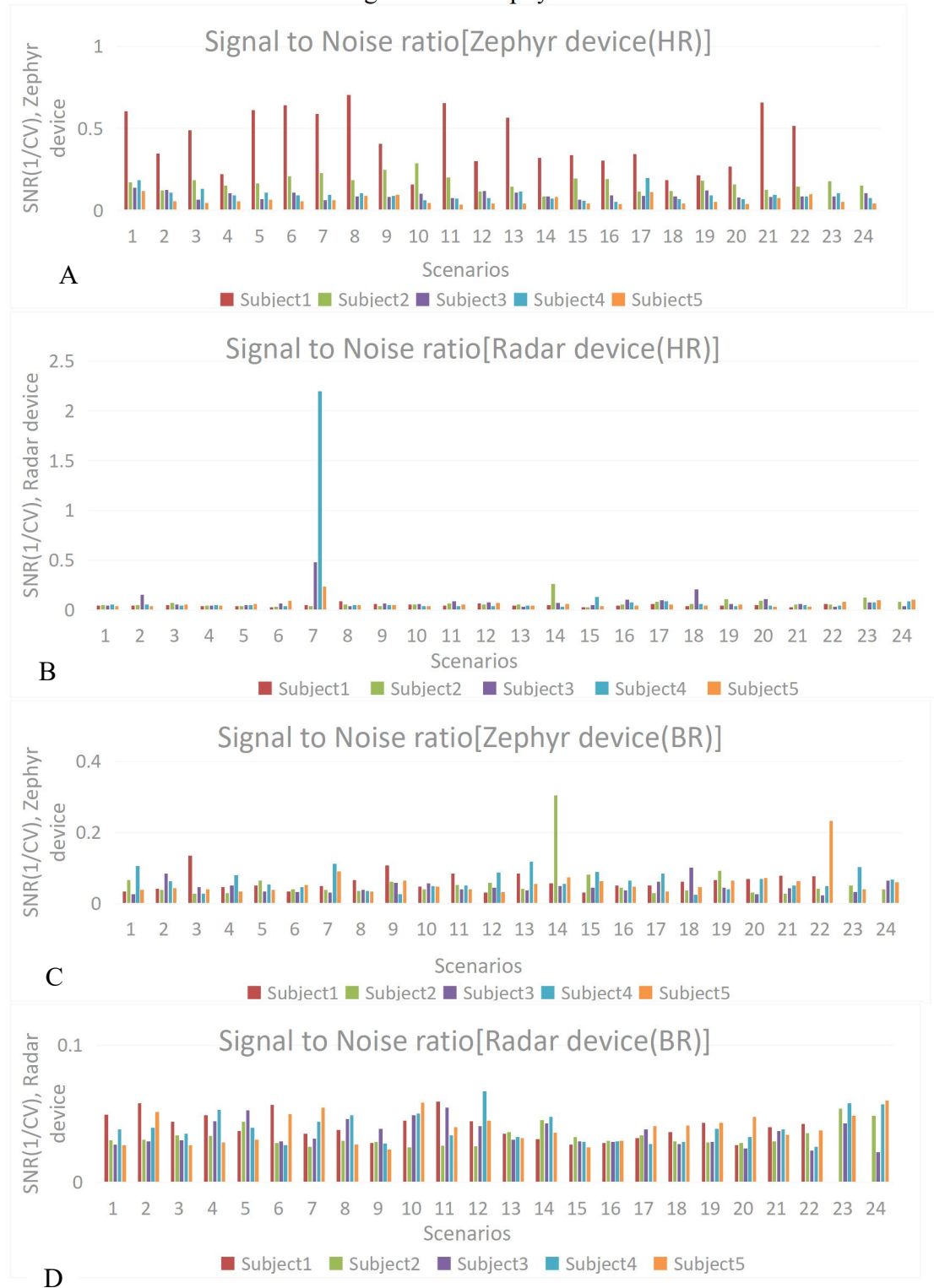
Figure 28. Signal to noise ratio per scenario of A) Heart rate for reference device B) Heart rate for Radar device C) Breathing rate for reference device D) Breathing rate for Radar device.versus Tilt angle Plots for Front and Back measurement scenarios.

Appendix 7.

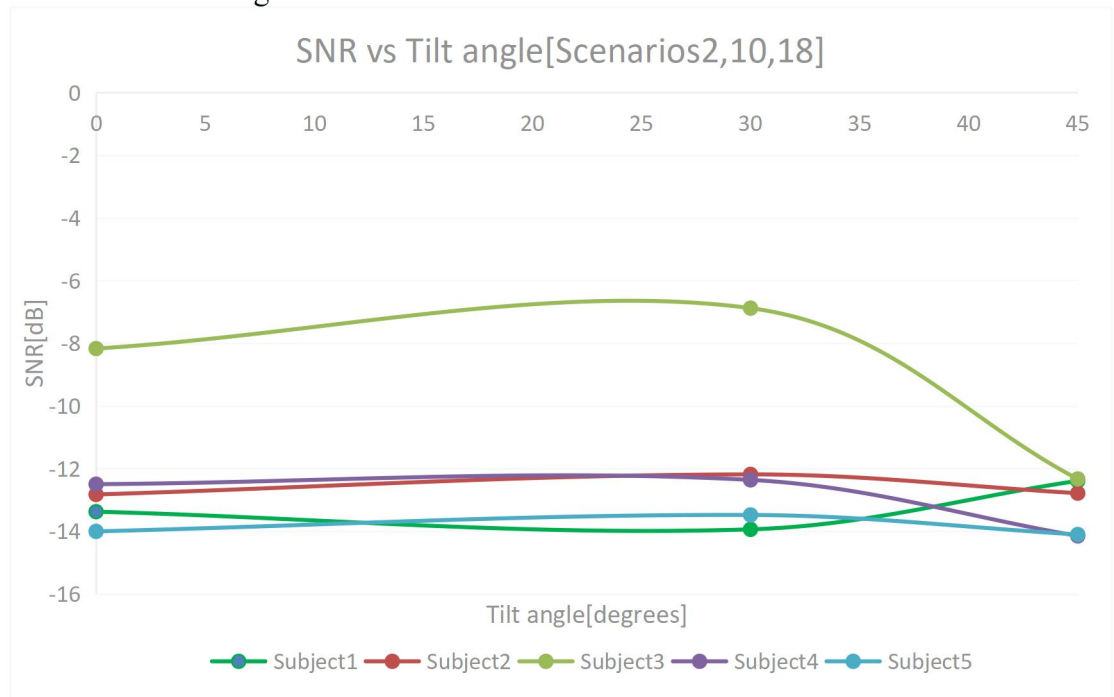SNR versus Tilt angle Plots for Front and Back measurement scenarios

Figure 31B. Signal to noise ratio versus tilt angle for front side scenarios(2, 10, 18).
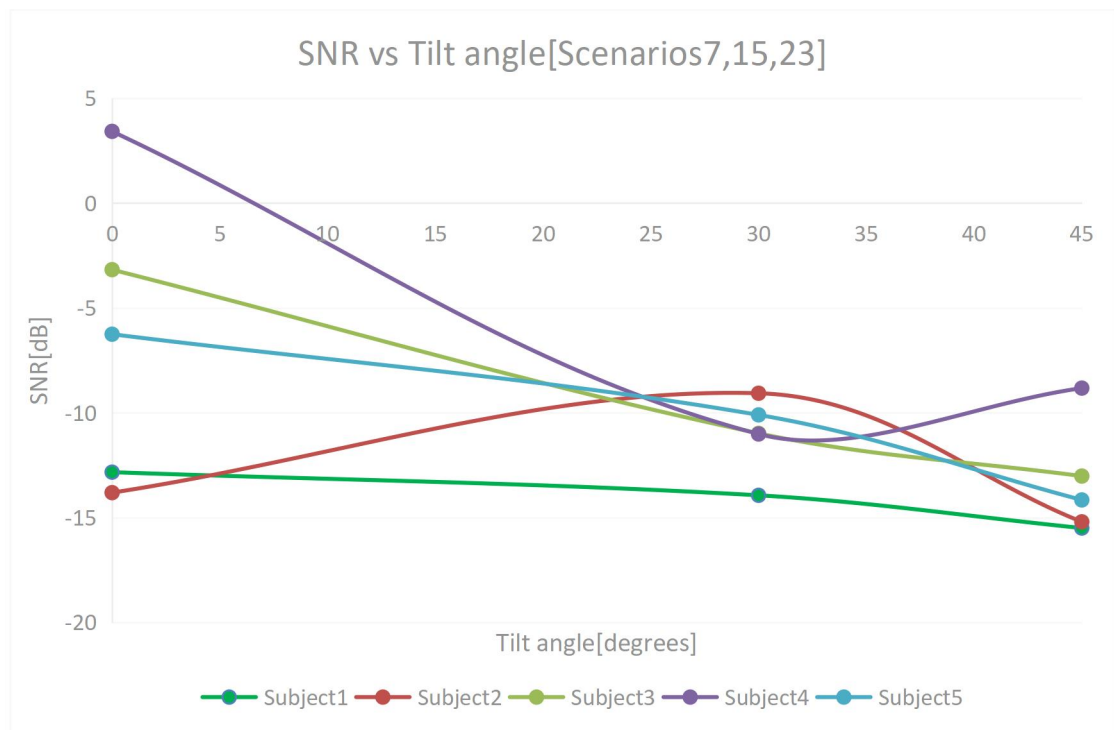

Figure 31G. Signal to noise ratio versus tilt angle for back side scenarios(7, 15, 23).

Appendix 8.

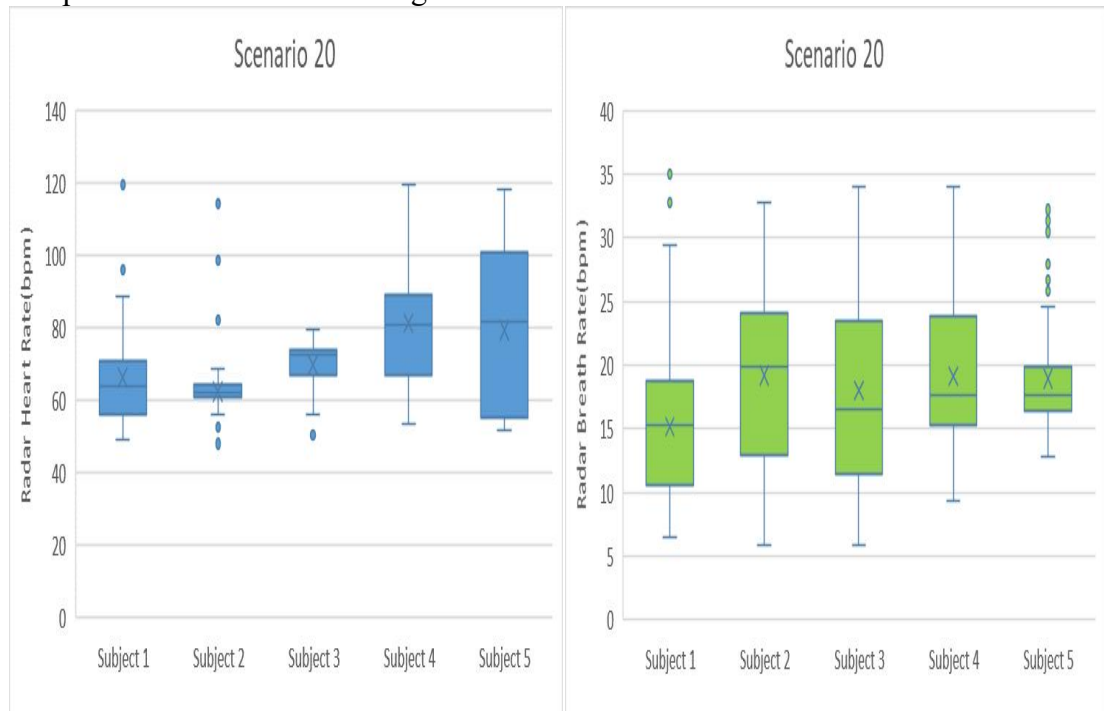Boxplots of Heart and Breathing rates for scenarios 20 and 7

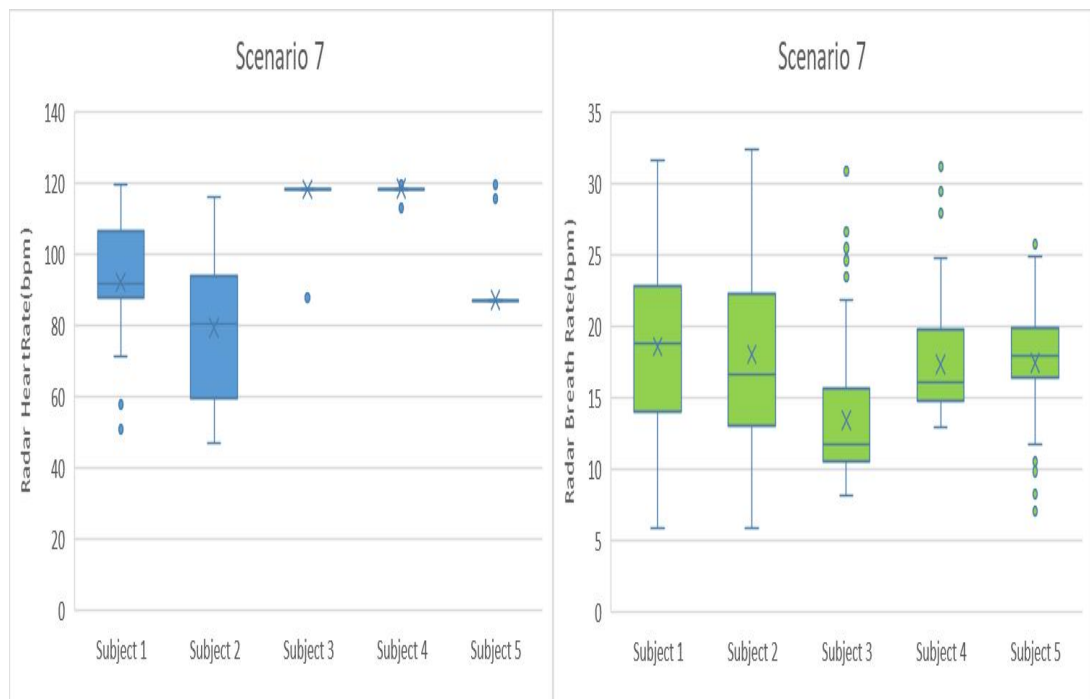Figure 32. Boxplots of Heart and Breathing rates for all subjects in scenario 20.

Figure 33. Boxplots of Heart and Breathing rates for all subjects in scenario 7.